FACULDADE DE ENGENHARIA DA UNIVERSIDADE DO PORTO



Bioengineered Decoys for *Helicobacter pylori*

Renato Filipe Mascarenhas Fernandes Pereira

Mestrado em Engenharia Biomédica

Supervisor: Paula Parreira, PhD

Co-Supervisor: Cristina Martins, PhD

September 19^{th}, 2020

© Renato Pereira, 2020

Bioengineered Decoys for *Helicobacter pylori*

Renato Filipe Mascarenhas Fernandes Pereira

Mestrado em Engenharia Biomédica

Faculdade de Engenharia da Universidade do Porto

September 19^{th}, 2020

The work described in this Dissertation was supervised by:
Paula Parreira, PhD
i3S - Instituto de Investigação e Inovação em Saúde, Universidade do Porto

and

M. Cristina L. Martins, PhD
i3S - Instituto de Investigação e Inovação em Saúde
ICBAS - Instituto de Ciências Biomédicas Abel Salazar, Universidade do Porto

The work described in this Dissertation was conducted at:
i3S - Instituto de Investigação e Inovação em Saúde / INEB – Instituto de Engenharia Biomédica, Universidade do Porto

and

Biocant - Centro de Inovação em Biotecnologia / CNC - Centro de Neurociências e Biologia Celular, Universidade de Coimbra

The work described in this Dissertation was financially supported by:
Projects (PyloriBinders: PTDC/CTM-BIO/4043/2014) and UID/BIM/04293/2019 funded by national funds through FCT/MCTES i3S Scientific platforms: Biointerfaces Nanotechnology and Portuguese Platform of Bioimaging (PPBI-POCI-01-0145-FEDER-022122).

Resumo

A *Helicobacter pylori* (*H. pylori*) é uma bactéria que coloniza o estômago humano, infetando 50% da população mundial. É o agente etiológico de gastrite crónica e cancro gástrico. O tratamento mais comum para a sua erradicação consiste na combinação de dois antibióticos e uma bomba inibidora de protões. No entanto, as taxas crescentes de resistência a antibióticos, aliadas a um esquema de tratamento complexo, que levam à falha do seu cumprimento, contribuem para o insucesso da terapia. Assim, o desenvolvimento de novos tratamentos é essencial.

Como a *H. pylori* necessita de obter/assimilar colesterol exógeno para a sua sobrevivência, o desenvolvimento de estratégias baseadas em lípidos (colesterol) imobilizados em nanopartículas para serem usados como "iscos/atraentes" é bastante apelativo. Nanopartículas funcionalizadas têm sido exploradas para controlo de infeções bacterianas, uma vez que possuem uma variedade de propriedades que as tornam interessantes para aplicações biológicas.

Neste trabalho, "*Self-Assembled Monolayers*" em ouro (SAMs) foram utilizadas como prova de conceito. As SAMs foram desenvolvidas imobilizando colesterol-$(etilenoglicol)_{75}$-SH (Chol-PEG) e um $(etilenoglicol)_4$-SH (EG4) mais pequeno para uma melhor orientação do Chol-PEG. Estas SAMs mistas (Chol-PEG-SAMs) foram produzidas com proporções diferentes de Colesterol-PEG/EG4 de 0 a 100%.
As Chol-PEG-SAMs foram caracterizadas através de Elipsometria, Ângulo de Contato Óptico (OCA) e Espectroscopia Fotoelectrónica de Raios-X (XPS). A elipsometria e o OCA revelaram um aumento da espessura e do ângulo de contato das SAMs, respetivamente, com o aumento da concentração de colesterol. A análise por XPS forneceu a caracterização elementar das SAMs. A Microbalança de Cristal de Quartzo com Dissipação (QCM-D) foi também usada para realizar a quantificação total de colesterol nas SAMs. No entanto, tal não foi possível por falta de especificidade da enzima/anti-corpo utilizados.

A capacidade das SAMs mistas à base de colesterol de atraírem a *H. pylori* foi avaliada através de ensaios de adesão. Para isso, a estirpe *H. pylori* J99 foi incubada com as superfícies durante 2 horas. Posteriormente, a bactéria aderida foi marcada com DAPI e as superfícies visualizadas no Microscópio de Fluorescência Invertido. Os resultados revelaram maior adesão nas 25% Chol-PEG-SAMs (25% Chol-PEG/75% EG4), indicando que existe um rácio ideal de colesterol para induzir a adesão bacteriana. A viabilidade da *H. pylori* aderida às SAMs foi avaliada, sendo que esta não foi comprometida. Foram também realizados estudos de seletividade de adesão a estas superfícies. Para tal, foram selecionadas bactérias Gram positivas e negativas, *Lactobacillus acidophilus* e *Escherichia coli*, respetivamente, de forma a serem representativas do microbioma gastro-intestinal. Os estudos de prova de conceito utilizando SAMs validaram o racional de que superfícies modificadas com lípidos, neste caso colesterol, têm capacidade de atrair a *H. pylori* seletivamente. Estes resultados encorajaram a translação desta estratégia para uma aplicação do

"Mundo real", tal como as Nanopartículas de ouro (Au-NPs).

Au-NPs funcionalizadas com EG4 (EG4-Au-NPs) e Chol-PEG/EG4 (Chol-Au-NPs) foram desenvolvidas e caracterizadas relativamente ao seu tamanho, carga e índice de polidispersão (PdI). As EG4-Au-NPs revelaram um tamanho de 17.17 ± 1.34 nm, enquanto as Chol-Au-NPs um tamanho de 19.88 ± 1.25 nm. A caracterização do potencial-Zeta e PdI mostrou uma carga de -18 mV e 0.5 de PdI para as EG4-Au-NPs, enquanto que a carga das Chol-Au-NPs foi de aproximadamente 4 mV e 0.3 PdI.
A resposta das EG4- e Chol-Au-NPs a soluções de diferentes valores de pH (2.6, 4.0, 6.0 e 7.4) também foi avaliada. As Chol-Au-NPs mantiveram o seu potencial-Zeta em todos os pHs testados, indicando serem apropriadas para uso em ambiente gástrico, enquanto que as EG4-Au-NPs aumentaram substancialmente a sua carga em soluções acídicas, para valores neutros.

A capacidade das EG4- e Chol-Au-NPs de interferirem com a *H. pylori* foi avaliada após 2, 6 e 24 horas de incubação com diferentes concentrações (62.5, 125, 250, 500 e 750 μg/ml). A concentração mínima bactericida para as EG4- e Chol-Au-NPs foi de 500 e 125 μg/ml, respetivamente. Um ensaio preliminar usando a linha celular AGS de carcinoma gástrico humano mostrou que tanto as EG4- como as Chol-Au-NPs são não citotóxicas em todas as concentrações testadas, à exceção de 750 μg/ml de EG4-Au-NPs.

Os resultados obtidos sugerem que as Au-NPs decoradas com grupos funcionais de colesterol interferem com o crescimento da *H. pylori*, atingindo valores bactericidas. Estas NPs são estáveis numa ampla gama de valores de pH e apresentam baixa citotoxicidade. Assim, esta estratégia apresenta-se como promissora no desenvolvimento de novas abordagens para o controlo da infeção gástrica por *H. pylori*.

Abstract

Helicobacter pylori (*H. pylori*) is a bacterium that inhabits the human stomach, infecting 50% of world population. It is the etiological agent of chronic gastritis and gastric cancer. The most common treatment for its eradication is based on a combination of two antibiotics and a proton pump inhibitor. However, the increasing rates in antibiotic resistance, allied with a complex therapeutic scheme that leads to lack of compliance, contributes to treatment failure. In this sense, the development of novel treatments is essential.

As *H. pylori* needs to obtain/assimilates exogenous cholesterol for its survival, the development of strategies based on lipids (cholesterol), immobilized on nanoparticles to be used as decoys, is appealing. Functionalized nanoparticles have been explored for the control of bacterial infections since they possess a variety of proprieties that make them interesting for biological applications.

During this work, Self-Assembled Monolayers on gold (SAMs) were used as proof-of-concept study. SAMs were developed immobilizing cholesterol-(ethylene glycol)$_{75}$-SH (Chol-PEG) and a smaller (ethylene glycol)$_4$-SH (EG4) for better orientation of Chol-PEG thiol. These mixed SAMs (Chol-PEG-SAMs) were produced in different Chol-PEG/EG4 ratios, from 0 to 100%.
Chol-PEG-SAMs were fully characterized using Ellipsometry, Optical Contact Angle (OCA) and X-Ray Photoelectron Spectroscopy (XPS). Ellipsometry and OCA showed increasing SAMs thickness and contact angle, respectively, with increasing cholesterol concentration. The XPS analysis provided elemental characterization of SAMs. Characterization using Quartz Crystal Microbalance with Dissipation (QCM-D) was also used for quantification of total cholesterol moiety on SAMs. However, this was not possible due to the lack of specificity of the enzyme/antibody used.

The ability of these mixed cholesterol based SAMs to attract *H. pylori* was accessed by adhesion assays. The *H. pylori* J99 strain was incubated with the surfaces for 2 hours. After, the adhered bacteria were stained with DAPI and the surfaces visualized under the Inverted Fluorescence Microscope. Results showed higher adhesion at 25% Chol-PEG-SAMs (25% Chol-PEG/75% EG4) indicating an optimum ratio of cholesterol to induce bacterial adhesion. The viability of the *H. pylori* adhered to SAMs was accessed and it was not compromised. Adhesion selectivity studies were also performed. For that, Gram positive and negative bacteria, *Lactobacillus acidophilus* and *Escherichia coli*, respectively, were selected in order to be representative of the gastro-intestinal microbiome. The proof-of-concept studies using SAMs validated the rational that modified surfaces with lipids, in this case cholesterol, have the ability to attract *H. pylori* selectively. These results encouraged the translation of this strategy to a more "real-world" application as Gold Nanoparticles (Au-NPs).

Functionalized Au-NPs with EG4 (EG4-Au-NPs) and Chol-PEG/EG4 (Chol-Au-NPs) were de-

veloped and characterized in relation to their size, charge and polydispersity index (PdI). EG4-Au-NPs revealed a size of 17.17 ± 1.34 nm, while Chol-Au-NPs had a mean size of 19.88 ± 1.25 nm. Zeta-potential and PdI characterization showed a charge around -18 mV and 0.5 PdI for the EG4-Au-NPs, while Chol-Au-NPs charge was approximately 4 mV and 0.3 PdI.
EG4- and Chol-Au-NPs response to different pH solutions (2.6, 4.0, 6.0 and 7.4) was also evaluated. Chol-Au-NPs maintained their zeta-potential in all pHs, indicating they are suitable for use in gastric environment, while EG4-Au-NPs increased substantially their charge in acidic solutions to neutral values.

The ability of EG4- and Chol-Au-NPs to interfere with *H. pylori* was accessed after 2, 6 and 24 hours of incubation with different concentrations (62.5, 125, 250, 500 and 750 μg/ml). Minimal bactericidal concentration for EG4-Au-NPs and Chol-Au-NPs was 500 and 125 μg/ml, respectively. A preliminary assay using Human gastric carcinoma AGS cell line showed both EG4- and Chol-Au-NPs are not cytotoxic in all tested concentrations, with the exception of 750 μg/ml EG4-Au-NPs.

The obtained results suggest that Au-NPs decorated with cholesterol groups interfere with *H. pylori* growth reaching bactericidal values. These NPs are stable over a wide range of pH values and have low cytotoxicity. Thus, this strategy presents itself as promising in the development of new approaches for the control of gastric infection by *H. pylori*.

Acknowledgements

A realização e conclusão deste trabalho marca o fim de uma das etapas mais importantes e determinantes na minha vida. No entanto, não seria possível sem o apoio e motivação de todos os que me rodeiam. Por isso expresso toda a minha honesta gratidão pelo seu contributo crucial nesta conquista.

À minha orientadora, a quem eu salvei a vida, Doutora Paula Parreira, pelo grande acompanhamento, enorme disponibilidade e dedicação. Não há palavras para descrever a sua rara e excecional orientação! Um enorme eterno Obrigado!

À minha co-orientadora, Professora Doutora Cristina Martins, por toda a ajuda, motivação e preocupação na realização deste trabalho.

Ao Dr. Lino Ferreira e Dr. Akhilesh Rai por aceitarem a colaboração com o nosso grupo, muito importante para a realização deste trabalho.

A todos os professores do Mestrado de Engenharia Biomédica, por todo o conhecimento transmitido e contributo para a minha formação académica.

A todos os membros do Bioengineered Surfaces Group, por toda a ajuda dada e pela ótima equipa que são. Um laboratório cheio de vida, pronto a ajudar e cheio de qualidade!

Ao Duarte e Diana, meus companheiros de laboratório, por toda a diversão, conversas e companheirismo.

Aos meus amigos, companheiros de vida, Leonor, Juca, Pipi, Marta, Rita, Diogo, Adriano, Maria, Tesouras e Clapy. Obrigado pela nossa amizade e por estarem sempre presentes!

Ao Pedro, meu melhor amigo, amor de uma vida, por me aturar! Obrigado pelo amor, carinho e amizade, por fazeres parte da minha vida nos bons e maus momentos.

À minha querida família, exemplo de dedicação e trabalho árduo, que nunca deixou que me faltasse nada. Obrigado pelo amor, carinho, preocupação e apoio incondicional! Se sou alguma coisa hoje é graças a vocês. Obrigado.

"Stay hungry
stay foolish"

Steve Jobs

Contents

Resumo iii

Abstract v

1 Introduction 1
1.1 Framework and motivation . . . 1
1.1.1 Objective . . . 1
1.2 Dissertation structure . . . 2

2 *Helicobacter pylori* - an overview 3
2.1 Infection by *H. pylori* . . . 4
2.1.1 Worldwide prevalence - The world conqueror . . . 5
2.1.2 Transmission . . . 5
2.1.3 Morphology, Colonization & Virulence factors . . . 6
2.1.4 Human immune system vs. *H. pylori* (the devil in disguise) . . . 9
2.2 Current treatments for *H. pylori* . . . 10
2.3 Alternative treatments . . . 12
2.4 *H. pylori* and Cholesterol - A love story and a new Target . . . 13
2.4.1 Cholesterol recognition . . . 14
2.4.2 Cholesterol "digestion" - Glycosylation . . . 14
2.4.3 A new Target: taking advantage of uniqueness . . . 16

3 New strategies for *H. pylori* treatment: from proof-of-concept to real-world applications 17
3.1 Self-Assembled Monolayers - on gold (SAMs) . . . 17
3.1.1 *H. pylori* and surface interaction (on SAMs) . . . 18
3.1.2 SAMs characterization techniques . . . 19
3.2 Real-world application - Gold Nanoparticles (Au-NPs) . . . 22
3.2.1 Nanoparticles against Bacteria . . . 23
3.2.2 SAMs on Au-NPs . . . 24
3.2.3 Biocompatibility of Au-NPs . . . 25
3.2.4 Gastric bioavailability & PEG functionalization . . . 25
3.2.5 Nanoparticles characterization techniques . . . 26

4 Materials and Methods 29
4.1 SAMs preparation . . . 29
4.1.1 Pure Cholesterol SAMs (PC-SAMs) . . . 29
4.1.2 Mixed Cholesterol SAMs (MC-SAMs) . . . 30
4.2 SAMs characterization . . . 30

4.2.1 Ellipsometry . . . 30
4.2.2 Optical Contact Angle . . . 30
4.2.3 X-Ray Photoelectron Spectroscopy . . . 31
4.2.4 Quartz Crystal Microbalance with Dissipation . . . 31
4.3 *In vitro* adhesion assays . . . 31
4.3.1 Bacteria culture . . . 31
4.3.2 Bacterial adhesion . . . 32
4.3.3 Planktonic cells viability . . . 32
4.3.4 Live/Dead assay . . . 32
4.4 Gold nanoparticles production and functionalization . . . 33
4.5 Gold nanoparticles characterization . . . 33
4.5.1 Size, charge and polydispersity index measurements . . . 33
4.5.2 Gold nanoparticles behavior in a pH range . . . 33
4.6 Gold nanoparticles *in vitro* antibacterial performance . . . 34
4.6.1 Growth conditions . . . 34
4.6.2 Antibacterial effect . . . 34
4.7 Gold Nanoparticles Cytotoxicity . . . 34
4.7.1 AGS cell culture . . . 34
4.7.2 Direct contact assay . . . 34
4.7.3 Cell metabolic activity . . . 35
4.8 Statistics . . . 35

5 Results and Discussion **37**
5.1 Pure Cholesterol SAMs (PC-SAMs) . . . 37
5.1.1 Surface Characterization . . . 37
5.2 Mixed Cholesterol SAMs (MC-SAMs) . . . 38
5.2.1 Surface Characterization . . . 39
5.2.2 *In vitro* adhesion assay - *Helicobacter pylori* . . . 42
5.2.3 *In vitro* adhesion assay - Viability study . . . 43
5.2.4 *In vitro* adhesion assay - Selectivity study . . . 45
5.3 Gold nanoparticles . . . 46
5.3.1 Size, charge and polydispersity index characterization . . . 46
5.3.2 Gold nanoparticles *in vitro* assay . . . 48
5.3.3 Gold Nanoparticles Cytotoxicity . . . 49

6 Conclusions and Future work **53**

A Au-NPs characterization after production **57**
A.1 Materials and Methods . . . 57
A.2 Results . . . 57

B i3S Annual Meeting (2019): "Lipid-based Decoys for Gastric Infection Management: A Proof of Concept Study" **59**

References **63**

List of Figures

2.1 Scanning electron micrograph of *H. pylori* (from [1]). . . . 4
2.2 **Correa's cascade:** model for the development of gastric cancer triggered by *H. pylori*. The point of no return marks the point of irreversible genetic alterations (adapted from [2]). . . . 4
2.3 *H. pylori* global geographic prevalence (adapted from [3]). . . . 5
2.4 Suggested *H. pylori* transmission routes (adapted from [4]). . . . 6
2.5 a) Gastric mucosal surface; b) pH gradient on the gastric mucus layer (adapted from [5]). . . . 7
2.6 Colonization of gastric mucus layer and adherence on gastric epithelial cells by *H. pylori* (adapted from [6]). . . . 7
2.7 Model of intracellular colonization by *H. pylori*. . . . 8
2.8 Translocation of CagA and VacA from *H. pylori* to epithelial gastric cells and cellular effects. . . . 9
2.9 Treatment regimens employed for *H. pylori* eradication. Tetracycline (TET), doxycycline (DOX), furazolidone (FZ), moxifloxacin (MXF) and rifabutin (RFB) (adapted from [7]). . . . 10
2.10 Prevalence of a) CLA; b) LEV and c) MET resistance (adapted from [8]). . . . 12
2.11 Cholesterol molecule. . . . 13
2.12 Cholesterol placement in the cellular plasmatic membrane. . . . 13
2.13 Predominant PE molecular species of *H. pylori* and *E. coli*. Saturated fatty acids highlighted in red (adapted from [9]). . . . 14
2.14 a) Cholesterol uptake and processes inside *H. pylori*; b) Cholesterol and DMPE affinity (adapted from [10]). . . . 15
2.15 Chronic inflammation due to cholesterol glycosylation model (adapted from [11]). 16

3.1 Illustration of the main three components of an ordinary thiol-based SAMs (Schematic representation not to scale). . . . 18
3.2 Schematic operation principle of Ellipsometry. . . . 19
3.3 Schematic operation principle of OCA. . . . 20
3.4 OCA methods (θ: Angle of the tangent between the solid surface and the liquid droplet, θr: Receding contact angle, θa: Advancing contact angle). . . . 20
3.5 Schematic operation principle of XPS. . . . 21
3.6 Schematic operation principle of QCM-D. Frequency of vibration shift (Δf) represented in blue and Dissipation shift (ΔD) represented in orange. . . . 21
3.7 Schematic representation of Au-NPs (Not to scale). . . . 22
3.8 Schematic representation of SAMs on a) planar and b) curved surface. Blue cones represent free volume of the alkanethiols chains to move. . . . 24
3.9 Schematic operation principle of DLS (adapted from [12]). . . . 27

3.10 Representation of ionic concentration and Zeta-potential as a function of distance from the charged surface of a positive charged NP. 27

4.1 Alkanethiols used: a) EG4 and b) Chol-PEG. 29

5.1 SAMs characterization: a) Ellipsometry; b) Optical contact angle. $*$ - statistically significant different, # - statistically significant from all the other tested surfaces (ANOVA; p<0.05). (n=3) 37
5.2 SAMs characterization: a) Ellipsometry; b) Optical contact angle. $*$ - statistically significant different, # - statistically significant from all the other tested surfaces (One way ANOVA; p<0.05). (n=3) 39
5.3 EG4 and Chol-PEG coverage on gold surface as a function of Nitrogen relative percentage, obtained through XPS analysis. 40
5.4 Quantification of linked Chol-PEG using MβCD through QCM-D. 41
5.5 Quantification of linked Chol-PEG using DPPE through QCM-D. 42
5.6 Representative images of *H. pylori* J99 labelled with DAPI after 2 hours adhesion. a) EG4-SAMs, b) 12.5% Chol-PEG-SAMs, c) 25% Chol-PEG-SAMs, d) 50% Chol-PEG-SAMs and e) 100% Chol-PEG-SAMs. 42
5.7 *H. pylori* J99 adhesion to Chol-PEG-SAMs after 2 hours. $*$ - statistically significant different, # - statistically significant from all the other tested surfaces (One way ANOVA; p<0.05). (n=3) 43
5.8 Representative images of *H. pylori* J99 labelled with LIVE/DEAD^{TM} Baclight^{TM} after 2 hours adhesion. Green colour represents live bacteria (SYTO9 stained), red colour represents dead bacteria (PI stained). a) EG4-SAMs, b) 12.5% Chol-PEG-SAMs, c) 25% Chol-PEG-SAMs, d) 50% Chol-PEG-SAMs and e) 100% Chol-PEG-SAMs. 44
5.9 *H. pylori* J99 adhesion to Chol-PEG-SAMs after 2 hours. a) surface adherent cells and b) planktonic cells. Total adhesion corresponds to the number of live + dead cells. # - statistically significant from all the other tested surfaces (One way ANOVA; p<0.05), green for Live and red for Dead. 44
5.10 Adhesion to Chol-PEG-SAMs after 2 hours. a) *E. coli* surface adherent cells, b) *E. coli* planktonic cells, c) *L. acidophilus* surface adherent cells, d) *L. acidophilus* planktonic cells. $*$ - statistically significant different, # - statistically significant from all the other tested surfaces (One way ANOVA; p<0.05). (n=3) 45
5.11 Histograms of size distribution of the produced Au-NPs. All statistically significant different (One way ANOVA; p<0.05). (n=2) 46
5.12 a) Zeta-potential and b) PdI Au-NPs. All Au-NPs have statistically significant differences in Zeta-potential. # - statistically significant from all the other tested surfaces (One way ANOVA; p<0.05). (n=2) 47
5.13 Au-NPs response on MilliQ water, and solutions of pH values of 7.4, 6.0, 4.0 and 2.6. 48
5.14 Antibacterial performance of a) EG4- and b) Chol-AuNPs against *H. pylori* J99. Assays were performed in BB + 10% FBS after 2, 6 and 24 hours of incubation. (n=3) 49
5.15 Metabolic activity of AGS cells assessed by the direct method. 50
5.16 Images of AGS cells after 24 hours incubation with EG4- and Chol-Au-NPs. EG4-Au-NPs: a) AGS cells, b) 62.5 μg/ml, c) 125 μg/ml, d) 250 μg/ml, e) 500 μg/ml, f) 750 μg/ml. Chol-Au-NPs: g) AGS cells, h) 62.5 μg/ml, i) 125 μg/ml, j) 250 μg/ml, k) 500 μg/ml, l) 750 μg/ml. 51

A.1 Histogram of size distribution of the produced Au-NPs after production, revealing a size diameter between 7.1 and and 8.3 nm. 57

List of Tables

3.1 Biological studies using SAMs. 18
3.2 Studies using NPs for bacterial infections. 23

5.1 Relative percentage of chemical elements Carbon (C), Oxygen (O), Nitrogen (N) and Sulfur (S) for EG4 and PC-SAMs. 38
5.2 Relative percentage of chemical elements Carbon (C), Oxygen (O), Nitrogen (N) and Sulfur (S) for EG4 and Chol-PEG-SAMs. 40

Abbreviations

AGS	Atypical Glandular cells
AlpA	Adherence-associated lipoprotein A
AlpB	Adherence-associated lipoprotein B
AMP	Antimicrobial peptide
AMX	Amoxicillin
Au-NPs	Gold nanoparticles
Au-S	Gold-Sulfur bond
$AuCl_3$	Gold Chloride
BabA	Blood group antigen binding Adhesin
BB	Brucella Broth medium
BB+10% FBS	BB supplemented with 10% FBS
BCE	Basal Cell Epithelioma
Blood Agar plates	Trypticase Soy Agar plates supplemented with horse blood
BS	Bismuth Salts
C	Carbon
$C_{14:0}$	Saturated fatty acid of myristic acid of 14 carbons
$C_{16:0}$	Saturated fatty acid of palmitic acid of 16 carbons
CAG	Cholesteryl-6-O-tetradecanoyl-α-D-glucopyranoside
CagA	Cytotoxin-associated A protein
cagPAI	cag pathogenicity island
CEMUP	Centro de Materiais da Universidade do Porto
CFUs	Colony-forming units
CGL	Cholesteryl-α-D-glucopyranoside
CGLAT	CGL acyltransferase
CGLPT	CGL phosphatidyltransferase
CGT	α-glucosyltransferase
Chol-Au-NPs	Au-NPs of EG4/Chol-PEG mixture
Chol-PEG	Cholesterol PEG Thiol/Sulfhydryl
CLA	Clarithromycin
CLSI	Clinical
Laboratory Standards Institute	
CNC	Centro de Neurociências e Biologia Celular
CPG	cholesteryl-6-O-phosphatidyl-α-D-glucopyranoside
D_{eff}	Diffusion coefficient
DLS	Dynamic Light Scattering
dMβD	2,6-di-O-methyl-β-cyclodextrin
DMPE	dimyristoyl-PE
DOX	Doxycycline
DPPE	1,2-dipalmitoyl-*sn*-glycero-3-phosphoethanolamine

E. coli	*Escherichia coli*
EG4	1- Mercapto-11-undecyl tetra(ethylene glycol)
EG4-Au-NPs	Pure Au-NPs of EG4
FBS	Fetal Bovine Serum
FTIR	Fourier Transform Infrared Spectroscopy
Full RPMI	RPMI medium supplemented with 10% FBS and Pen/Strep
FZ	Furazolidone
H. pylori	*Helicobacter pylori*
hβD3	Human β-defensin 3
HCO_3^-	Bicarbonate ion
HDF	Human Dermal Fibroblasts
HopZ	*Helicobacter* outer membrane protein Z
HPLC	High Performance Liquid Chromatography
IFM	Inverted Fluorescence Microscope
IFN-γ	interferon-γ
IL-22	Interleukin-22
IL-8	Interleukin-8
K. pneumoniae	*Klebsiella pneumoniae*
KBr	Potassium Bromide
L. acidophilus	*Lactobacillus acidophilus*
LEV	Levofloxacin
Logs	Logarithms
LPS	Lipopolysaccharides
MBC	Minimal Bactericidal Concentration
MβCD	Methyl-β-cyclodextrin
MC-SAMs	Mixed Cholesterol SAMs
MET	Metronidazole
MilliQ	MilliQ water
MRS	Rogosa and Sharpe agar
MTS	3-(4,5-dimethylthiazol-2-yl) 5-(3-carboxymethoxyphenyl)-2-(4- sulfophenyl)-2H- tetrazolium
MW	Molecular weight
MXF	Moxifloxacin
N	Nitrogen
NPs	Nanoparticles
O	Oxygen
OCA	Optical Contact Angle
P. aeruginosa	*Pseudomonas aeruginosa*
PBS	Phosphate Buffer Solution
PC-SAMs	Pure Cholesterol SAMs
PCABs	Potassium-Competitive Acid Blockers
PdI	Polydispersity Index
PE	phosphatidylethanolamine
PEG	Poly(ethylene glycol)
Pen/Strep	Penicillin and Streptomycin
PI	Propidium Iodide
PPI	Proton Pump Inhibitor
QCM-D	Quartz Crystal Microbalance with Dissipation
r.p.m	rotations per minute

RFB	Rifabutin
ROS	Reactive Oxygen Species
RPMI	Roswell Park Memorial Institute
S	Sulfur
SabA	Sialic acid-binding Adhesin
SAMs	Self-Assembled Monolayers
TCPS	Tissue Culture Polystyrene
TEM	Transmission electron microscopy
TET	Tetracycline
θ	Angle of the tangent between the solid surface and the liquid droplet
θa	Advancing contact angle
θr	Receding contact angle
Th1	Type 1 T helper cells
TSA	Trypticase Soy Agar
T4SS	Type IV secretion system
VacA	Vacuolating cytotoxin A protein
XPS	X-Ray Photoelectron Spectroscopy

Chapter 1

Introduction

1.1 Framework and motivation

Helicobacter pylori (*H. pylori*) is a Gram negative bacterium that infects the human gastric mucosa of nearly 4.4 billion individuals worldwide (50% of human population) [13, 14]. It causes several gastric disorders, such as gastritis and 90% of the global non-cardia cancer burden is attributed to infection by this bacterium [15]. Its success relies on several features namely the ability to penetrate and destroy the stomach protective lining, the release of cytokines and establishment of chronic inflammatory processes as well as to deceive the human immune system by camouflaging itself [5, 16, 17].

The most common therapeutic scheme consists in a triple therapy prescribed with two antibiotics and one proton pump inhibitor [18]. However, the increasing rates in antibiotic resistance allied with low patient compliance largely contribute to treatment failure [4, 19]. Overall, there are limited drug options available for *H. pylori* treatment. Currently, this gastric pathogen ranks as one of the most dangerous bacteria to human health in the 21^{st} century, making the development of novel treatments an urgent need [20, 21].

Cholesterol takes an important role in the biological processes, being a key constituent of cells plasmatic membranes [22]. Unlike any other bacteria, *H. pylori* assimilates exogenous cholesterol and incorporates it in its cell membrane for its survival. Also, this cholesterol uptake allows *H. pylori* to acquire resistance to antibacterial agents [10, 23]. In this sense, lipid-based (cholesterol) bioengineered strategies can be developed as decoys to be used against *H. pylori*.

1.1.1 Objective

The aim of this work was to develop a lipid-based (cholesterol) decoy specific for *H. pylori*. Ideally, this strategy would enhance *H. pylori* eradication, either by internalization onto the bacterial cells leading to death or by acting as a chemo attractant, which can be explored as co-adjutant to enhance other therapeutic strategies.

To validate this rational, proof-of-concept studies using Self-Assembled Monolayers on gold (SAMs) functionalized with the lipid of interest (cholesterol) were first performed. These studies comprised SAMs development and characterization, followed by *in vitro* testing (ability to act as chemo attracts and selectivity studies). Then, the knowledge obtained with model surfaces was translated to Au-NPs, a biocompatible "real-world" strategy, followed by anti *H. pylori* and cytotoxicity screening.

1.2 Dissertation structure

This dissertation is divided in 6 chapters. The second chapter (Chapter 2) aims to give the reader a broad overview on *H. pylori* biology and infection. It focuses on infection, worldwide prevalence, current treatments and new therapeutic alternatives, as well as the importance of cholesterol for its survival. The third chapter (Chapter 3) introduces the proof-of-concept studies using SAMs, followed by the translation of knowledge to nanoparticles as a real-world strategy. Chapter 4 includes the materials and methods. Chapter 5 focuses on the obtained Results and Discussion. Finally, Chapter 6 presents the main conclusions and future work.

Chapter 2

Helicobacter pylori - an overview

A spiral shaped organism, still unidentified, was first observed by Italian researcher Bizzozero in dogs stomach in the second part of the 19th century [24]. Later on, W. Jaworski, Professor of Medicine at the Jagiellonian University of Cracow, Poland, reported the presence of spiral shaped organisms in gastric washing of human's stomachs, being the first to associate their presence with a possible pathogenic effect in the gastric tract. However, his work had little visibility since it was written in polish [25]. In 1924, Luck *et al.* observed high urease activity in the human stomach that would decrease following a course of antibiotics treatment [26]. Nonetheless, the association between these events and the presence of a microorganism in the stomach was not made, since at the time it was believed that the "stomach secrets acid to keep its lumen sterile and that acid may cause mucosal lesions". Also, the inability to culture those bacteria was a major hindrance to recognize their presence and role in the human stomach [25].

In 1982, Warren and Marshal successfully isolated and cultured a spiral-shaped bacterium from the gastric biopsy of a patient with duodenal ulcer [27]. For their discovery of *H. pylori* and its role on the development of several gastric disorders, namely peptic ulcer disease, they were awarded with the Nobel Prize of Medicine in 2005 [28, 29]. Later studies reported that the eradication of *H. pylori* alone was sufficient to treat duodenal and gastric ulcers. However, these reports found medical reluctance, since stress or lifestyle were associated to ulcers development and simple treatments, such as acid-suppressive therapies, were considered enough [24, 30]. Several years passed until the medical community accepted the link between *H. pylori* infection and gastric diseases and even more time until the association between infection with this pathogen and gastric cancer was established [31].

Currently, *H. pylori* is classified by the World Health Organization as one of the 16-antibiotic resistant bacteria that pose the greatest threat to human health [19]. Overall, there are limited drug options available for *H. pylori* and novel alternative treatments are needed [20, 32]. Also, more specific targeting for this gastric pathogen is required, since the use of broad-spectrum drugs disrupts the balance of the gut microbiota that nowadays is known to play a pivotal role in human health [33].

2.1 Infection by *H. pylori*

H. pylori is a microaerophilic Gram negative bacterium (Figure 2.1) found in the human gastric mucosa [13]. It has a spiral shaped body (2.4-4.0 μm long and 0.5-1.0 μm wide) with four to six unipolar flagella allowing its mobility [34]. This morphology is associated with the gastric infection [35]. The spiral shape and the flagella enable the stomach protective lining penetration (the mucus layer covering the gastric epithelial cells) in a cork screw motion that, in association with the release of cytokines and chronic inflammatory process, lead to disease development [16, 36]. When the environmental conditions are unfavourable for survival and growth, *H. pylori* has the ability to enter the coccoid form, a viable but not cultivable state [37].

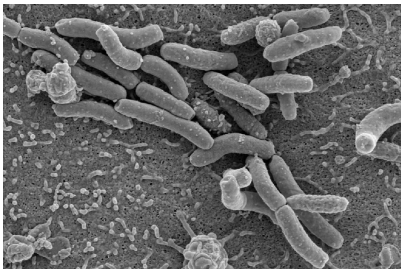


Figure 2.1: Scanning electron micrograph of *H. pylori* (from [1]).

Persistent gastric infection by this pathogen accounts for 90% of the global non-cardia cancer burden, the 5th most common and 3rd deadliest cancer worldwide [15]. The majority of individuals infected with *H. pylori* are asymptomatic, which contributes to the delayed diagnosis of gastric cancer. This is often identified only when it has progressed to advanced stages, reflecting poor prognosis and low patient survival rates [38]. *H. pylori* eradication is now being recommended to reduce the risk of cancer development and other diseases [39]. The main symptoms reported by the symptomatic individuals are heartburn, dyspepsia, nausea, vomiting or halitosis. Those subjects who present erosive gastritis or ulcers may also suffer from hematemesis or melena [40].

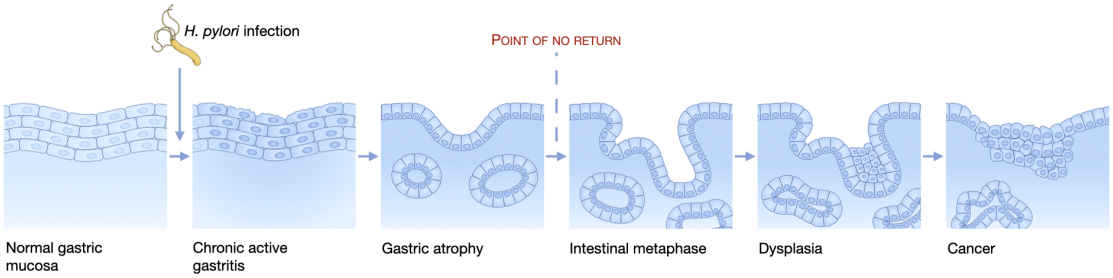


Figure 2.2: **Correa's cascade:** model for the development of gastric cancer triggered by *H. pylori*. The point of no return marks the point of irreversible genetic alterations (adapted from [2]).

Correa *et al.* (1992) described a cascade of events triggered by *H. pylori* (Correa's cascade, Figure 2.2) that culminate in gastric carcinogenesis as a result of a variety of mutations [2]. This cascade begins with a superficial chronic gastritis that evolves to gastric atrophy and achlorhydria. This is followed by gastric intestinal metaplasia, dysplasia and lastly gastric carcinoma [41].

2.1.1 Worldwide prevalence - The world conqueror

H. pylori infects 4.4 billion people worldwide, being considered one of the most successful human pathogens [42]. However, *H. pylori* prevalence is not uniform around the world [3]. Rates of infection are higher in Africa (79.1%), Latin America (63.4%), and Asia (54.7%), while lowest rates are reported in Northern America (37.1%) and Oceania (24.4%) [3]. Figure 2.3 illustrates *H. pylori* global geographic prevalence.

Countries with higher socioeconomic status, better hygiene conditions and less household overcrowding are thought to have a vital contribution for lower *H. pylori* prevalence [43], while in less developed countries the lack of clean drinking water, inadequate handling of food and lack of adequate disposal of wastewater contributes to higher infection rates [44].

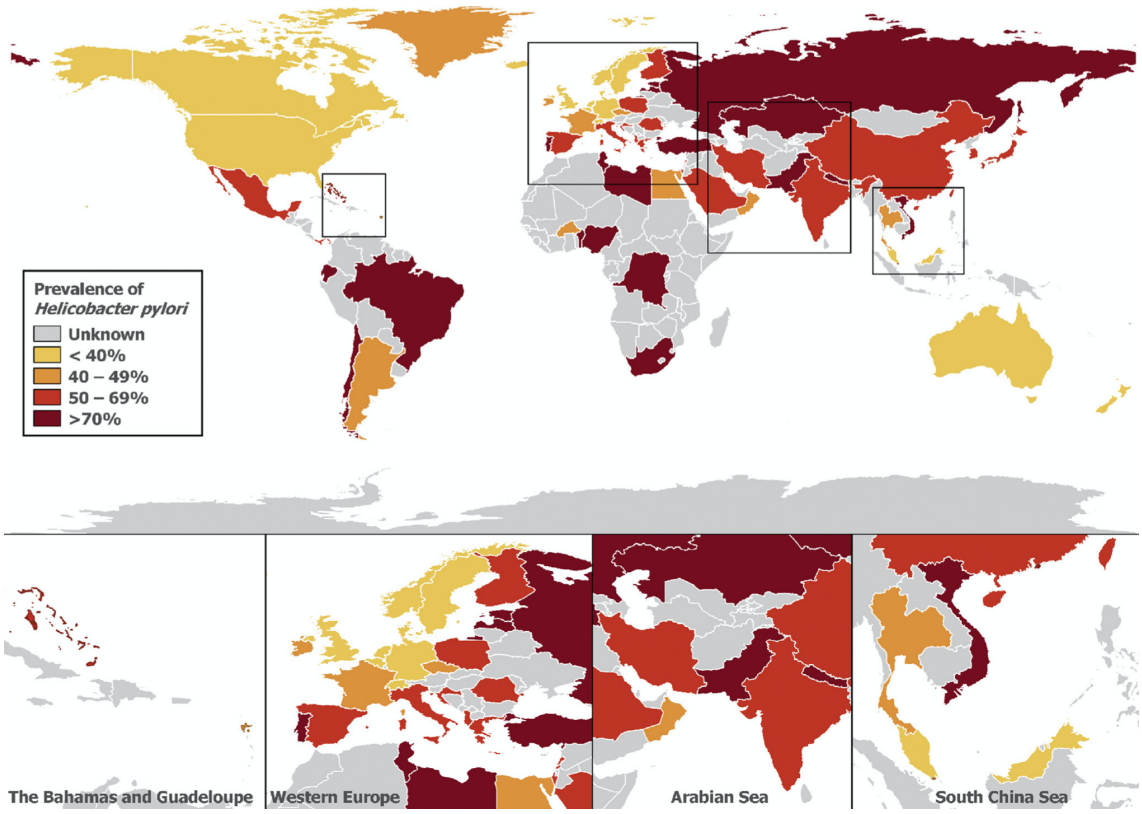


Figure 2.3: *H. pylori* global geographic prevalence (adapted from [3]).

Portugal has the highest mortality rates for gastric cancer in Western Europe as well as the highest incidence of *H. pylori* infection [45]. The infection prevalence is 66.2% at children of 13 years old [46] and 84.2% in adults [47].

2.1.2 Transmission

Infection by *H. pylori* is usually acquired in early childhood and commonly persists for life [40]. The most common transmission route to the host occurs from person-to-person, via oral-oral

and/or oral-faecal routes. Water and food can also be a possible transmission vehicle mainly due to poor hygienic conditions [48]. Figure 2.4 summarizes possible transmission routes for *H. pylori*.

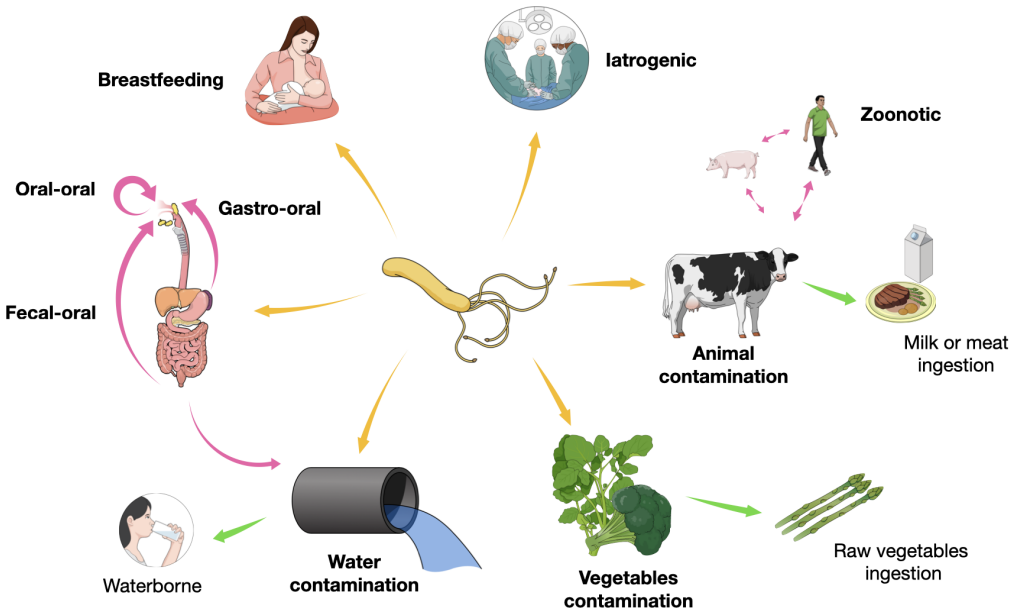


Figure 2.4: Suggested *H. pylori* transmission routes (adapted from [4]).

2.1.3 Morphology, Colonization & Virulence factors

The mucosal surface, represented in Figure 2.5 a), acts as a barrier of defense against pathogens. In order to cause disease, they need to disrupt or penetrate it. In gastric settings, bacteria have initial contact with a highly hydrated mucus gel that covers the gastric mucosal surface. This mucus gel protects the epithelial cells against chemical, enzymatic, microbial and mechanical attacks [5]. This hydrated gel is a combination of high-molecular-mass oligomeric glycoproteins (mucins) with reinforced defense factors as lysozyme, defensins, Secretory IgA, among others. The existence of a firmly and a loosely adherent mucins layer is thought to be explained by differences in its concentration. Going deeper into the mucosal surface, the pathogen encounters a dense surface of highly diverse glycoproteins and glycolipids (glycocalyxes) attached to the epithelial cells membrane. These glycolalyxes have an average renewal time of 6-12 hours, renewing continuously the mucosal surface [5]. The mucus layer above epithelial cells acts as a barrier for large molecules but also promotes a static environment. This static environment is important by hindering protons diffusion, as H^+ ions from gastric acid and bicarbonate (HCO_3^-) released by epithelial cells, causing a pH range in the mucus layer (Figure 2.5 b)) [5]. In this sense, epithelial cells keep a favourable neutral pH as the gastric space keeps an acid pH of 1-3 [5].

In its majority, *H. pylori* is found in the mucus (about 80%) or adhered to gastric epithelial cells

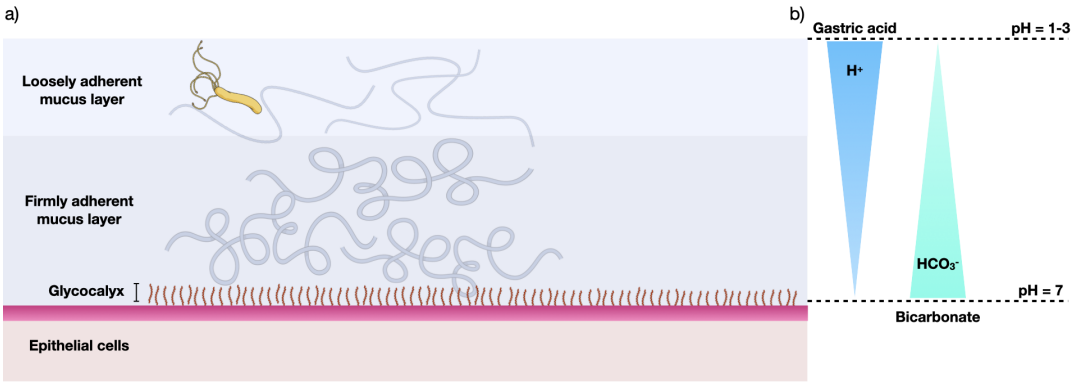


Figure 2.5: a) Gastric mucosal surface; b) pH gradient on the gastric mucus layer (adapted from [5]).

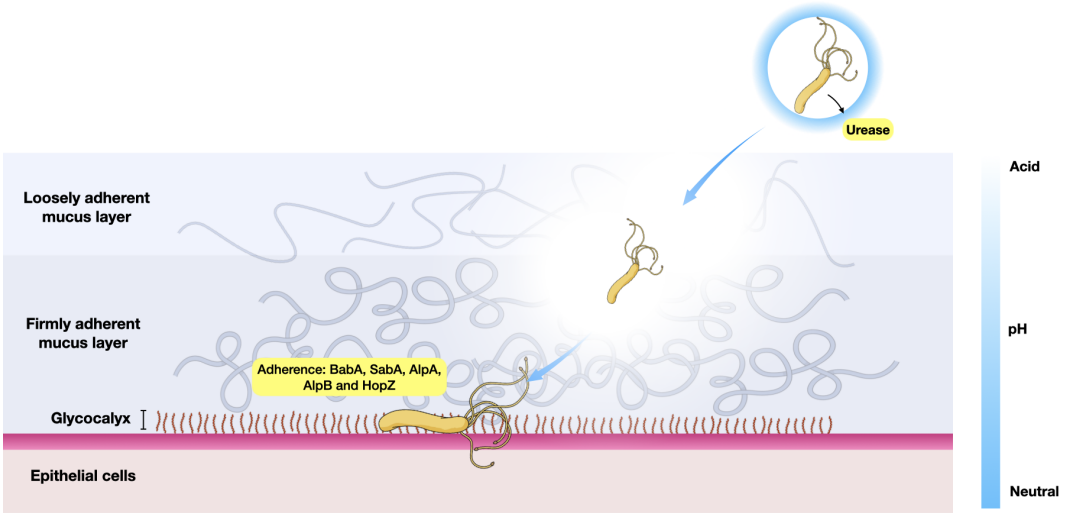


Figure 2.6: Colonization of gastric mucus layer and adherence on gastric epithelial cells by *H. pylori* (adapted from [6]).

[49]. Besides its spiral shape and flagella that help it to penetrate the gastric mucus layer, *H. pylori* developed mechanisms that allow its survival in the harsh acidic conditions of the human stomach, namely its ability to regulate urease production, an enzyme that hydrolyses urea to ammonia [6, 50]. Urea enters into the bacterium through proton-gated urea channel UreI located in the inner membrane. UreI opens at pH = 5, allowing urea to enter the bacterium and closes at pH = 7. This channel only permits urea to enter in acidic conditions to hinder lethal alkalization [50]. This reversion of pH in the bacterium surrounding also reduces the viscoelasticity of the highly hydrated mucus gel surface turning it more permeable, thus enabling *H. pylori* to penetrate it (Figure 2.6) [5, 51]. *H. pylori* attachment to gastric epithelial cells is enabled by the presence of outer membrane proteins as Blood group antigen binding Adhesin (BabA), Sialic acid-binding Adhesin (SabA), adherence-associated lipoprotein A and B (AlpA and AlpB) and *Helicobacter* outer membrane protein Z (HopZ) [6]. *H. pylori* adherence to gastric epithelial cells results in activation of numerous signalling pathways and allows efficient delivery of toxins or other effector

molecules into the cells.

Even though *H. pylori* is associated as an extracellular invader, Chu *et al.* (2010) showed that *H. pylori* could invade and replicate inside epithelial cells and, in this sense, be considered a facultative intracellular pathogen. In Atypical Glandular cells (AGS) human gastric cancer line and MKN45 epithelial cell lines, the number of colony-forming units (CFUs) of the invading bacteria increased over time, showing it can replicate in cells [52]. *H. pylori* is thought to invade the epithelial cells (Figure 2.7) when the outside environment becomes unfavourable [53]. The entrance of *H. pylori* into the host cells is made by a zipper-like mechanism, i.e. *H. pylori* induces the formation of pseudopod structures on the cells membrane that, after some time, "zipps" along *H. pylori* length [54]. Inside the cell, *H. pylori* is able to replicate either attached to cellular membrane or in the cytoplasm bulk (Figure 2.7). Regarding the cellular membrane as a replicative niche, *H. pylori* can freely detach from the membrane and be released into the extracellular space at any point [52]. On the other hand, replication in the cytoplasm bulk initiates with *H. pylori* located on the periplasmic membrane and then, as infection proceeds, it gradually migrates into the cytoplasm. The migration occurs in double-layer membrane vesicles (the autophagosome) and the bacterium replicates in it. As infection carries on, lysosomes fuse with the vesicles to digest the bacteria. After the external conditions become desirable, *H. pylori* can be released for further recolonization [53].

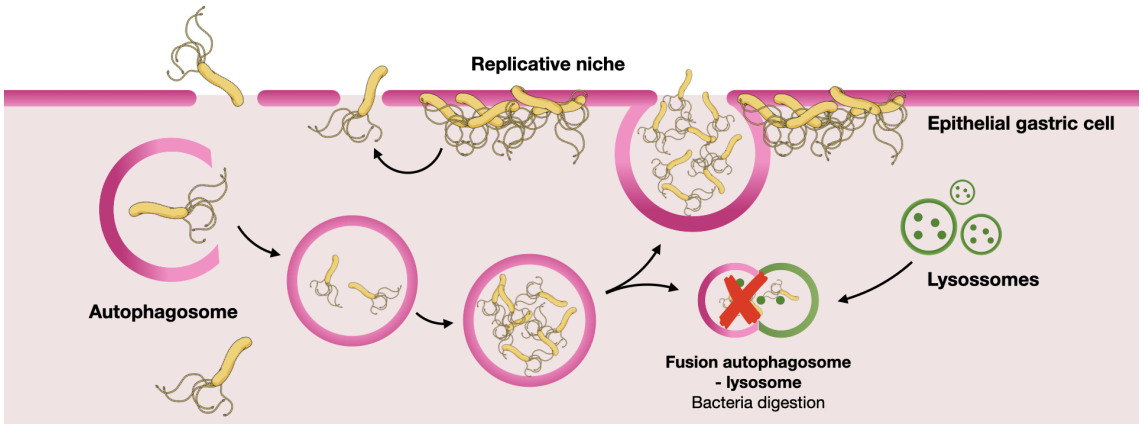


Figure 2.7: Model of intracellular colonization by *H. pylori*.

Other studies showed *H. pylori* is also capable of replicate inside macrophages and dendritic cells [55, 56]. However, the intracellular replication of this gastric pathogen is not completely established and still is a matter of divergence in the scientific community.

2.1.3.1 Cytotoxin-associated A (CagA) & Vacuolating cytotoxin A (VacA) proteins

H. pylori possesses the *cagA* gene, a specific gene for human gastric infection, which is associated with increased risk of peptic ulcer disease and gastric cancer [34, 57, 58, 59]. The *cag* pathogenicity island (*cag*PAI) contains six genes that are responsible for encoding a type IV secretion system

(T4SS). T4SS, a hallow conduit, translocates CagA protein into the host cells [50, 60], leading to the activation of cell signalling transduction pathways [4]. Once in the host gastric cell cytoplasm, CagA impairs cell signalling by affecting cell-cell junction, cytoskeleton, spreading and migration of the cell. CagA can also stimulate secretion of Interleukin-8 (IL-8), a proinflammatory cytokine. Besides local cell effects, CagA also has widespread cellular effects as a cellular emergency response (proinflammatory cytokines and β-defensins) [50, 60].

All *H. pylori* strains have the *vacA* gene that encodes the VacA protein. VacA is specially adapted to the human stomach, being activated by acid and resistant to acid and pepsin degradation. VacA increases the pathogenic advantage of *H. pylori* by producing pores in the cell membranes that are capable to efflux metabolic substrates for bacterial growth and bicarbonate and anions into the host cytoplasm [60]. VacA is also responsible for the formation of vacuoles, increasing permeability, cytoskeleton changes and inducing apoptosis [61]. As CagA, this protein also induces acute inflammation by the release of IL-8.
Figure 2.8 schematically shows CagA and VacA entry mode on epithelial gastric cells and effects.

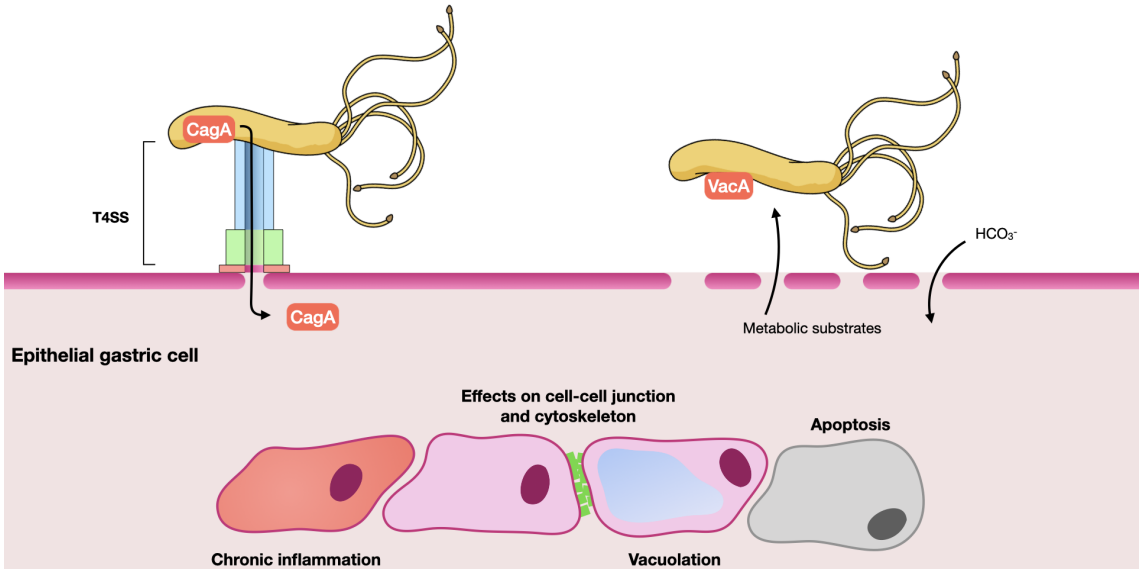


Figure 2.8: Translocation of CagA and VacA from *H. pylori* to epithelial gastric cells and cellular effects.

2.1.4 Human immune system vs. *H. pylori* (the devil in disguise)

Although *H. pylori* induces a strong inflammatory state, it has developed several mechanisms to minimize the host immune responses, important for chronic infection and persistent colonization [62].
The continued secretion of IL-8, from CagA and VacA, functions as an activator of the innate immune system. *H. pylori* also stimulates cell-mediated immune responses, responsible for the eradication of bacteria and clearance of disease. The immune response to *H. pylori* is mainly Type

1 T helper cells (Th1) and, therefore, linked to proinflammatory cytokine release and macrophage activation. High Th1 responses are associated with aggravated gastritis and peptic ulcers but reduced bacterial numbers. However, CagA and VacA are also responsible for the decrease in T cells activation and thus Th1 response [60].
Another human defense mechanism is the production of human β-defensin 3, (hβD3) an antimicrobial peptide (AMP), produced by the gastric epithelial cells and capable of killing *H. pylori* [63, 64]. However, CagA production inhibits hβD3 and therefore increases *H. pylori* survival rate [63].
The immune system recognizes bacteria for the presence of membrane structures such as lipopolysaccharides (LPS), flagellin and bacterial nucleic acids [17]. LPS is a proinflammatory glycolipid found on the membrane of Gram negative bacteria that is composed by three structures: a lipid A, responsible for toxic effects; a core oligosaccharide; and O-antigen, exposed to the extracellular space. However, *H. pylori* is capable to evade the immune recognition system by adapting its LPS to a less proinflammatory state [6]. It is able to modify the lipid A and expression of Lewis antigens on O-antigen to structures that resemble human Lewis antigens and related blood groups antigens. In this sense, O-antigen is not detected as an intrusive molecule but comparatively as a "self"-antigen, "neutralizing" the host immune system [17].

2.2 Current treatments for *H. pylori*

Due to the high incidence of *H. pylori* worldwide, antibiotic-based treatments began to appear, which were popular and effective [65]. However, eradication of *H. pylori* has become more and more challenging, mainly because of the increasing antibiotic resistance rates [19]. Figure 2.9 shows the most common lines of therapies for *H.pylori*. In the beginning of the 21st century, the

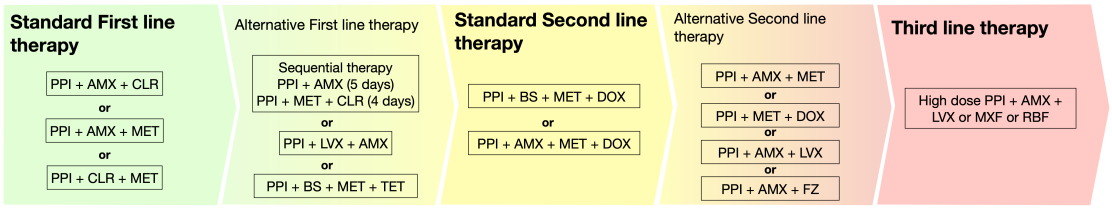


Figure 2.9: Treatment regimens employed for *H. pylori* eradication. Tetracycline (TET), doxycycline (DOX), furazolidone (FZ), moxifloxacin (MXF) and rifabutin (RFB) (adapted from [7]).

European Guidelines on the management of *H. pylori* recommended a triple therapy composed of two antibiotics: clarithromycin (CLA) and amoxicillin (AMX) or metronidazole (MET); plus a proton pump inhibitor (PPI) as first line of therapy [66]. Another triple therapy with similar efficacy results was the bismuth therapy consisting in taking ranitidine bismuth citrate together with two antibiotics: CLA or AMX or MET [67]. However, bismuth salts (BS) are not allowed in some European countries due to their potential neurotoxic effects [7]. There are other first line therapies, such as the sequential treatment, which consists in the uptaking of a PPI with AMX followed by five days of PPI and CLA and nitroimidazole; the quadruple therapy that comprises

a PPI plus three antibiotics in a concomitant regimen; and a Levofloxacin (LEV) based therapy, with similar effectiveness to the standard triple therapy. LEV can also be used in a triple therapy regime with a PPI and one antibiotic [68, 69, 70].
Some studies suggest that the addition of probiotics could improve the eradication rates of the current treatments, as they may be able to reduce the antibiotic associated side effects and, therefore, improve compliance [21, 71].
In recent years, already three authorities have issued treatment guidelines: the Canadian Association of Gastroenterology/Canadian *Helicobacter* Study Group [72], the American College of Gastroenterology [73] and the European *Helicobacter* and Microbiota Study Group (Maastricht V/Florence report) [39]. Large clinical trials and meta-analyses set the failure of standardized therapeutic treatments in approximately 20–30% of patients, also showing it might be higher in the clinical environment [74]. There are several factors that account for this scenario:

(a) **Bacterial factors**
During chronic infection *H. pylori* appears to have high mutation rates (10^5 mutations/site/year) encoding faster outer membrane proteins than other functional groups [75]. Also, as infection is multi-strain, one treatment may affect a specific strain but not another due to variations in antibiotic susceptibility [76].

(b) **Antibiotics**
The over consumption of antibiotics in the medical and veterinary fields are responsible for the increasing antibiotic resistance in a great number of bacteria worldwide [77]. Figure 2.10 shows worldwide resistance distribution of CLA, LEV and MET, common antibiotics used for *H. pylori* treatment.
Also, given that the gastric mucus layer serves as a protective barrier, the antibiotics cannot easily reach the surface of the gastric epithelial cells where *H. pylori* is adhered [78]. To eradicate possible intracellular *H. pylori* cells, it is recommended that cell membrane penetrating antibiotics, such as CLA and MET, capable of diffusing through gastric cell membranes and reach *H. pylori* are used [53].
Moreover, with pH varying from 2 near the stomach's lumen to 5.5 and higher on the cell-mucus interface, only few antibiotics are capable to be active in both extreme pHs [76]. The low pH value in the stomach also accelerates the degradation of antibiotics such as AMX and CLA [79].

(c) **Patient**
The complicated protocol of the treatment regimes, involving multiple drug combinations in different times of the day conjugated with adverse side effects, e.g. diarrhea from dysbiosis, boost the lack of patient compliance [19]. Patient life style, as coffee ingestion or smoking may also contribute to treatment failure [4].

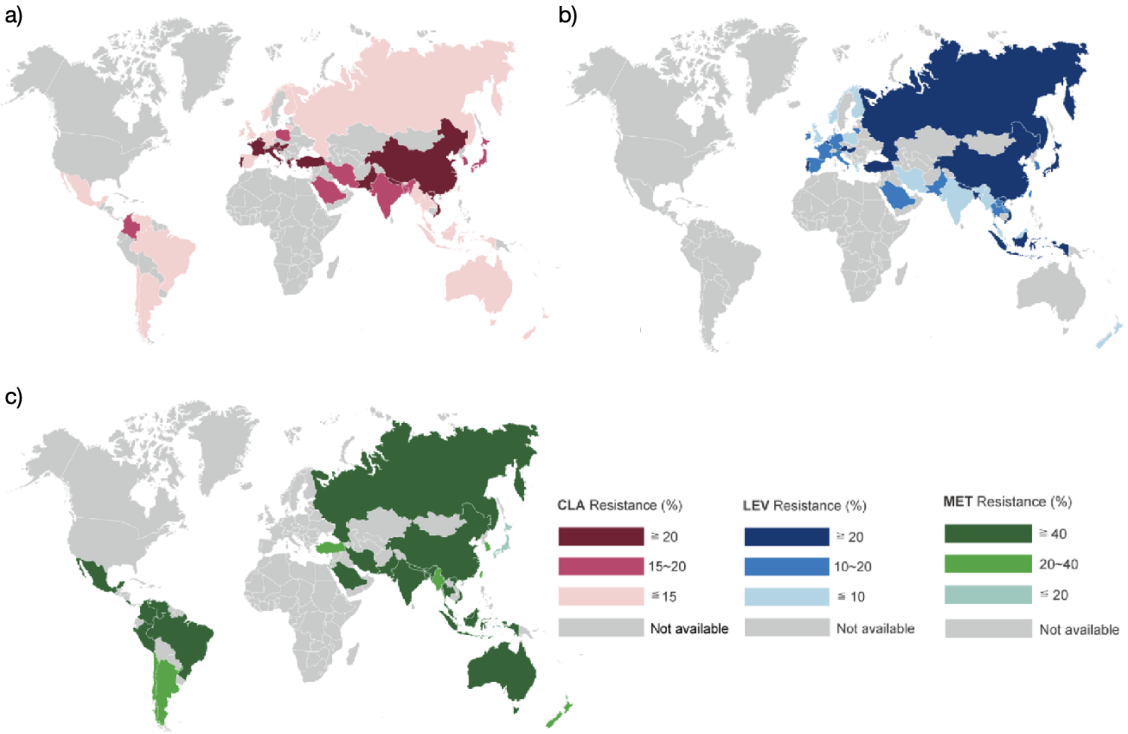


Figure 2.10: Prevalence of a) CLA; b) LEV and c) MET resistance (adapted from [8]).

2.3 Alternative treatments

Overall, there are limited drug options available for *H. pylori* and, with the increasing antimicrobial resistance, alternatives are needed [20, 21]. The use of potent acid suppression with potassium-competitive acid blockers (PCABs) substituting the usage of PPIs, has revealed to improve CLA base triple therapy with 10-20% higher eradication rates [80]. The same happens with AMX therapies [81]. Due to the more potent acid suppressive effect, CLA and AMX have a slight increase on their effectiveness against *H. pylori* [21].

Another alternative strategy being developed is a vaccine [18]. Vaccines would prevent the problem of increasing antibiotic resistance but would also protect the patient from reinfection [21, 82]. *In vivo* studies showed promising results but when translated to clinical settings the results were disappointing [83, 84]. Phytotherapy also demonstrated potential against *H. pylori* but to date no pre-clinical studies were yet reported [16].

Bioengineering has also been used within the scope of novel treatments. This will be discussed in more detail in Chapter 3 but, as an example, chitosan microspheres, lipid nanoparticles and surface grafted AMPs have been explored as alternatives [85, 86, 87, 88].

2.4 *H. pylori* and Cholesterol - A love story and a new Target

Exogenous cholesterol assimilation is an unique biological characteristic of this gastric pathogen. Cholesterol assimilation into the cell membranes is essential not only for *H. pylori* survival, but also for resistance acquisition against antibacterial compounds [10, 23].

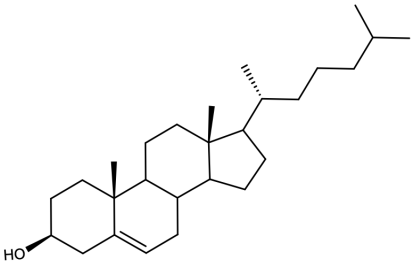


Figure 2.11: Cholesterol molecule.

Cholesterol (Figure 2.11) is a lipid found in the plasmatic membranes of the cells, composed by a hydrophilic and a hydrophobic region. Its hydrophilic group is placed between the phospholipid heads, while the hydrophobic portion is located in-between the phospholipids hydrophobic region, as shown in Figure 2.12. The amount of cholesterol in the membrane controls the membranes fluidity and therefore its functionality [22]. In the stomach, cholesterol is bound to mucins and in epithelial cell membranes, forming cholesterol-rich microdomains (lipid rafts) [89].

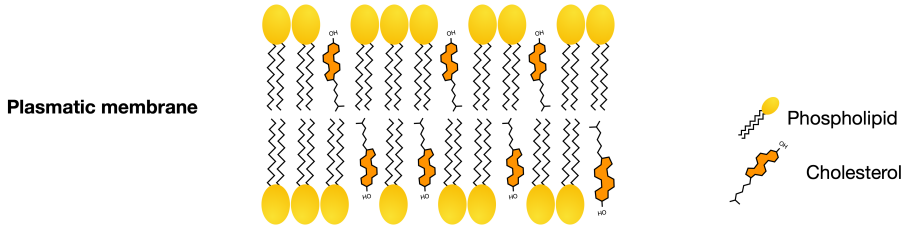


Figure 2.12: Cholesterol placement in the cellular plasmatic membrane.

The inability of *H. pylori* to synthesize cholesterol, crucial to its survival, leads the bacterium to acquire it from the host [23].
Wunder *et al.* (2006) showed that the *H. pylori* P12 strain has the ability to follow a cholesterol gradient, sensing cholesterol as low as 250 μM in the environment and moving along increasing concentrations of cholesterol. In an attempt to comprehend how *H. pylori* acquires this lipid, NBD-cholesterol (marked cholesterol) was introduced in AGS cell line and then these cells were infected with *H. pylori*. This assay, besides showing that the bacteria is time dependent in cholesterol assimilation, also demonstrated that *H. pylori* acquires the lipid from the plasmatic membrane of the AGS cells and not from free secreted cholesterol in the supernatant of those same cells [23].

2.4.1 Cholesterol recognition

The recognition and uptake mechanism of cholesterol by *H. pylori* is explained by the presence of phosphatidylethanolamine (PE), the most common glycerophospholipid in cell membranes of Gram negative bacteria [9]. However, PE molecular species in *H. pylori*, more specifically dimyristoyl-PE (DMPE), differ from the typical Gram negative ones. While *Escherichia coli* (*E. coli*), *Klebsiella pneumoniae* (*K. pneumoniae*) and *Pseudomonas aeruginosa* (*P. aeruginosa*) possess a palmitic acid of 16 carbons ($C_{16:0}$), *H. pylori* has a myristic acid of 14 carbons as the saturated fatty acid ($C_{14:0}$) attached to PE (Figure 2.13) [9]. Shimomura *et al.* (2012) conducted an

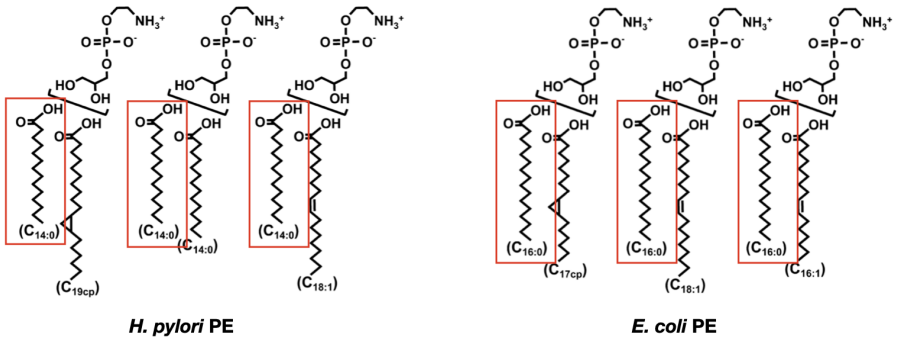


Figure 2.13: Predominant PE molecular species of *H. pylori* and *E. coli*. Saturated fatty acids highlighted in red (adapted from [9]).

experiment to understand if $C_{14:0}$ attached to PE is responsible for the *H. pylori* selective binding to cholesterol. PE-$C_{14:0}$, or DMPE, was incubated with both cholesterol and cholesterol ester in paper disks. The results showed that DMPE interacts selectively with cholesterol, while the binding of cholesterol ester to DMPE did not occur, concluding that DMPE plays an important role in the selective binding of cholesterol. In the same study, it was established that 2,6-di-O-methyl-β-cyclodextrin (dMβD) enhances cholesterol absorption by *H. pylori* and elutes DMPE from the dead bacteria. When *H. pylori* dead cells were incubated with dMβD, the amount of DMPE was exceptionally low when compared with the absence of dMβD. Altogether, since dMβD establishes more contact with the outer layer of the pathogen, the authors concluded that there are large amounts of DMPE in this outer layer [9].

2.4.2 Cholesterol "digestion" - Glycosylation

H. pylori has an unique potential to manipulate cellular cholesterol. Cholesterol assimilated by *H. pylori* is modified by α-glucose resulting in cholesteryl glycoside (cholesterol glycosylation). This cholesteryl glycoside is used as an *H. pylori* cell membrane constituent. *H. pylori* has at least three different types of cholesteryl glucoside:

- cholesteryl-α-D-glucopyranoside (CGL)
- cholesteryl-6-O-tetradecanoyl-α-D-glucopyranoside (CAG)
- cholesteryl-6-O-phosphatidyl-α-D-glucopyranoside (CPG)

CGL is synthesized by the action of α-glucosyltransferase (CGT), the key cholesterol enzyme. For the synthesis of CAG and CPG it is known that PE is used as a substrate for their synthesis. CAG results by a transfer of a fatty acid derived from PE to CGL by CGL acyltransferase (CGLAT). On the other hand, CPG is a result of a phosphatidyl group derived from PE to CGL by CGL phosphatidyltransferase (CGLPT) [10].
Figure 2.14 schematically represents these processes.

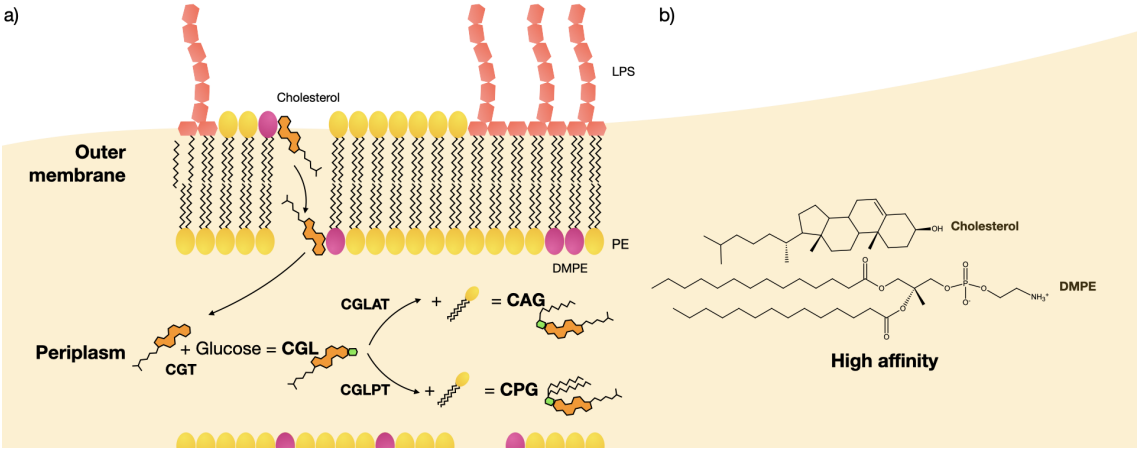


Figure 2.14: a) Cholesterol uptake and processes inside *H. pylori*; b) Cholesterol and DMPE affinity (adapted from [10]).

The disruption of CGT compromises cholesterol modifications and thus the synthesis of all cholesterol glucosides [90]. Wunder *et al.* (2006) also demonstrated that mice infected with disrupted CGT *H. pylori* type were unable to colonize the mice stomach [23].

Lipid rafts in eukaryotic cells are used as structures for various cellular receptors [91]. Extracting cholesterol from cells causes lipid raft destruction and/or alteration of cell membrane structure, serving as an entry door for *H. pylori* [92, 93]. For example, the take over of this lipid rafts is used to place the T4SS and translocate CagA protein [89].

Cholesterol glycosylation also takes a significant role in defeating immune system surveillance [23]. As previously mentioned, the infection by *H. pylori* induces the release of the proinflammatory cytokine IL-8. However, cholesterol glycosylation by this pathogen hinders T cell-mediated immune response, preventing infected cells to respond to interferon-γ (IFN-γ) and Interleukin-22 (IL-22), among others. Neighbouring cells, nevertheless, still receive these inflammatory responses producing AMPs against *H. pylori*. Therefore, *H. pylori* is able to create protective niches of diminished inflammation, while simultaneously builds a chronic inflammation status in the neighbouring environment [62, 11]. The chronic inflammation model caused by *H. pylori* is resumed in Figure 2.15.

In the same study, Wunder *et al.* (2006) fed mice a cholesterol rich diet and found a decline in

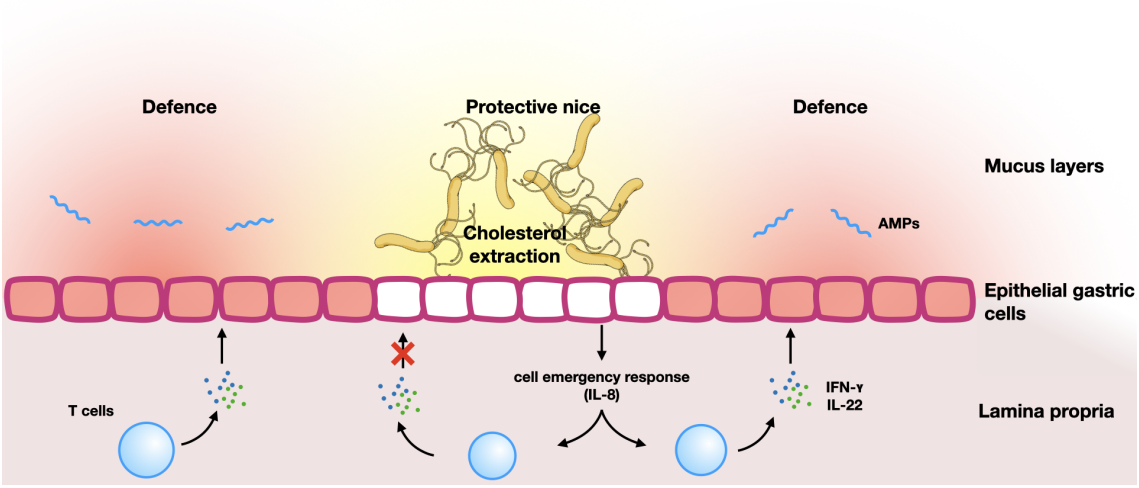


Figure 2.15: Chronic inflammation due to cholesterol glycosylation model (adapted from [11]).

H. pylori colonization when compared to the one obtained on mice on a normal diet. This decline was due the increasing regulation of IFN-γ by Th1 cells [23].

2.4.3 A new Target: taking advantage of uniqueness

As described in the previous sections, cholesterol takes an important role in *H. pylori* metabolism, from specific receptors to recognize it, to protection and structure, being vital for *H. pylori* survival. In this sense, a bioengineered approach, such as nanoparticles with immobilized cholesterol, could be developed as a strategy to deceive *H. pylori*, attracting it and improving its clearance from the host.

Chapter 3

New strategies for *H. pylori* treatment: from proof-of-concept to real-world applications

Proof-of-concept studies are extremely useful to demonstrate the validity of the rational, to better understand the interactions between *H. pylori* and an immobilized lipid (cholesterol) and to optimize the strategy prior to translation onto real-world materials/strategies. Self-assembly is possibly the most effective and versatile strategy for surface functionalization, making Self-Assembled Monolayers extremely useful for these studies.

3.1 Self-Assembled Monolayers - on gold (SAMs)

SAMs are well-defined model surfaces that allow control at the molecular scale [30]. SAMs are very stable, spontaneous molecular assemblies that adsorb from a solution in an orderly manner to a surface [94]. There are several SAMs systems, such as chlorosilanes on silicon, carboxylic acids on metal oxides and organosulfur compounds on gold. However, organosulfur compounds on gold present the highest structural order, ease of preparation and analysis. These SAMs functionality is achieved by choosing the right alkanethiol to the desired application [95]. There are numerous advantages in using SAMs of alkanethiols on gold, namely: gold is a relatively inert metal without oxide surface formation; gold and sulfur bond is highly specific; and alkanethiol chains form a densely packed monolayer on gold [96]. In addition, there are several extremely surface-sensitive techniques that can be used for SAMs characterization. SAMs can be divided in three structures: Gold-Sulfur bond (Au-S) to anchor each thiol to the surface; an alkyl chain, which is used as a spacer and to stabilize the monolayer by van der Waals interactions; and an ending functional group that defines the chemical reactivity of the SAM surface (Figure 3.1) [94].

SAMs have been widely used for studies with proteins, cells and bacteria. Table 3.1 summarizes some biological assays that have used SAMs.

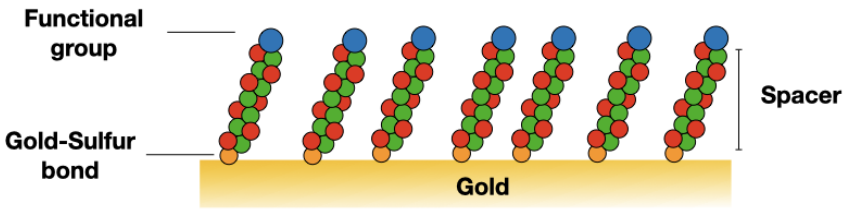


Figure 3.1: Illustration of the main three components of an ordinary thiol-based SAMs (Schematic representation not to scale).

Table 3.1: Biological studies using SAMs.

Rational	**SAMs**	**Reference**
E. coli detection	Streptavidin (protein)	[97]
Adsorption of fibrinogen and lysozyme, adhesion of *Staphylococcus aureus* and *S. epidermidis*, attachment and spreading of Basal Cell Epithelioma (BCE) cell line	Hexadecanethiolate, Hexamethylphosphoramide, Poly(ethylene glycol)$_3$-OH, (and others)	[98]
Albumin adsorption	OH- and CH_3-terminated thiols	[99]
E. coli adhesion	Mixed SAMs of alkanethiolates terminated in oligo(ethylene glycol) groups and in a mannoside ligand	[100]
Neurons patterned growth	Silane-based	[101]
H. pylori adhesion and viability	EG4-, OH- and CH_3-terminated thiols	[102]
H. pylori adhesion and binding specificity	EG4- and biotin-terminated thiols	[103, 104]

3.1.1 *H. pylori* and surface interaction (on SAMs)

As shown in Table 3.1, previous studies were developed concerning *H. pylori* and surface interaction using SAMs. In the study from Parreira *et al.* (2011), adhesion, viability and morphology of several *H. pylori* strains (J99, 17875/Leb and 17875 babA1A2) were evaluated on SAMs with dif-

ferent functional groups: EG4-, CH_3- and OH- on gold. The kinetics of adhesion was also tested, concluding that after 2 hours of incubation with SAMs, bacterial adhesion reaches a plateau. The results of this study highlighted that *H. pylori* tends to adhere preferentially to more hydrophobic surfaces, i.e. CH_3- terminated SAMs. Less bacteria adhered to EG4-SAMs with a significant loss of viability, which was not observed on the other surfaces. In what concerns the morphology, the typical *H. pylori* spiral shape was only observed on the CH_3-SAMs and control group (Tissue Culture Polyethylene) proving to be more favourable for bacteria [102].

3.1.2 SAMs characterization techniques

There are several surface characterization techniques that can be applied on SAMs, namely Ellipsometry, Optical Contact Angle (OCA), X-Ray Photoelectron Spectroscopy (XPS) and Quartz Crystal Microbalance with Dissipation (QCM-D). A short overview on each will be given in the next subsections.

3.1.2.1 Ellipsometry

Ellipsometry is generally used to characterize thin films thickness, in the nanometer range, through measurements in changes of polarization, as light reflects from the surface and the refractive index of the surface [105, 106]. A polarized laser beam is reflected from the surface and the polarization detection made with a compensator/detector couple [107]. Figure 3.2 schematically demonstrates the function mechanism of a typical Ellipsometer apparatus.

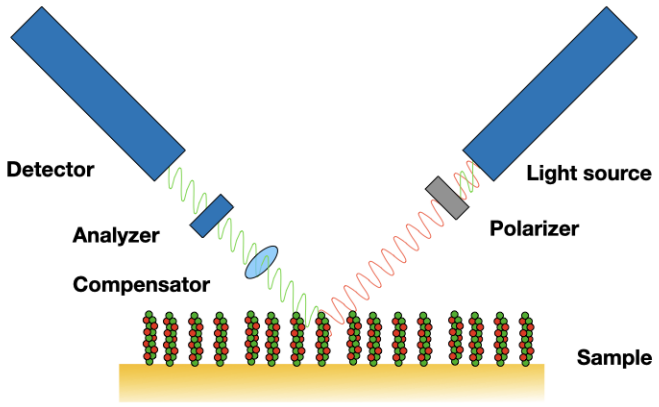


Figure 3.2: Schematic operation principle of Ellipsometry.

3.1.2.2 Optical Contact Angle (OCA)

OCA is used to evaluate the wettability of a solid surface as it describes the morphology of a liquid droplet on the surface under study. In the Sessile drop method, it is defined as the angle θ of the tangent between the solid surface and the liquid droplet. Solid surfaces with $\theta < 90^\circ$ are hydrophilic and with $\theta > 90^\circ$ hydrophobic [108]. Figure 3.3 represents a typical setup of

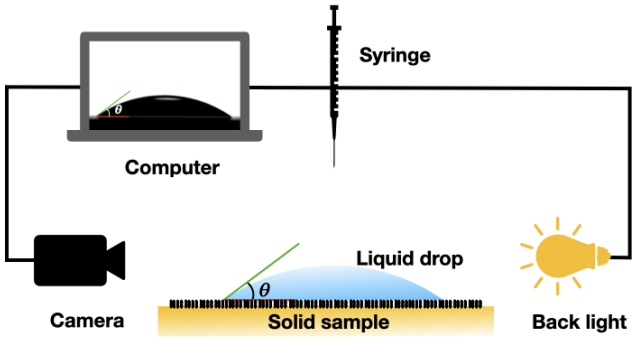


Figure 3.3: Schematic operation principle of OCA.

OCA measurements using the Sessile drop method. Other methods are available depending on the solid-liquid-gas system [108] as shown in Figure 3.4.

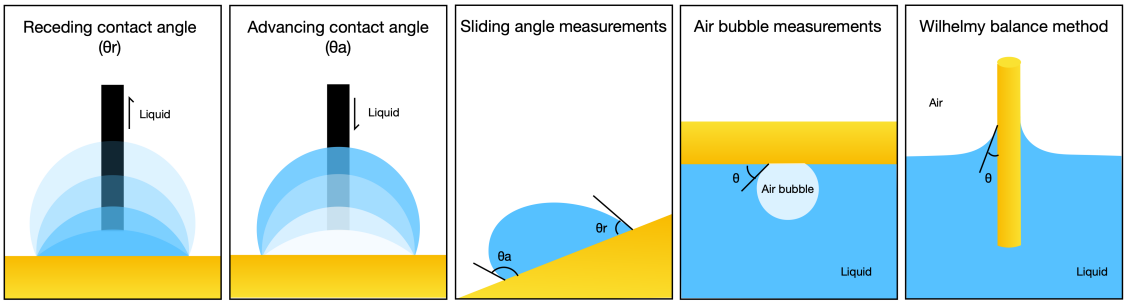


Figure 3.4: OCA methods (θ: Angle of the tangent between the solid surface and the liquid droplet, θr: Receding contact angle, θa: Advancing contact angle).

3.1.2.3 X-Ray Photoelectron Spectroscopy (XPS)

XPS analyses allow inferring the elemental composition of SAMs. In ultra-high vacuum conditions, X-Ray beams irradiate the samples and measurements of the energy (ekV) of the ejected electrons from the inner shell are performed. These energies are specific for each individual chemical element and, consequently, SAMs elemental composition is possible to determine [96]. Figure 3.5 demonstrates the function of a typical XPS apparatus.

3.1.2.4 Quartz Crystal Microbalance with Dissipation (QCM-D)

QCM-D allows measuring changes of mass, in the nanograms range, on surfaces in real time and under controlled conditions of temperature and at a desired flow rate. This technique is based on the oscillation of a piezoelectric quartz crystal at specific resonance frequencies (Figure 3.6). Changes in the resonance frequency result in ultra-sensitive determinations of absorbed or desorbed mass that can be quantified [107]. QCM-D also gives information on the viscoelastic properties of the adsorbed molecules, as it simultaneously measures the frequency and energy

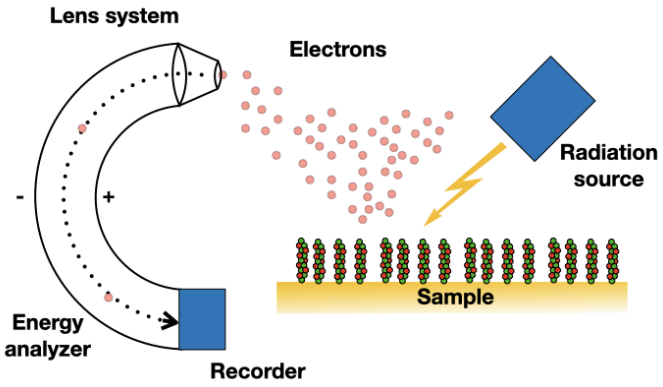


Figure 3.5: Schematic operation principle of XPS.

dissipation. If the adsorbed mass is viscous and soft, it won't synchronize to the sensor oscillation leading to dissipation [109]. The Sauerbrey equation (Equation 3.1) or Voigt model (Equation 3.2) can be used to estimate the adsorbed mass on the sensor, depending on the dissipation values [110]:

$$\Delta m = \frac{\Delta f}{n} C \tag{3.1}$$

$$G^* = G' + i'' = \mu_1 + i2\pi f \eta_1 \tag{3.2}$$

where from Equation 3.1, Δm represents the adsorbed mass per unit surface, Δf the frequency shift, C the mass sensitivity and n the overtone number. From Equation 3.2, G^* is the complex shear modulus, G' the storage modulus and G'' is the loss modulus [110].

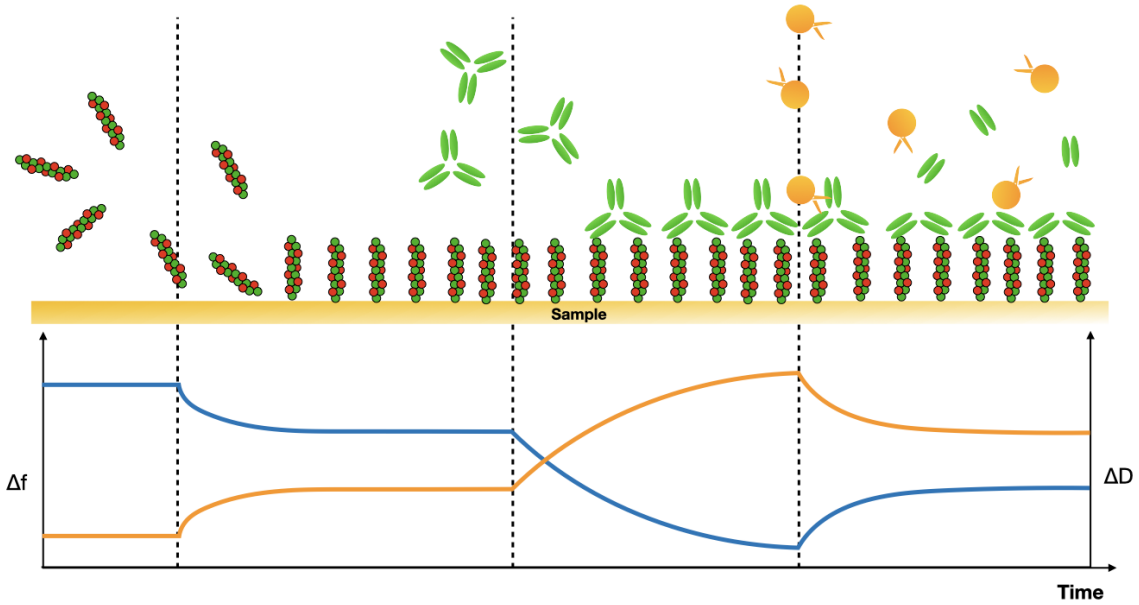


Figure 3.6: Schematic operation principle of QCM-D. Frequency of vibration shift (Δf) represented in blue and Dissipation shift (ΔD) represented in orange.

3.2 Real-world application - Gold Nanoparticles (Au-NPs)

After the proof-of-concept studies, the obtained knowledge may be translated to a bio-applicable approach as, for example, Nanoparticles (NPs).
NPs with attached biomolecules have attracted much interest specially for bringing new applications to biological systems [111]. In particular, Gold nanoparticles (Au-NPs) have been used as tools for diagnostic and therapies, including biosensors applications, target delivery of anticancer drugs, bioimaging for cells and tissues and immunoassays [112].

Au-NPs possess a variety of properties that make them interesting for biological applications: they are chemically very stable; allow controlling size during fabrication; are easily surface functionalized with amines or thiols and gold is highly biocompatible [113].
Typically, the Au-NPs core is produced using a reducing agent in gold salts, as Gold Chloride ($AuCl_3$). This leads to the nucleation of the gold ions to NPs.
To increase NPs stability, a charged surfactant is linked to the gold surface to prevent NPs aggregation, thus being colloidally stable [114]. In aqueous solutions, citric acid can be used to first induce nucleation and second to provide the colloidal stability by adsorption of its negative charges to gold surface. In organic solvents/solutions, however, the reducing and stabilizing agent must be different. Usually the stabilizing agent is based on hydrophobic alkane chains on the Au-NPs surface for the colloidal stability [114].

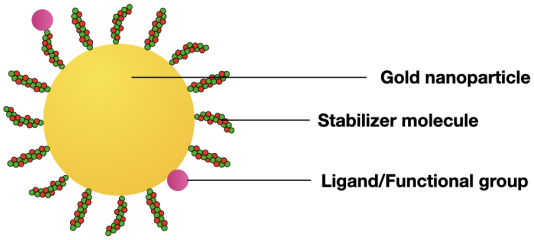


Figure 3.7: Schematic representation of Au-NPs (Not to scale).

Alkanethiols can easily replace stabilizer molecules after Au-NPs are produced [114]. The anchoring of these thiols moieties on Au-NPs is due to the formation of the Au-S bond, similar to what occurs in planar surfaces (Section 3.1) [115]. This exchange allows transferring Au-NPs from aqueous solution to organic solvents and *vice versa*, by switching hydrophilic to hydrophobic molecules, as cholesterol. Also, this allows controlling the surface properties of Au-NPs.
Poly(ethylene glycol) (PEG) is commonly used as a stabilizer, providing colloidal stability for steric reasons, while it also reduces adsorption of particles and other (bio)molecules (non-fouling behaviour). Biological molecules can also be used for Au-NPs surface covering, either directly to the Au-NPs surface with a terminal-functional group as thiols, or linked to the stabilizer molecules by bioconjugate chemistry [114].

3.2.1 Nanoparticles against Bacteria

NPs have been widely explored in the quest for controlling bacterial infections. With simple NPs or with surfactants, these NPs have proven to be efficient for killing Gram positive and negative bacteria (Table 3.2).

Table 3.2: Studies using NPs for bacterial infections.

Bacteria		Nanoparticles	Reference
Gram positive	*S. aureus*	Chitosan and Copper-loaded Chitosan	[116]
	Bacillus Calmette-Guérin	Gold and Silver	[117]
Gram negative	*E. coli*	Silver	[118]
	E. coli, *Salmonella choleraesuis*, *S. typhimurium*	Chitosan and Copper-loaded Chitosan	[116]
	E. coli and *Pseudomonas aeruginosa*	Gold (Pyrimidine-capped Gold NPs)	[119]
	E. coli	Gold and Silver	[117]
	H. pylori	Chitosan/Heparin	[120]
	H. pylori	Lipid NPs	[87]
	H. pylori	AGS epithelial membrane-coated NPs	[121]

When compared to other bacteria, fewer studies using NPs against *H. pylori* were found. Also, studies using NPs as decoys were scarce, as most of the studies report the use of antibiotic-based approaches. In particular, only one study reported the use of NPs as a decoy. Its aim was to attract

H. pylori and avoid colonization of the epithelial gastric cells. For that, Angsantikul *et al.* (2018) coated poly(lactic-co-glycolic acid) polymeric and AMX cores with AGS cells. The authors expected that these NPs could mimic natural pathogen–host binding interactions and, following their administration, *H. pylori* would preferentially bind to them, followed by an antibiotic release on-site. Results showed superior bactericidal effect *in vitro* and reduced *H. pylori* colonization in a mouse model [121].
Very other few studies describing NPs as decoys for other bacteria are reported elsewhere [122, 123], as this strategy has gained interest only over the last few years.

3.2.2 SAMs on Au-NPs

In the sense of a more direct translation of the obtained knowledge from the proof-of-concept studies using SAMs, these can be built on Au-NPs as well. Au-S interface both on curve or plane gold surfaces have a lot of similarities [115]. SAMs on Au-NPs can be correlated and are representative of SAMs on flat surfaces, since the NPs surface at the nanoscale mirrors locally the flat surface, granting the same stability and functionality [124, 125]. A previous report from Badia *et al.* (1996), which performed kinetic and thermodynamics studies, concluded that SAMs on Au-NPs have a large surface area similar to SAMs on planar gold surfaces [126]. Therefore, Au-NPs allows using the same alkanethiols (with the same functional group) previously tested. Although using the same functional group and taking advantage of the same nano-surface chemistry, building SAMs on Au-NPs may require the careful evaluation of some aspects. SAMs on Au-NPs need to be as robust and densely packed as SAMs on flat surfaces while remaining colloidal disperse [125]. This can be achieved using the Brust-Schiffrin method [127]. In this method, $AuCl_3$ is transferred to an organic phase using tetraoctylammonium bromide as the phase-transfer agent and then the gold salts are reduced by sodium borohydride with the alkanethiols. The change of color from orange to deep brown confirms the formation of the Au-NPs [127]. Also, the change in geometry of the gold surface, from planar to spherical, must be taken into consideration. Because of the NPs curvature, the alkanethiols chains have more free volume/space to move even if they are densely packed [128]. Figure 3.8 compares the free space of the alkanethiols chains to move on planar and curved surfaces.

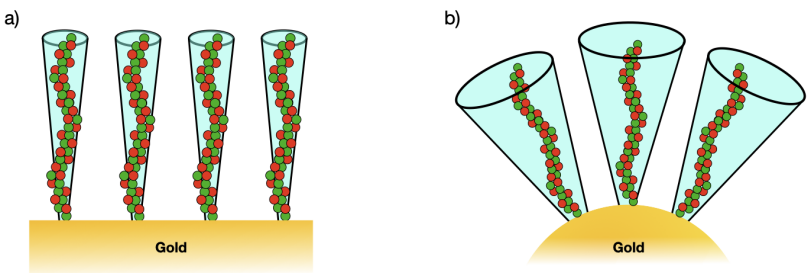


Figure 3.8: Schematic representation of SAMs on a) planar and b) curved surface. Blue cones represent free volume of the alkanethiols chains to move.

Another important aspect is the chain length. As the chain increases length, thiols density decreases. A mixture of thiols with different chain lengths can also supply extra volume for the longer thiols to bend over shorter thiols [128].

3.2.3 Biocompatibility of Au-NPs

With the great deal of variables in NPs optimization, such as their physic-chemical properties (size, shape, coating, surface functional groups, uptake, metabolism, degradation, ...) and the use of different cell types, there was an increase in mismatching data and conclusions about Au-NPs cytotoxicity over the literature [129].
In what concerns size, as particles become smaller, their surface area to volume ratio increases meaning an increased contact area to external or internal cellular components. These NPs are also capable to arrive at intracellular locations as the nucleus, being considered less biocompatible than bigger NPs [112, 130].
A study performed by Chuang *et al.* (2013), using several mammalian cell lines (AGS human gastric adenocarcinoma cells, A549 human lung adenocarcinoma epithelial, NIH3t3 mouse embryonic fibroblast, PK-15 porcine kidney, Vero African green monkey kidney and MRC5 human normal lung tissue), showed that Au-NPs cytotoxicity is related to the cellular context and not only directly to the Au-NPs size or cellular uptake. For example, AGS cells are more sensible to Au-NPs than A549 cells [112].
On the other hand, Penders *et al.* (2017) observed no significant cytotoxic effects on nanospheres, nanostars and nanoflowers chapped Au-NPs. The different shaped Au-NPs were incubated with adult Human Dermal Fibroblasts (HDF cell line), with concentrations raging from 0.5 to 1000 μg/ml. The safety of these Au-NPs was evaluated by 3- (4,5- dimethylthiazol - 2- yl) - 5- (3- carboxymethoxyphenyl) - 2- (4- sulfophenyl) - 2H- tetrazolium (MTS) assay and confocal microscopy and showed neither viability impairment or changes in the cell morphology at the concentrations tested [131].
A more recent study showed low cytotoxicity of nanospheres and nanostars chapped Au-NPs in AGS, HeLa and HT29 cell lines when in lower concentrations, with cell viability near 100%. However, nanorods shaped Au-NPs showed increased cytotoxicity in all cell lines, independently of Au-NPs concentration [132].
Therefore, Au-NPs biocompatibility should be accessed using the appropriate settings that match the envisioned application.

3.2.4 Gastric bioavailability & PEG functionalization

Bioengineered strategies for delivery systems on mucosal surfaces are being increasingly studied for local and/or systemic drug activity, such as for the gastric mucosa [133]. However, and as previously described, the mucosal surface acts as a protection mechanism against pathogens and foreign particles [5]. The reduced permeability of drugs, allied to rapid renewal of the mucus barrier, reduces treatment effectiveness at non-toxic dosages [134]. Since the *H. pylori* cells bulk

is found in the mucus, designing a gastric available system (i.e. that does not leach to other organs as kidneys and liver) and that is simultaneously mucus penetrating is essential for its eradication.

In an experiment conducted by Hinkley *et al.* (2015) the bioavailability of coated and uncoated 23 nm PEG-Au-NPs was compared. Mice were orally gavaged with these particles and after 30 days the retention of the absorbed NPs was evaluated. High amounts of gold were found in the tissues of the gastric tract such as in the stomach, small intestine, cecum and large intestine. Using the Transmission Electron Microscopy (TEM) technique, it was observed that PEG-coated Au-NPs were primarily observed as colloids near the tissue surface, even interacting with microvilli, while the uncoated Au-NPs were found as agglomerates and mainly on the gastric lumen. The authors suggest that this low absorption can be explained by the extensive agglomeration of these NPs [135].

A previous and unique study from Lai *et al.* (2008), contradicted that NPs were incapable of diffusing efficiently through mucus layers. 100, 200 and 500 nm polystyrene NPs were produced and covered with different molecular weight (MW) PEG chains (2, 5 and 10 kDa). Then, the diffusion coefficient (D_{eff}) was tested in fresh undiluted human mucus. Results showed that NPs densely coated with 2 and 5 kDa PEG, were able to penetrate rapidly through the mucus, but NPs covered with 10 kDa PEG chains showed slower transport. It was concluded that highly packed surface coverage and low MW are required for PEG-coated NPs to rapidly penetrate the mucus [134].

3.2.5 Nanoparticles characterization techniques

As for planar SAMs, there are several techniques for NPs characterization. Some will be briefly introduced in the next subsections.

3.2.5.1 Dynamic light scattering (DLS)

DLS (Figure 3.9) is one of the most common tools used to analyze the hydrodynamic size (i.e. in liquid environment) of NPs. It measures intensity variation of the scattered light dispersed in different angles that goes through a liquid sample with NPs. This variation is due to the movement of the NPs [12, 136]. Au-NPs scatter light remarkably well at or near their surface plasmon resonance wavelength [137]. Because small particles are more sensitive to random forces, their scatter light intensity fluctuates more rapidly when compared to bigger particles [12]. DLS has a spectrum resolution from a few nanometers to 3 microns being suitable to characterize NPs but unqualified for larger particles as microspheres [136].

3.2.5.2 Zeta-potential

Zeta-potential refers to the electrical potential at or near the NPs surface where the liquid's relative velocity is zero [138]. Measuring the Zeta-potential allows estimating the colloidal dispersion

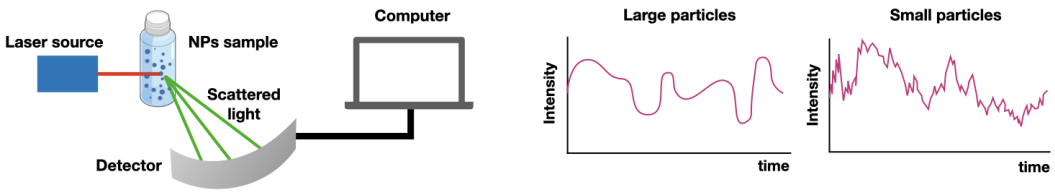


Figure 3.9: Schematic operation principle of DLS (adapted from [12]).

storage stability. Ordinarily, due to electrical repulsion, particle aggregation of charged particles (high Zeta-potential) is less likely to occur. This rule, however, cannot be applied strictly to systems containing steric stabilizers, as their adsorption will decrease the Zeta-potential [136]. Figure 3.10 schematically represents the dependence between ionic concentration and Zeta-potential as a function of the distance from the NP charged surface.

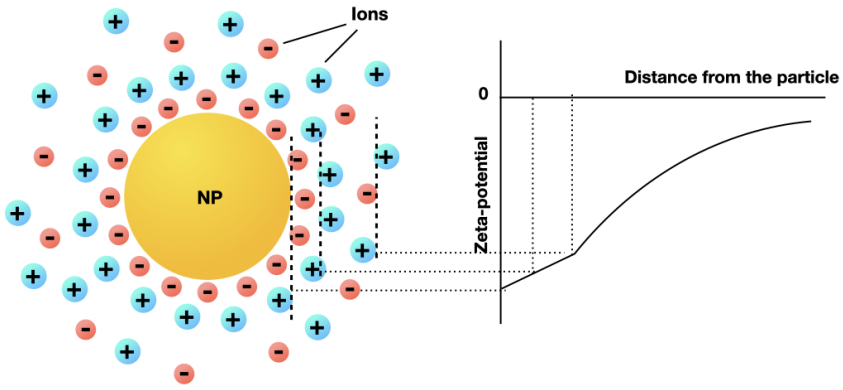


Figure 3.10: Representation of ionic concentration and Zeta-potential as a function of distance from the charged surface of a positive charged NP.

Chapter 4

Materials and Methods

4.1 SAMs preparation

4.1.1 Pure Cholesterol SAMs (PC-SAMs)

4.1.1.1 Alkanethiols solutions

Ethanolic (Merck) solutions of 1-Mercapto-11-undecyl-tetra(ethylene glycol) (EG4, Sensopath) (Figure 4.1 a)); and Cholesterol-(ethylene glycol)$_{75}$ Thiol/Sulfhydryl, MW 3400 Da (Chol-PEG, Nanocs) (Figure 4.1 b)); were prepared with a concentration of 1 mM.
Final solutions of 0.1 mM EG4 (EG4-SAMs) and 0.025, 0.050, 0.075, 0.100 and 0.200 mM Chol-PEG were done.

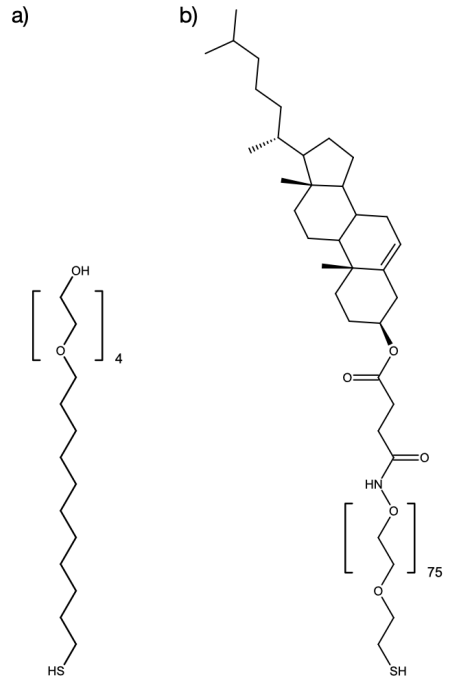


Figure 4.1: Alkanethiols used: a) EG4 and b) Chol-PEG.

4.1.1.2 Gold-coated substrates

Gold-coated substrates of 1 x 1 cm^2 (INESC) were cleaned twice in acetone (Merck) in an ultrasonic bath for 2 minutes for the removal of the photoresist coating.
For QCM-D assays, Gold-coated quartz-crystals (QSX301-Standard Gold, 4.95 Hz. 78 mm^2 active sensor area, Biolin Scientific) were treated in an UV/Ozone chamber for 10 minutes.
Then, gold substrates, either gold-coated surfaces or gold-coated quartz-crystals, were immersed in a "piranha solution" (7:3 v/v concentrated H_2SO_4 (Prolabo) and 30% H_2O_2 (Merck)), for 5 minutes for the removal of any organic residues present. A final wash was performed with absolute ethanol (Merck), *dd*H_2O and absolute ethanol (Merck), sequentially, for 2 minutes in an ultrasonic bath.
Finally, the cleaned gold substrates were immersed in the alkanethiol solutions and incubated under a Nitrogen atmosphere, protected from light for 24 hours. Afterwards, the prepared monolayers were washed twice with absolute ethanol (Merck) in an ultrasonic bath for 2 minutes, dried with a gentle Argon stream and stored under inert atmosphere protected from light until further use.

4.1.2 Mixed Cholesterol SAMs (MC-SAMs)

Alkanethiols preparation was done as described in Section 4.1.1. MC-SAMs were assembled from final solutions with mixture of different Chol-PEG/EG4 ratios: (0 (100% EG4); 12.5; 25; 50; 75; 100% (0% EG4)) at a final thiol concentration of 0.1 mM.

Gold substrates used and monolayer incubation proceeded as stated in Section 4.1.1.

4.2 SAMs characterization

4.2.1 Ellipsometry

Thickness of the SAMs was determined by ellipsometry measurements, using EP3 model (Nanofilm Surface Analysis). Ellipsometer was used in polarized-compensator-sample-analyzer mode (null ellipsometry). A solid-state laser was used as the light source at 532 nm. The readings were performed with a variable angle ranging from 62º to 76º and in 4 zones. Results are expressed as the average of 3 measurements on each of the 3 replicates per sample.

4.2.2 Optical Contact Angle

Contact angle measurements were performed on SAMs using the sessile drop method on measuring system from Data Physics, model OCA 15, equipped with a electronic syringe, a video CCD-camera and SCA 20 software. A ddH_2O drop of 6 μl volume was dispensed on the samples and the angle between the surface and the tangent of the drop was measured. The measurements

were performed at room temperature (25ºC). Results are expressed as the average of 2 measurements on each of the 2 replicates per sample.

4.2.3 X-Ray Photoelectron Spectroscopy

XPS analysis was carried out at Centro de Materiais da Universidade do Porto (CEMUP). SAMs were submitted to XPS analysis using Kratos AXIS Ultra HSA, with VISION and CasaXPS software for data acquisition and analysis, respectively. The XPS analyses were performed with a monochromatic Al X-ray source, operating at 15kV (90W), in FAT mode (Fixed Analyses Transmission), with a pass energy of 20 eV for regions ROI and 80 eV for survey. Data acquisition was performed with a pressure lower than 10^{-6} Pa, along a charge neutralization system. Spectra's convolution was performed using CasaXPS software for peaks adjustment using peak fitting with Gaussian-Lorentzian peak shape and Shirley type background subtraction.

4.2.4 Quartz Crystal Microbalance with Dissipation

Cholesterol oxidase (Sigma-Aldrich), Methyl-β-cyclodextrin (MβCD, Sigma-Aldrich) and 1,2-dipalmitoyl-*sn*-glycero-3-phosphoethanolamine (DPPE, Sigma-Aldrich) adsorption onto SAMs assembled onto Quartz Crystals were performed with a Q-Sense E4 system (Biolin Scientific) at 37 ºC.

For Cholesterol oxidase and MβCD, Phosphate buffer solution (PBS, pH = 7.4) was injected into the system at 0.1 ml/minute flow rate until a stable signal was obtained. Afterwards, Cholesterol oxidase (300 μl, 5 U) and MβCD (2 mM) in PBS were added to the system and allowed to incubate under static conditions for 1 hour at 37 ºC. Then, rinsing with PBS to remove any non-adherent Cholesterol oxidase and MβCD was performed.

For DPPE, absolute ethanol (Merck) was injected into the system at 0.1 ml/minute flow rate until a stable signal was obtained. Afterwards, 18 mg/ml DPPE solution 9:1 (v/v) Chloroform (Prolabo) and methanol (Merck) was prepared, diluted in ethanol to a final concentration of 0.5 mg/ml, added to the system and allowed to incubate under static conditions for 1 hour at 37 ºC. Then, rinsing with absolute ethanol to remove any non-adherent DPPE was performed.

Results were treated with Q-Tools Software Version 3 using Sauerbrey equation (Equation 3.1).

4.3 *In vitro* adhesion assays

4.3.1 Bacteria culture

H. pylori J99 (ATCC 700824) strain was obtained from the Department of Medical Biochemistry and Biophysics, Umeå University and routinely cultured in Trypticase Soy Agar plates supplemented with 5% horse blood (Probiologica) and an antibiotic cocktail (Blood Agar plates) [87], in a microaerophilic environment (GenBox system, BioMérieux) at 37 ºC for 48 hours. Afterward, some colonies were streaked onto Blood Agar plates and incubated for 48 hours under identical conditions.

E. coli ATCC®25922 strain was streaked in Trypticase Soy Agar (TSA, Sigma-Aldrich) at 37 ºC overnight. Then, *E. coli* was incubated with Tryptic soy broth (Merck) at 37 ºC, at 150 rotations per minute (r.p.m) overnight (∼16h).

Lactobacillus acidophilus-01 strain (*L. acidophilus*) was streaked in De Man, Rogosa and Sharpe agar (MRS plates, Biokar Diagnostics) at 37 ºC for 24 hours in microaerophilic environment. *L. acidophilus* was harvest and incubated with MRS broth (Biokar diagnostics) at 37 ºC, at 150 r.p.m. overnight, in microaerophilic environment.

4.3.2 Bacterial adhesion

Bacteria were harvested from the agar plates with sterile PBS (pH=7.4, Sigma). Before incubation with the bacteria, SAMs were hydrated with sterile PBS for 15 minutes.
For *H. pylori* inoculum, the optical density was adjusted to 0.03, $\lambda = 600$ nm ($\sim 1 \times 10^7$ CFU/ml) [102]. Initial inoculum was confirmed by inoculation of 20 μl drops of bacterial suspension onto Blood Agar plates and CFUs were counted after 5 days of incubation. *E. coli* and *L. acidophilus* bacterial suspensions were adjusted to a final concentration of $\sim 1 \times 10^5$ CFU/ml. Initial inoculum was confirmed by inoculation of 10 μl drops of bacterial suspension onto TSA and MRS plates, respectively. *E. coli* CFUs were counted after 24 hours and *L. acidophilus* after 48 hours of incubation using the above-mentioned settings. All inoculums were adjusted in accordance with guidelines recognized by Clinical Laboratory Standards Institute (CLSI) [139].
Incubation of bacteria with the surfaces was done at 37 ºC, at 150 r.p.m for 2 hours according to Parreira *et al.* (2011) [102]. Afterwards, SAMs were rinsed twice with PBS at 150 r.p.m for 15 minutes to remove any non-adherent bacteria and then stained with Vectashield with DAPI (Vector Laboratories, Inc.). Adherent bacteria were visualized with Inverted Fluorescence Microscope (IFM, Zeiss Axiovert 200 MOT) at 40x magnification. Bacterial counts were performed based on photographs from 9 random fields per sample and were expressed as number of bacteria/mm^2. Results are representative of 3 independent assays using 3 replicates for each condition.

4.3.3 Planktonic cells viability

Supernatants (planktonic cells) of the adhesion assay were removed, serially diluted and platted either in Blood agar plates for *H. pylori*, or TSA and MRS for *E. coli* and *L. acidophilus*, respectively, for CFUs determination. *H. pylori* CFUs were determined after 5 days of incubation at 37 ºC in microaerophilic conditions, while *E. coli* and *L. acidophilus* were counted after 24 hours and 48 hours, respectively, of incubation at 37 ºC.

4.3.4 Live/Dead assay

Incubation of bacteria with surfaces followed Section 4.3.2 conditions. After, SAMs were rinsed with PBS and 0.9% NaCl (VWR International) at 150 r.p.m for 15 minutes to remove any non-

adherent bacteria. Afterwards, bacteria were stained with LIVE/DEAD^{TM} BacLight^{TM} (ThermoFisher Scientific) and mounted with Vectashield (Vector Laboratories, Inc.). Adherent bacteria were visualized with IFM at 40x magnification. Bacterial counts were performed based on photographs from 9 random fields per sample and were expressed as number of bacteria/mm^2. Results were obtained using 3 replicates for each condition.

4.4 Gold nanoparticles production and functionalization

150 ml of Sodium Citrate (2.2 mM, Sigma-Aldrich) solution containing Potassium Carbonate (150 mM, Sigma-Aldrich) and Tannic acid (2.5 mM, Sigma-Aldrich) was heated at 70 ºC in a 3 necked round bottom flask under vigorous stirring. Then 1 ml of $HAuCl_4$ (25 mM, Sigma-Aldrich) was added in solution and heated for another 5 minutes to ensure complete reduction of gold ions. The resultant NPs (3.5 nm) were used as seeds. To prepare 5 nm AuNPs, immediately after the synthesis of the seeds, 55 ml of seeds solution was extracted and replaced with 55 ml of Sodium Citrate solution. When the temperature reached 70 ºC, 2 subsequent injections of 0.5 ml of $HAuCl_4$ (25 mM) on a time interval of 10 minutes was added in the solution. The growing step was repeated one more time to get 8 nm Au-NPs. The synthesized Au-NPs were ultracentrifuged at 25000 r.p.m. for 20 minutes to prepare 2 mg/ml of Au-NP solution.
To functionalize Au-NPs with Chol-PEG/EG4, 1 mg of Chol-PEG was added in 2 mg/ml of Au-NPs and incubated for 24 hours at room temperature. Then 1 mg of EG4 was added in the solution and incubated for 4 hours followed by centrifugation at 25000 r.p.m. for 20 minutes to collect Chol-Au-NPs. Similarly, EG4-Au-NPs were prepared by incubation of 1 mg of EG4 with 2 mg/ml of Au NPs.

4.5 Gold nanoparticles characterization

4.5.1 Size, charge and polydispersity index measurements

Size surface, charge (Zeta-potential) and polydispersity index (PdI) of the Au-NPs were characterized using a Malvern Zetasizer Nano ZS (Malvern Instruments). Diluted Au-NPs (1:200 in MilliQ water (MilliQ)) were placed on a disposable capillary cell and triplicate measurements were conducted at a backscattering angle of 173º at 25 ºC.

4.5.2 Gold nanoparticles behavior in a pH range

Citrate-Phosphate buffer solutions at pH equal to 2.6, 4.0 and 6.0 were prepared as described elsewhere [140]. NPs (EG4- and Chol-Au-NPs) were immersed in the prepared buffers, MilliQ water and PBS (pH=7.4) and incubated at 37 ºC for 3 to 5 minutes. After, readings of PdI, size and charge, were obtained in the same conditions as in Section 4.5.1.

4.6 Gold nanoparticles *in vitro* antibacterial performance

4.6.1 Growth conditions

Bacteria were cultured as stated in Section 4.3.1. Then, pre-inoculum was prepared by harvesting *H. pylori* J99 from the agar plates with sterile Brucella Broth medium (BB, Oxoid) supplemented with 10% (v/v) of heat inactivated Fetal Bovine Serum (FBS, Gibco), (BB+10% FBS). Bacteria were then transferred to a T-flask (SPL Life Sciences) containing BB+10% FBS and adjusted to an optical density of 0.1, $\lambda = 600$ nm. Incubation was performed under microaerophilic conditions, 150 r.p.m, 37 ºC overnight.

4.6.2 Antibacterial effect

H. pylori was adjusted to a final optical density of 0.03 ($\sim 1 \times 10^7$ CFU/ml), $\lambda = 600$ nm and incubated with NPs, both EG4- and Chol-Au-NPs, in different concentrations (62.5, 125, 250, 500 and 750 μg/ml) in BB+10% FBS for 2, 6 and 24 hours, in a 96-well plate, under microaerophilic conditions, at 37 ºC and 150 r.p.m. Initial inoculum and viability of bacteria was confirmed by inoculation of 10 μl drops of bacterial suspension onto Blood Agar plates. CFUs were counted after 5 days of incubation using the previously mentioned settings.

4.7 Gold Nanoparticles Cytotoxicity

NPs (EG4- and Chol-Au-NPs) cytotoxicity was evaluated following international standard ISO 10,993–5;12 [141, 142]

4.7.1 AGS cell culture

AGS cells were grown in Roswell Park Memorial Institute 1640 medium supplemented with L-glutamine (RPMI, Corning), 10% FBS (v/v, Gibco), Pen/Strep (10 U/ml penicillin (Biowest) and 10 μg/ml streptomycin (Biowest)) (Full RPMI), at 37 ºC in a humidified atmosphere of 5% CO_2, until 80-90% of confluence was reached. Then, cells were washed with PBS, trypsin (Sigma-Aldrich) added and incubated at 37 ºC in a humidified atmosphere of 5% CO_2 for 5 minutes, to detach adhered cells. Cells were then collected using Full RPMI and number of cells counted using a Neubauer chamber. After, cells were seeded in 96-well Tissue Culture Polystyrene (TCPS) plates ($\sim 3 \times 10^3$ cells/well) in Full RPMI for 24 hours under the same conditions as previously mentioned.

4.7.2 Direct contact assay

Different concentrations of the EG4- and Chol-Au-NPs, as in Section 4.6.2, were suspended in Full RPMI. Culture medium was then replaced by 50 μl of either EG4- or Chol-Au-NPs, in the

desired concentration adjusted in fresh medium and cells were incubated at 37 ºC in a humidified atmosphere of 5% CO_2, for 24 hours. After, resazurin assay was performed to evaluate cell metabolic activity. Cells in Full RPMI were used as negative control of cytotoxicity.

4.7.3 Cell metabolic activity

Resazurin (20% v/v, Sigma-Aldrich) was added to each well and incubated for 4 hours at room temperature. Then, fluorescence was measured ($\lambda_{ex} = 530$ nm, $\lambda_{em} = 590$ nm) in a microplate fluorometer (Synergy Mx, BioTek). Blanks for fluorescence emission subtraction were performed with Full RPMI, without cells. Cell viability was determined using the average of 2 replicates, following Equation 4.1.

$$Metabolic\ activity\ (\%) = \frac{Treated\ cells}{Untreated\ cells\ in\ medium} \times 100 \tag{4.1}$$

4.8 Statistics

Statistical significance was accessed using GraphPad Prism 8 Software (V. 8.2.1). One-Way Anova test for multiple comparisons was used with a 95% confidence interval (p<0.05).

Chapter 5

Results and Discussion

5.1 Pure Cholesterol SAMs (PC-SAMs)

5.1.1 Surface Characterization

PC-SAMs were developed and fully characterized with Ellipsometry, OCA, XPS and QCM-D. Cholesterol-based SAMs were obtained as the results in Figure 5.1 indicate. There was an increase in SAMs thickness and hydrophobicity with increasing Chol-PEG concentration and when compared to the control group, EG4-SAMs.

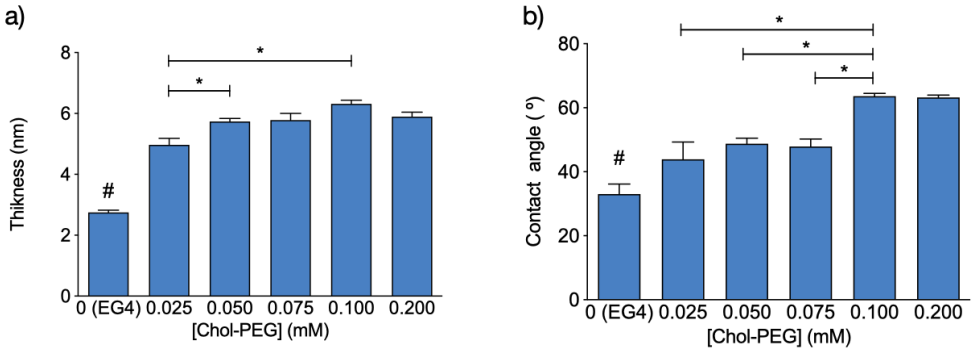


Figure 5.1: SAMs characterization: a) Ellipsometry; b) Optical contact angle. $*$ - statistically significant different, # - statistically significant from all the other tested surfaces (ANOVA; p<0.05). (n=3)

EG4-SAMs had a thickness of approximately 2.5 nm as expected [30]. A plateau in thickness was reached when using 0.050 mM of Chol-PEG, yielding a maximum thickness of approximately 6 nm. Significant statistical differences ($p < 0.05$) in thickness between Chol-PEG concentrations of 0.025 and 0.050 mM; and between 0.025 and 0.100 mM, were seen. EG4-SAMs presented a contact angle of approximately 35º as expected [30]. PC-SAMs at 0.025, 0.050 and 0.075 mM Chol-PEG presented a contact angle of 50º. PC-SAMs prepared using 0.100 and 0.200 mM of Chol-PEG had a contact angle of 65º, also reaching a plateau, suggesting that the gold surface is fully covered with Chol-PEG moieties. Water contact angle of PC-SAMs prepared by 0.100 mM

Chol-PEG showed significant differences to all concentrations with the exception of 0.200 mM. All PC-SAMs were statistically significantly different from the control group (EG4-SAMs).

Table 5.1: Relative percentage of chemical elements Carbon (C), Oxygen (O), Nitrogen (N) and Sulfur (S) for EG4 and PC-SAMs.

[Chol-PEG] (mM)	C	N	O	S
0 (EG4)	73.1	0.0	25.9	1.0
0.025	72.4	0.4	26.3	0.9
0.050	74.4	0.6	24.1	0.8
0.100	74.1	0.5	25.0	0.4

Concerning the XPS study, SAMs demonstrated that no chemical element other than expected were detected, showing no elementary contamination on the surfaces. Carbon (C), Oxygen (O), Nitrogen (N) and Sulfur (S) were detected in all SAMs (Table 5.2), except for EG4-SAMs, which contained no N, as expected. Regarding PC-SAMs with different concentrations of Chol-PEG, an increase in the amount of N was seen from 0.025 mM to 0.050 mM. Interestingly, from 0.050 mM to 0.100 mM, no increase in N was observed, which also leads to the assumption that a plateau is reached. The amount of S in all SAMs should be similar, however there is a decrease in S relative percentage as Chol-PEG concentration increases. As with higher concentrations there is a bigger packaging and thickness of the monolayers, the ejected electrons may have some hindrance reaching the surface to be detected. Altogether, these results suggest that at 0.100 mM Chol-PEG concentration the gold surface is fully covered with Chol-PEG moieties.

In order to quantify the amount of Chol-PEG present on the surfaces, a QCM-D assay using a Cholesterol oxidase was designed. Cholesterol oxidase has the ability to cleave the cholesterol moieties [143]. However, no difference in frequency values was observed after addition of this enzyme to the system. It was expected that the frequency values would increase, as a result of mass loss on the system (cholesterol cleavage). A possible explanation is that the enzyme is not able to cleave the cholesterol moiety once immobilized onto SAMs, as the cleavage site might be hindered or not available. Another hypothesis is that the PC-SAMs did not expose the Cholesterol moieties fully, due to dense lipid coverage. Therefore, mixed Chol-PEG/EG4-SAMs were engineered to develop a more organized surface and enhance the cholesterol exposure from the surface.

5.2 Mixed Cholesterol SAMs (MC-SAMs)

Mixed EG4- and Chol-PEG-SAMs were developed. As the PEG chain helps to expose the cholesterol molecule, the addition of the EG4-thiol on the gold surfaces, allows having a more compacted and ordered surface [103].

5.2.1 Surface Characterization

Thickness and wettability were determined by ellipsometry and optical contact angle measurements. Results are expressed in Figure 5.2.

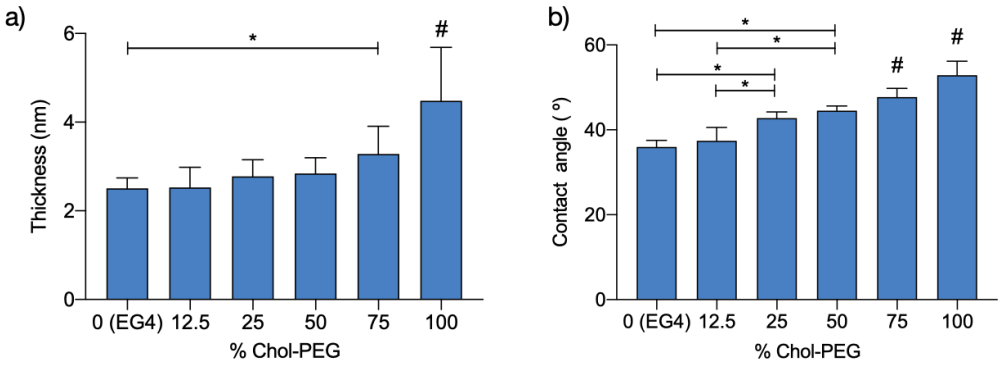


Figure 5.2: SAMs characterization: a) Ellipsometry; b) Optical contact angle. $*$ - statistically significant different, # - statistically significant from all the other tested surfaces (One way ANOVA; p<0.05). (n=3)

As shown in Figure 5.2 a), SAMs thickness increased with increasing Chol-PEG concentration as expected, from 2.5 nm (0% Chol-PEG) to 5 nm (100% Chol-PEG). Regarding surface contact angle (Figure 5.2 b)), it increased from approximately 37º (0% Chol-PEG) to 50º (100% Chol-PEG). As with higher concentration of Chol-PEG there is a bigger packaging of the monolayer, the alkanethiols tend to adopt a more up right orientation increasing in thickness. Hydrophobicity of the monolayers also increases because of the increasing addition of cholesterol, an hydrophobic molecule.
Differences were seen when comparing PC-SAMs and MC-SAMs thickness. MC-SAMs tend to be thinner than PC-SAMs as the addition of the EG4 chain enables Chol-PEG to bend over [128]. Significant statistical differences ($p < 0.05$) in thickness were found between 0% and 75% Chol-PEG-SAMs. Also 100% Chol-PEG-SAMs are significant different from all other the other surfaces. Regarding optical contact angle, 75% and 100% Chol-PEG-SAMs were significantly different from all the others, and no significant differences were found between 25% and 50% Chol-PEG-SAMs.

Regarding the XPS study, SAMs demonstrated that no chemical elements other than expected were detected. Elements C, O, N and S were detected in all SAMs (Table 5.2), except for EG4-SAMs, which contained no N, as expected. Regarding Chol-PEG-SAMs, an increase in the amount of N was seen with increasing cholesterol concentration, which was expected. The decrease in the S percentage from 25% to 100% Chol-PEG-SAMs can be correlated with increase in SAMs thickness, as with higher Chol-PEG concentrations there is a bigger packaging and thickness of the monolayers and the ejected electrons may have some hindrance reaching the surface and therefore

be detected. Gold surfaces were incubated with a mixture of EG4 and Chol-PEG alkanethiols at

Table 5.2: Relative percentage of chemical elements Carbon (C), Oxygen (O), Nitrogen (N) and Sulfur (S) for EG4 and Chol-PEG-SAMs.

Chol-PEG (%)	C	N	O	S
0 (EG4)	73.8	0.0	24.6	1.6
12.5	72.2	0.1	25.9	1.9
25	71.2	0.5	26.2	2.1
50	70.8	0.6	26.7	1.9
100	69.4	0.8	28.5	1.2

a specific ratio. However, this ratio might not be exactly reflected on the surface elemental composition. Considering that the binding kinetics onto the gold surface of EG4- and Chol-PEG are the same, it is expected that as Chol-PEG/EG4 ratio increases, relative percentage of N on the surface also increases, linearly, in a directly proportional relation, as demonstrated in Figure 5.3: Line of identity [144]. However, if one considers that EG4 adsorbs first onto the gold surface, it

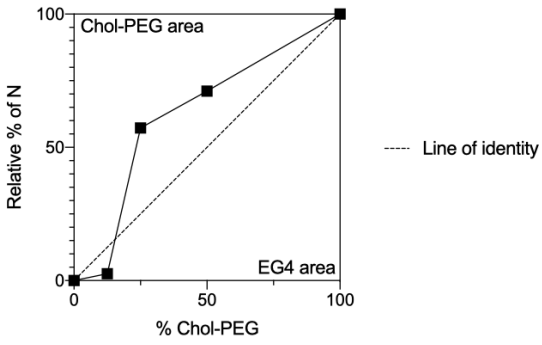


Figure 5.3: EG4 and Chol-PEG coverage on gold surface as a function of Nitrogen relative percentage, obtained through XPS analysis.

is expected to have lower relative percentage of N with increasing Chol-PEG ratio and N% values will lean more towards the EG4 area represented in Figure 5.3; and *vice-versa*. With the results of N relative percentage (in Table 5.2) normalized to 0-100% through Equation 5.1, it is possible to observe that at 12.5% Chol-PEG-SAMs (87.5% EG4), very low amount of N was observed on the surface, suggesting that surface is mostly composed with EG4. However, when both thiols are at same concentration in solution (50% Chol-PEG-SAMs), the N % on the surface is higher than 50% suggesting that Chol-PEG thiol linked faster to the surface than EG4-thiol. Even, at 25% Chol-PEG-SAMs (75% EG4) the N % on the surface is higher than 50%. This might be explained by the differences in solubility of the two alkanethiols [145].

$$N\%_{normalized}(n) = \frac{N\%_{n\%Chol-PEG}}{N\%_{100\%Chol-PEG}} \times 100 \tag{5.1}$$

The final mass of Chol-PEG onto the gold surface was attempted to be estimated using QCM-D. Tabaei *et al.* (2014) performed cholesterol quantification on lipid bilayers on silicon oxide surfaces using MβCD. MβCD was used to extract cholesterol and results showed an increase of frequency of vibration due to the loss of mass on the bilayer [146]. For that, MβCD was chosen to perform cholesterol quantification, as it interacts with the cholesterol molecule.
As seen in Figure 5.4, after the injection of 2 mM MβCD into the system, there was a decrease of frequency in all surfaces. Although this result is opposite to the one obtained by Tabaei *et al.* (2014), this might be explained due to the fact that the existing cholesterol is linked covalently to the alkanethiol chain and so cannot be extracted. At 100% Chol-PEG-SAMs a significant decrease in frequency of surface vibration is observed, when comparing to the control group (EG4-SAMs), suggesting MβCD interacts with the cholesterol moiety/adsorbs to the surface. Nonetheless, there were no significant differences between the 0 (EG4, control group), 12.5, 25 and 50% Chol-PEG-SAMs, revealing lack of specificity, since MβCD also adsorbed to the control group. In Figure 5.4 it is also visible that after the re-injection of PBS into the system, the shift frequency values turn to zero, further highlighting that MβCD did not linked to the cholesterol moiety.
Altogether, this method demonstrated to be inadequate for the quantification herein required.

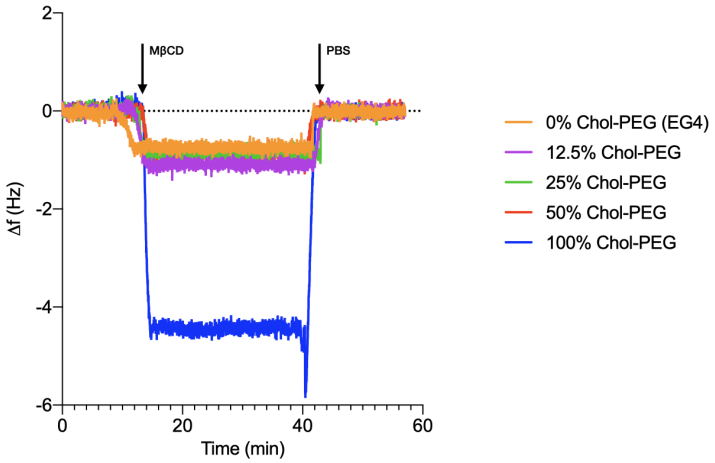


Figure 5.4: Quantification of linked Chol-PEG using MβCD through QCM-D.

Another QCM-D assay was performed using DPPE, a phospholipid with cholesterol recognition ability [10]. The obtained results are presented in Figure 5.5, showing a decrease in frequency, i.e. mass increase, in all surfaces when injecting the DPPE into the system. However, no significant differences were seen between EG4-SAMs and 25% Chol-PEG-SAMs, revealing lack of specificity, as described for MβCD. Similar to the results shown in Figure 5.4, 100% Chol-PEG-SAMs showed significant decrease in frequency, meaning DPPE adsorbed to the surface. Regardless, after the re-injection of ethanol (rinsing step), all the DPPE was removed (shift frequencies return to zero), meaning DPPE did not link to the cholesterol moiety.

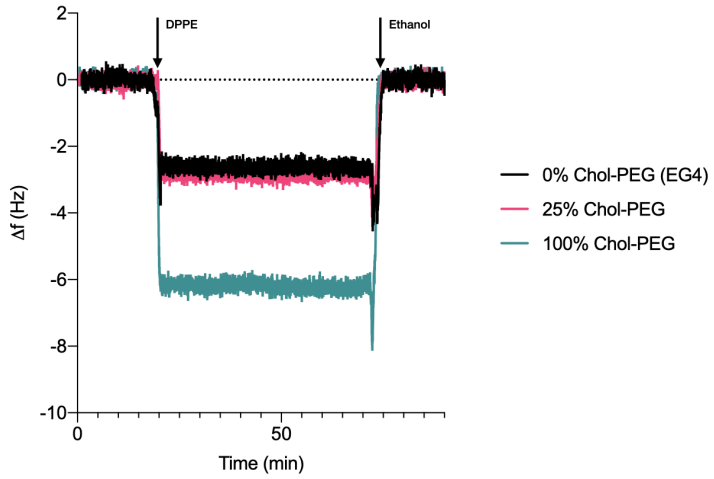


Figure 5.5: Quantification of linked Chol-PEG using DPPE through QCM-D.

5.2.2 *In vitro* adhesion assay - *Helicobacter pylori*

The ability of the designed bioengineered surfaces to attract *H. pylori* was accessed by *in vitro* adhesion assays. *H. pylori* J99 strain was chosen since it can successfully infect humans, is highly pathogenic and is associated to worst prognostic [147].
Figure 5.6 shows representative images of each surface taken with the IFM.

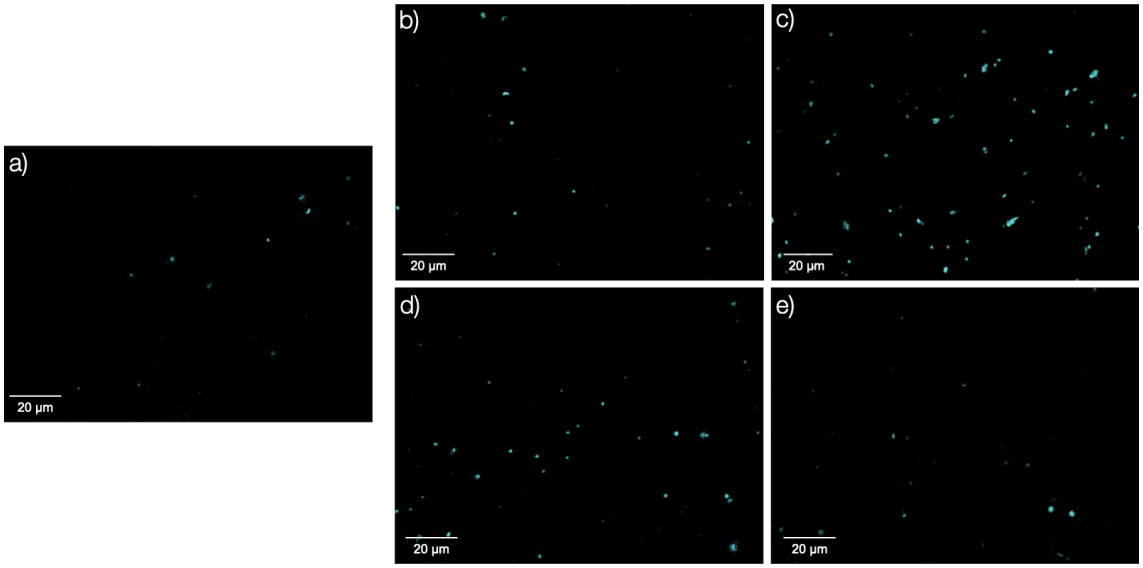


Figure 5.6: Representative images of *H. pylori* J99 labelled with DAPI after 2 hours adhesion. a) EG4-SAMs, b) 12.5% Chol-PEG-SAMs, c) 25% Chol-PEG-SAMs, d) 50% Chol-PEG-SAMs and e) 100% Chol-PEG-SAMs.

As it is possible to observe in Figure 5.6, the number of bacteria labelled with DAPI (blue in images), increases from EG4-SAMs control group to 25% Chol-PEG-SAMs (Figure 5.6 a) through Figure 5.6 c)) but decreases from 25% to 100% Chol-PEG-SAMs (Figure 5.6 c) through Figure 5.6 e)). Figure 5.7 represents the number of bacteria adhered to the different surfaces tested counted

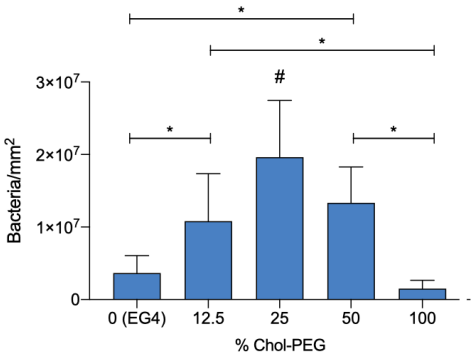


Figure 5.7: *H. pylori* J99 adhesion to Chol-PEG-SAMs after 2 hours. $*$ - statistically significant different, # - statistically significant from all the other tested surfaces (One way ANOVA; $p<0.05$). (n=3)

through IFM photographs.
As shown in Figure 5.7, after 2 hours, the number of adhered bacteria increased from 0% to 25% Chol-PEG-SAMs, being this surface the one with higher adhesion. A decrease in the number of adherent bacteria from 25 to 100% Chol-PEG-SAMs was seen and, more interestingly, the number of adhered bacteria at 100% Chol-PEG-SAMs is similar to the one in the control group (EG4; 0% Chol-PEG), in accordance to Figure 5.6. This may suggest that the alkanethiols are densely packed at higher Chol-PEG percentages and *H. pylori* cannot recognize the cholesterol molecule. In 25% Chol-PEG-SAMs, the adhered bacteria were evenly spread, suggesting the EG4 and Chol-PEG thiols are adsorbed homogeneously onto the gold surface. However, in surfaces with 50% Chol-PEG (50% EG4), agglomerates of bacteria could be observed randomly throughout the surface, with areas containing an increased density of bacteria (data not shown). This suggests that in this ratio of Chol-PEG/EG4 alkanethiols, these thiols are linked heterogeneously onto the gold surface, forming small 'clusters/islands'.
These results indicate that 25% Chol-PEG ratio would be an optimum ratio to induce bacterial adhesion and act as decoy for *H. pylori*.

5.2.3 *In vitro* adhesion assay - Viability study

The viability of surface adherent bacteria was evaluated using the LIVE/DEAD^{TM} Baclight^{TM} Kit. This kit allows distinguishing live from dead cells. It contains two fluorophores, SYTO9 and propidium iodide (PI) and works as a function of the integrity of the cells membrane: cells with a compromised membrane, considered dead or dying, will stain red (PI), while cells with an intact membrane will stain green (SYTO9) [88].

Figure 5.8 shows representative images of each surface taken with the IFM. Density of bacteria in each surface (live bacteria represented in green and dead bacteria represented in red) resembles images of Section 5.2.2.
Only on 100% Chol-PEG-SAMs (Figure 5.8 e)) a decrease in bacterial viability was seen.

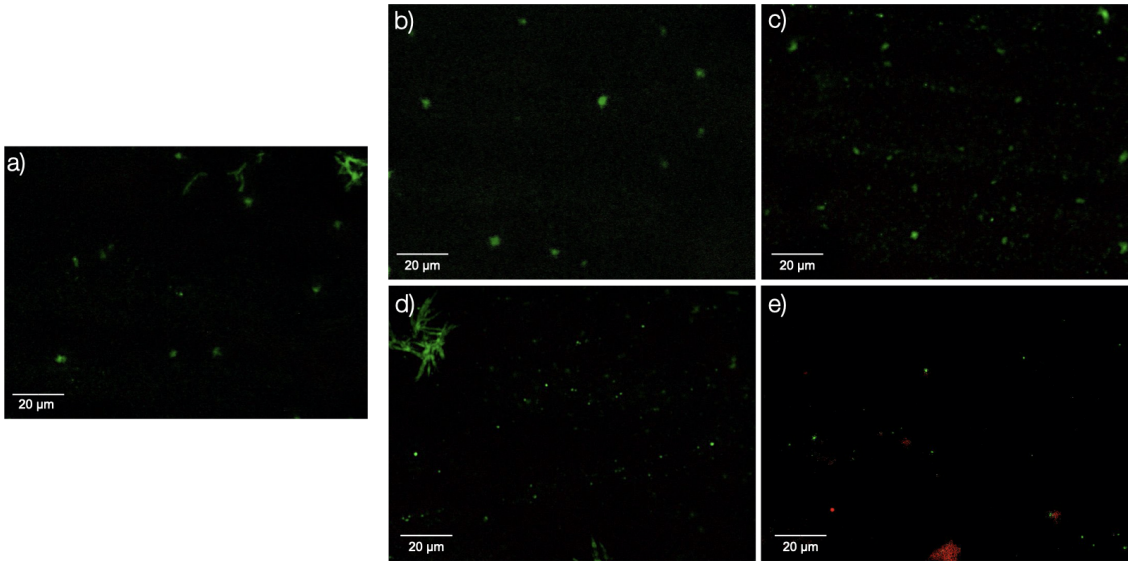


Figure 5.8: Representative images of *H. pylori* J99 labelled with LIVE/DEAD^{TM} Baclight^{TM} after 2 hours adhesion. Green colour represents live bacteria (SYTO9 stained), red colour represents dead bacteria (PI stained). a) EG4-SAMs, b) 12.5% Chol-PEG-SAMs, c) 25% Chol-PEG-SAMs, d) 50% Chol-PEG-SAMs and e) 100% Chol-PEG-SAMs.

Figure 5.9 a) represents the number of bacteria adhered to the different surfaces being the total the sum of live (represented in green) and dead (represented in red) bacteria and Figure 5.9 b) the planktonic bacteria of the living non-adhered bacteria. Results in Figure 5.9 a), showed that the viability of the adhered *H. pylori* was not compromised, while maintaining the same adhesion behaviour previously reported (Section 5.2.2). The majority of *H. pylori* appear to be alive for the exception of 100% Chol-PEG-SAMs that showed a small increase in mortality (less than 20%), congruent with what was already described for Figure 5.8 e). The viability of planktonic bacteria was also accessed to understand if the contact with these surfaces would lead to bacteria death. After 2 hours, the number of planktonic *H. pylori* cells (Figure 5.9 b)) was not affected by exposure to the Chol-PEG-SAMs.

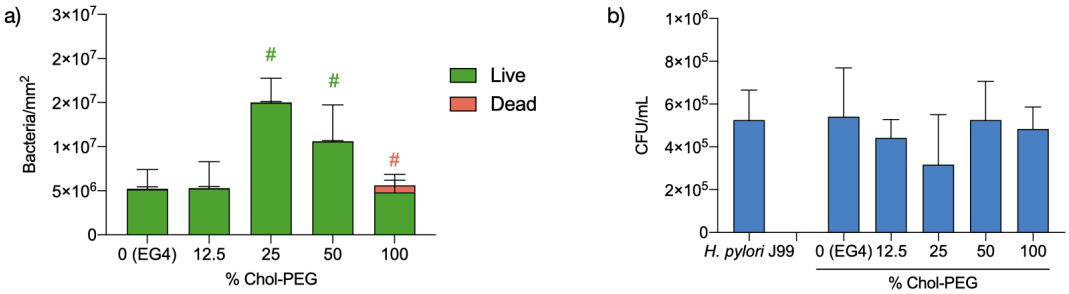


Figure 5.9: *H. pylori* J99 adhesion to Chol-PEG-SAMs after 2 hours. a) surface adherent cells and b) planktonic cells. Total adhesion corresponds to the number of live + dead cells. # - statistically significant from all the other tested surfaces (One way ANOVA; p<0.05), green for Live and red for Dead.

5.2.4 *In vitro* adhesion assay - Selectivity study

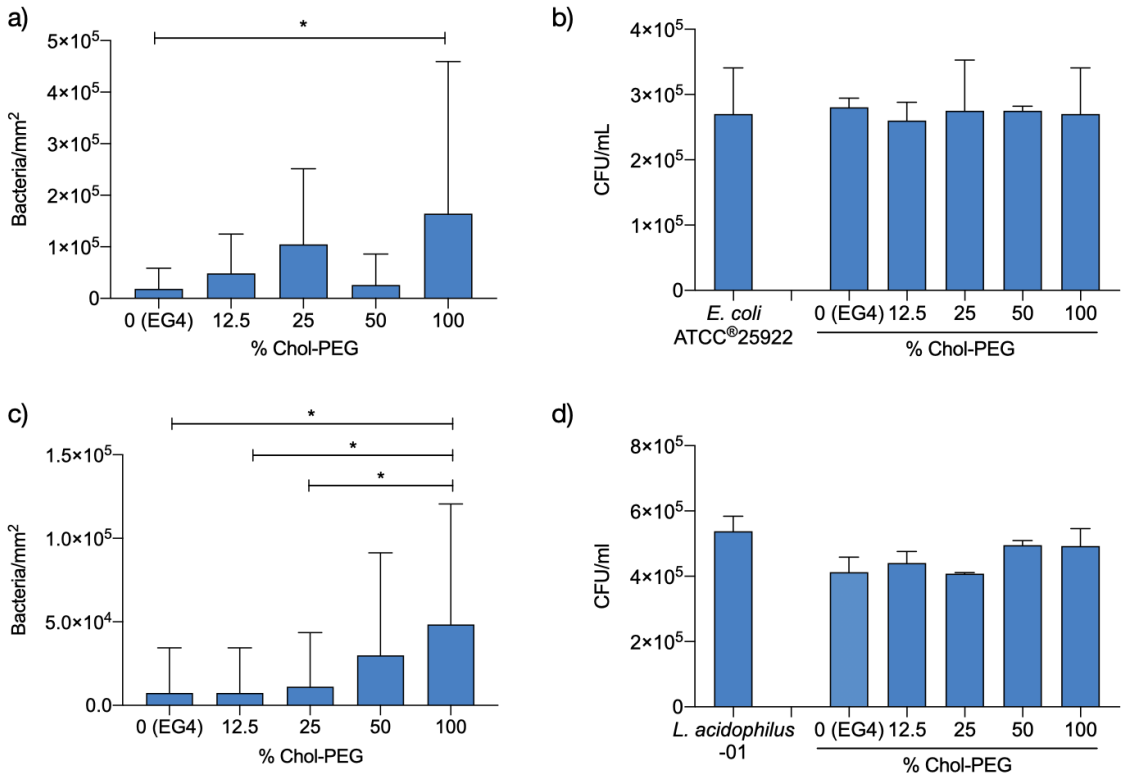


Figure 5.10: Adhesion to Chol-PEG-SAMs after 2 hours. a) *E. coli* surface adherent cells, b) *E. coli* planktonic cells, c) *L. acidophilus* surface adherent cells, d) *L. acidophilus* planktonic cells. $*$ - statistically significant different, # - statistically significant from all the other tested surfaces (One way ANOVA; $p<0.05$). (n=3)

In vitro adhesion assays with *E. coli* and *L. acidophilus* were also performed to study if the surfaces created could selectively target *H. pylori* and foresee the possible impact on the gut microbiota. *E. coli* and *L. acidophilus* were chosen since they are abundant in the human gastro-intestinal tract [148, 149]. Adhesion results (Figure 5.10 a) for *E. coli* and b) for *L. acidophilus*) showed approximately 200 times less adhesion, with the exception of the EG4 surface, which had almost no bacteria adhered as expected by the non-fouling nature of EG4 [102]. However, to verify if the order of magnitude of adhesion would change with different initial inoculums (*E. coli* and *L. acidophilus* were adjusted to $\sim 1 \times 10^5$ CFU/ml in accordance to CLSI standards), the same experiment was repeat with initial inoculums adjusted to $\sim 1 \times 10^7$ CFU/ml. Results revealed adhesion in the same order of magnitude as results shown in Figure 5.10 (data not shown).

E. coli and *L. acidophilus* preferentially adhered to surfaces with higher rates of Cholesterol (more hydrophobic), having the expected behaviour towards hydrophobic surfaces reported in the literature [150, 151]. Planktonic results (Figure 5.10 b) for *E. coli* and d) for *L. acidophilus*) showed no significant differences between all surfaces.

5.3 Gold nanoparticles

With the obtained results of the proof-of-concept study, the obtained knowledge was translated to a more bio-applicable approach. For that, Au-NPs were selected because of their high biocompatibility, stability, easy fabrication and straightforward surface functionalization [113]. This was performed in collaboration with Lino Ferreira, PhD and Akhilesh Rai, PhD at Center for Neurosciences and Cell Biology (CNC), University of Coimbra.
Au-NPs successful production was confirmed by the final dark ruby red colour of the solution [152]. After, Au-NPs were incubated with EG4 or with a mixture of Chol-PEG and EG4 thiols for Au-NPs surface functionalization.

5.3.1 Size, charge and polydispersity index characterization

For their characterization Au-NPs were diluted in MilliQ water and analyzed by Zetasizer gauging the following parameters: Size, Zeta-potential and PdI in accordance with [153].

Initial characterization after Au-NPs production, confirmed the intended 8 nm diameter (Appendix A). However, and due to the use of different equipment to perform the analysis, “naked" Au-NPs presented a size of 1.61 ± 0.34 nm. EG4-Au-NPs presented a size of 17.17 ± 1.34 nm while Chol-Au-NPs a size of 19.88 ± 1.25 nm, as expected from the size difference of EG4 and Chol-PEG alkanethiols. Size histogram (Figure 5.11) reveals good NPs preparation since only one population is found.

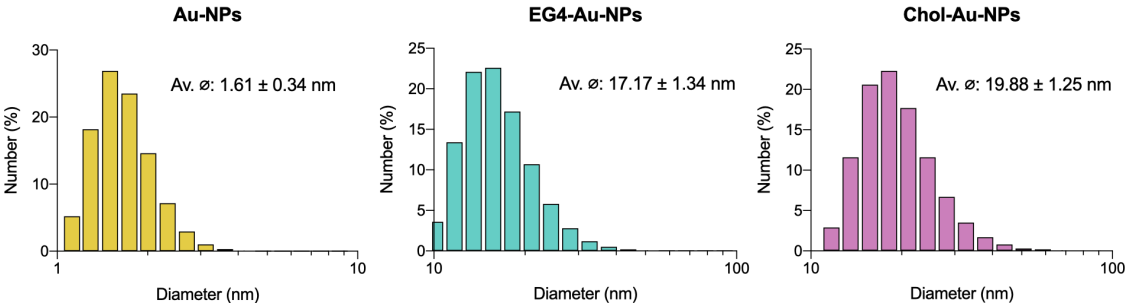


Figure 5.11: Histograms of size distribution of the produced Au-NPs. All statistically significant different (One way ANOVA; p<0.05). (n=2)

Zeta-potential evaluation showed that Au-NPs possess a negative charge around -35 mV, EG4-Au-NPs also have a negative charge of -18 mV, while Chol-Au-NPs charge was approximately 4 mV, close to neutral values (Figure 5.12 a)). As Au-NPs core are positively charged, Au-NPs are surrounded by negative ions at the slipping plane, thus Au-NPs presenting negative Zeta-potential. Although EG4- and Chol-Au-NPs were engineered using Au-NPs as cores, the presence of an ethylene glycol chain around it increases Zeta-potential. In Chol-Au-NPs, the presence of cholesterol increases even more the Zeta-potential to neutral or even more positive charges, depending on the concentration, as reported in the literature [154]. Similar EG4-Au-NPs found in the literature

have equivalent Zeta-potential [155]. Rod shaped NPs functionalized with similar Chol-EG$_n$-SH had neutral to positive Zeta-potential [156, 157].
Significant differences in size and Zeta-potential confirm the successful immobilization of the cholesterol moiety in Au-NPs.

In what concerns PdI, shown in Figure 5.12 b), Au-NPs, EG4-Au-NPs had values of approximately 0.5 and Chol-Au-NPs of 0.3. PdI represents the size population distribution, in this case, the NPs in a solution. It varies from 0, completely uniform regarding particle size, to 1.0, intensely polydisperse with multiple size populations. Although it is recommended that the values of PdI should be close to 0.2 for polymer-based NPs materials [158], similar results to the ones herein obtained were found in the literature when functionalizing Au-NPs with PEG chains [159].

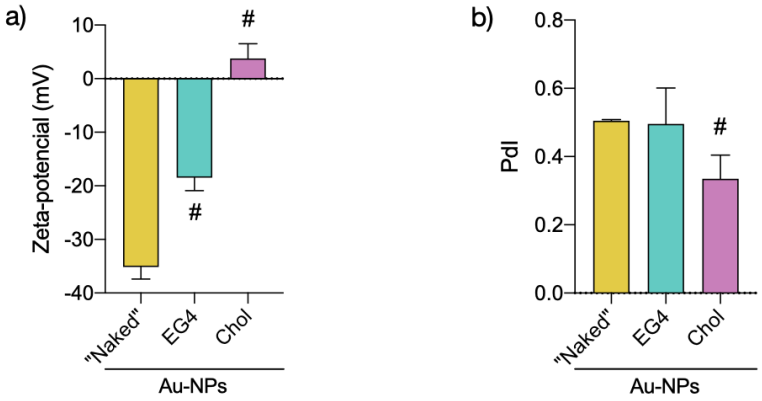


Figure 5.12: a) Zeta-potential and b) PdI Au-NPs. All Au-NPs have statistically significant differences in Zeta-potential. # - statistically significant from all the other tested surfaces (One way ANOVA; $p<0.05$). (n=2)

5.3.1.1 Gold nanoparticles interactions to different pH values

Since these Au-NPs are designed for application in gastric settings, the interaction with different solutions was tested measuring the Zeta-potential, PdI and size at different pH values: 2.6, 4.0 and 6.0 (Citrate-Phosphate buffer) and in pH = 7.4 (PBS) (Figure 5.13), mimicking the pH range found in the gastric environment.
Analysing the results represented in 5.13 a)), "Naked" Au-NPs Zeta-potential increases with increasing acidity, as well as EG4-Au-NPs, which Zeta-potential increased to neutral charges. In Au-NPs, although PdI values remained similar for the pH range tested (Figure 5.13 b)), with exception for the pH 6.0 solution, populations with 140 to 450 nm in diameter (Figure 5.13 c)) were observed, which indicates that these NPs are not stable and aggregated as expected [135]. As most NPs are not at an equilibrium state and exhibit a high surface energy, they are unstable and require a stabilizing coating, such as surfactants [160].
EG4-Au-NPs also showed tendency to agglomerate but only in pH 4.0 solution, that along with

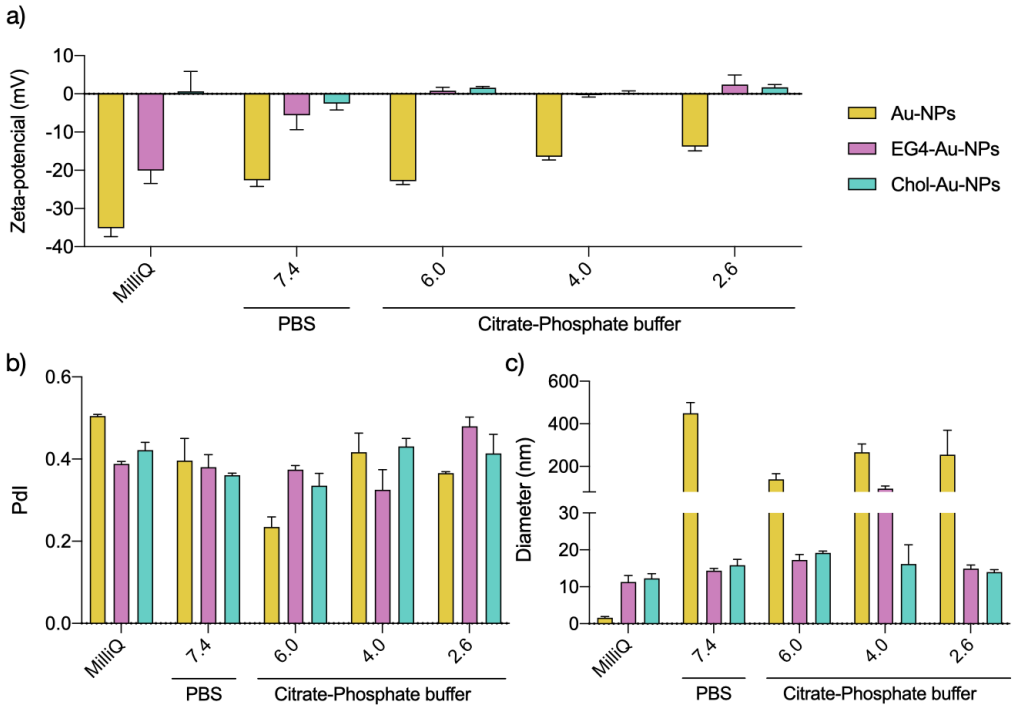


Figure 5.13: Au-NPs response on MilliQ water, and solutions of pH values of 7.4, 6.0, 4.0 and 2.6.

changes in Zeta-potential, demonstrates thin ability to preserve initial activity.
Analysing results of Figure 5.13 a) it is noticeable that Chol-Au-NPs are very stable, maintaining a neutral Zeta-potential along different acidic pH solutions, probably due to its long surfactant chain (75 ethylene glycol repetitions). Zeta-potential, PdI (Figure 5.13 b)) and Size (Figure 5.13 c)) of Chol-Au-NPs were stable along the pH range tested. Altogether, this indicates that these Chol-Au-NPs may be capable to preserve their functionality in a wide pH range and, therefore, are good candidates to become a gastric environment biomaterial.

5.3.2 Gold nanoparticles *in vitro* assay

The growth of *H. pylori* J99 over three time points (2, 6 and 24 hours), when exposed to a range of Au-NPs concentrations (62.5, 125, 250, 500 and 750 μg/ml) was accessed (Figure 5.14). This assay was performed to examine if the bioengineered NPs were capable of having bactericidal effect against *H. pylori per se*, as well as to understand if Chol-Au-NPs would behave differently from EG4-Au-NPs.

The Minimal Bactericidal Concentration (MBC) is the minimal concentration required to kill 99.9% (reduction of 3 logarithms (logs)) of bacteria in a 24 hours time frame [87]. EG4-Au-NPs were used as control groups. As seen in Figure 5.14, bacterial growth is conditioned by the presence of both NPs, decreasing over time. At the lowest concentration of NPs, 62.5 μg/ml, both

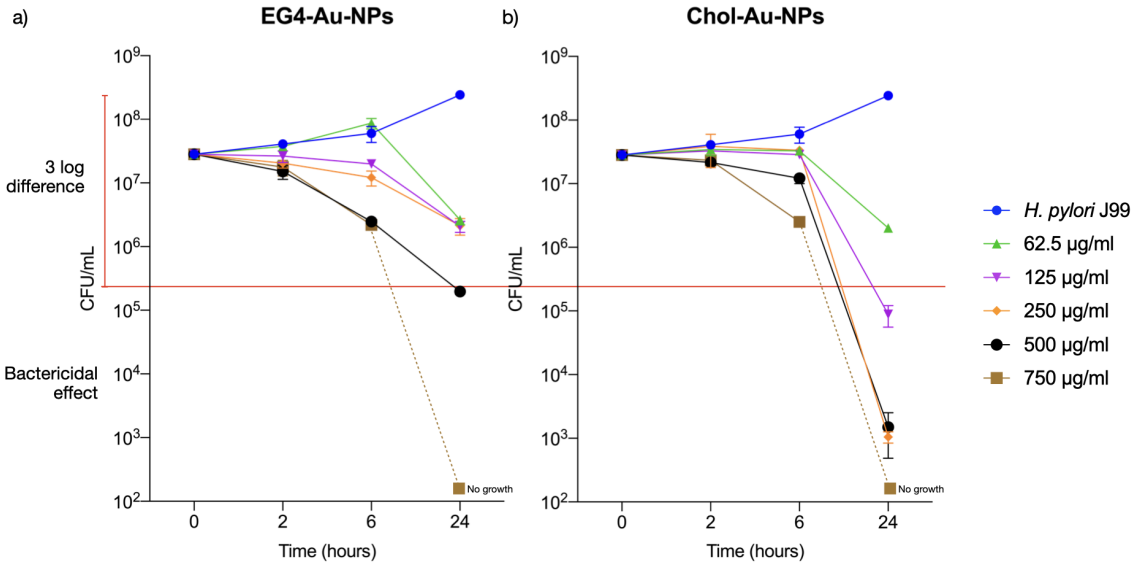


Figure 5.14: Antibacterial performance of a) EG4- and b) Chol-AuNPs against *H. pylori* J99. Assays were performed in BB + 10% FBS after 2, 6 and 24 hours of incubation. (n=3)

EG4- and Chol-Au-NPs had no bactericidal effect after 24 hours, with only a reduction of 2 logs on bacterial load. Looking at bacteria exposed to the EG4-Au-NPs (Figure 5.14 a)) in concentrations of 125 and 250 μg/ml there was also a 2 log reduction. However, at 500 μg/ml there was a 3 log reduction and a bactericidal effect for the EG4-Au-NPs was reached. For the Chol-Au-NPs (Figure 5.14 b)) all concentrations had bactericidal effect, with the exception of 62.5 μg/ml. The bactericidal effect was more pronounced with increasing Chol-Au-NPs concentration: 125 μg/ml had a 3 log reduction, while 250 and 500 μg/ml induced a 5 log reduction on the *H. pylori* load. Both particles completely impaired bacterial growth at the concentrations of 750 μg/ml. The MBC for EG4-Au-NPs was determined to be 500 μg/ml and 125 μg/ml for the Chol-Au-NPs.
These results reveal that Au-NPs decorated with cholesterol groups compromised *H. pylori* growth over time, suggesting a higher interaction between cholesterol groups and *H. pylori* than with EG4. The small size, concentration and, most importantly, the surface functionalization, revealed to be important to compromise *H. pylori* growth. However, at the highest concentration (750 μg/ml), the absence of growth of *H. pylori* with both Au-NPs, indicates that in this case, concentration of the NPs may be the limiting factor and not the surface functionalization. TEM analyzes would also prove if internalization was responsible for *H. pylori* death.

5.3.3 Gold Nanoparticles Cytotoxicity

Although several studies indicate low cytotoxicity of Au-NPs, Chol-Au-NPs cytotoxicity may be a concern, since human cells can also recognize cholesterol [161].
Here, biocompatibility was accessed using a gastric cell lines.
A preliminary assay was done using Human gastric carcinoma AGS cell line in a direct contact assay following the ISO 10,993–5;12 [141, 142]. Briefly, to evaluate the metabolic activity

and consequent cytotoxicity, a rezazurin assay was done. This assay is based on the ability of healthy cells to reduce resazurin intracellularly. This reduction of resazurin is a direct measure of metabolic activity in cell cultures and can be measured colorimetrically or fluorometrically, as the colour solution changes from deep blue to pink [162, 163].
Results are shown in Figure 5.15.

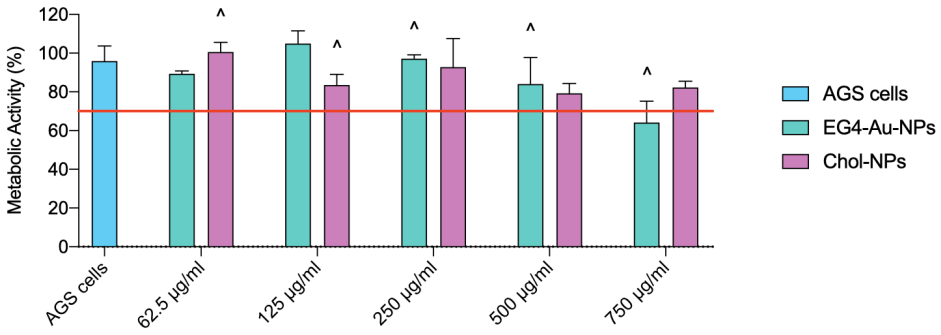


Figure 5.15: Metabolic activity of AGS cells assessed by the direct method.

The preliminary results represented in Figure 5.15 show a decrease in cell metabolic activity with increasing concentration of Au-NPs, more evident for EG4-Au-NPs. Nonetheless, according to the standard ISO, only a reduction in metabolic activity below 70% is considered as a cytotoxic effect. Therefore, only EG4-Au-NPs in the concentration of 750 μg/ml may be considered cytotoxic.
However, during experimental proceedings it was visible that after 24 hours incubation with the developed NPs and in certain concentrations, cells detached from the wells bottom. These results are marked with $\wedge$ symbol on Figure 5.15. In Figure 5.16 it is possible to observe cells attachment and morphology after 24 hours incubation with the developed Au-NPs.

In what concerns morphology it is noticeable that in both EG4- and Chol-Au-NPs and in all concentrations cells morphology changed from "random shaped tile" to a round morphology, indicating that although metabolic activity was not impaired, cells somehow were stressed in contact to these Au-NPs. Another point that should be taken in account is the concentration per well, as higher cell seeding may also be influencing the results. In the future, this should be optimized.

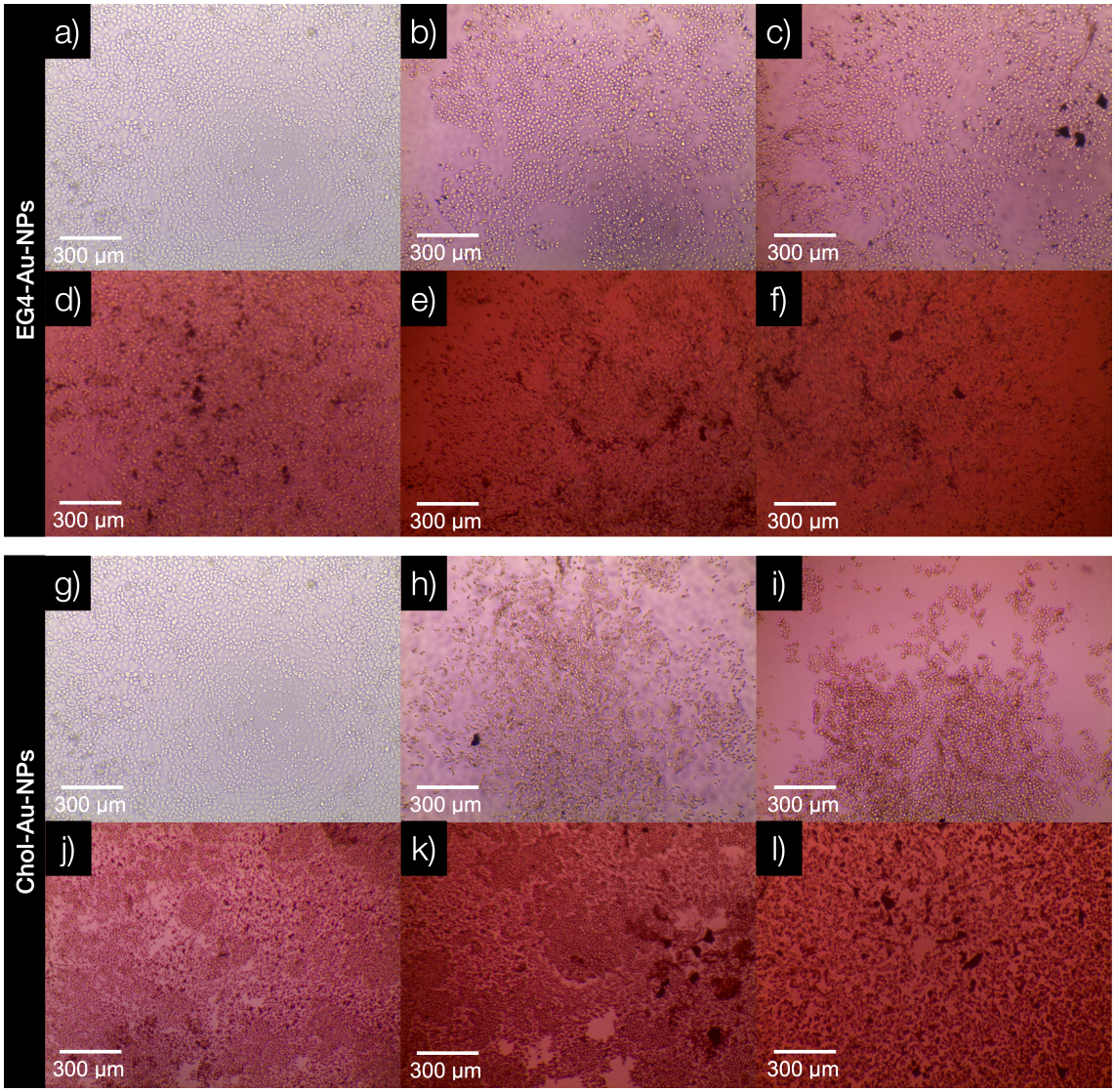


Figure 5.16: Images of AGS cells after 24 hours incubation with EG4- and Chol-Au-NPs. EG4-Au-NPs: a) AGS cells, b) 62.5 μg/ml, c) 125 μg/ml, d) 250 μg/ml, e) 500 μg/ml, f) 750 μg/ml. Chol-Au-NPs: g) AGS cells, h) 62.5 μg/ml, i) 125 μg/ml, j) 250 μg/ml, k) 500 μg/ml, l) 750 μg/ml.

Chapter 6

Conclusions and Future work

The goal of this dissertation was to develop a cholesterol based decoy specific for *H. pylori*. Ideally, this strategy would enhance *H. pylori* eradication, either by internalization onto the bacterial cells leading to death or by acting as a chemo attractant, which can be explored as co-adjutant to enhance the available therapeutic strategies.

First, proof-of-concept studies using SAMs functionalized with cholesterol were performed. Pure Cholesterol SAMs and Mixed Cholesterol/EG4-SAMs were designed with different ratios and characterization with Ellipsometry, OCA, XPS demonstrated that they were successfully done. Mixed-SAMs were selected to undergo further *in vitro* assays, as a more ordered surface is achieved. The ability of these surfaces to attract *H. pylori* was accessed by adhesion assays. For that, the *H. pylori* J99 strain was selected, since it is a human highly pathogenic strain. *H. pylori* J99 was incubated with Chol-PEG-SAMs for 2 hours. Results showed higher adhesion at 25% Chol-PEG-SAMs, indicating an optimum ratio to induce bacterial adhesion. The viability of *H. pylori* was also accessed and it was demonstrated that Chol-PEG-SAMs do not impair bacteria viability. Selectivity studies using 2 representative bacteria from the gut microbiota, *L. acidophilus* and *E. coli*, demonstrated that the engineered surfaces were highly selective towards *H. pylori*.

The main results of this proof-of-concept study were presented at the i3S Annual Meeting through poster: "Lipid-based Decoys for Gastric Infection Management: A Proof of Concept Study" (Appendix B).

The proof-of-concept study using SAMs validated the rational of using cholesterol based surfaces to specifically attract *H. pylori* selectively. This strategy was then translated to Au-NPs, a more bio-applicable approach.
EG4-Au-NPs and Mixed Chol(EG4)-Au-NPs were developed and characterized using Zetasizer. EG4-Au-NPs had 17 nm in diameter, charge of -18 mV, and 0.5 PdI, while Chol-Au-NPs had an average diameter of 20 nm, 4 mV charge and 0.3 PdI. The NPs response to different pH values (2.6, 4.0, 6.0 and 7.4) was also evaluated and it was demonstrated that Chol-Au-NPs were stable

in the range of pH tested, which suits their envisioned gastric application.
Different concentrations of both EG4- and Chol-Au-NPs (62.5, 125, 250, 500 and 750 μg/ml) were tested against *H. pylori* J99. Bactericidal effect was achieved at 500 μg/ml for EG4-Au-NPs and at 125 μg/ml for Chol-Au-NPs. Their cytotoxicity was evaluated against the AGS cell line (human gastric carcinoma) in a direct contact assay using the ISO 10,993–5;12 standard. The preliminary results of cells metabolic activity showed that Chol-Au-NPs were not cytotoxic at any of the concentrations tested. Only EG4-Au-NPs in a concentration of 750 μg/ml were cytotoxic (metabolic activity below 70%). Nonetheless, changes in cell morphology were observed after exposure to the NPs, which may indicate cellular stress. Further assays should be performed to better understand the interaction NPs-cells.
Overall, Chol-Au-NPs were stable in pH-gastric settings and compromised *H. pylori* viability without inducing cytotoxic effects (preliminary results). Therefore, this strategy appears as an excellent candidate for the development of a bioengineered decoy for gastric infection management.

To date and to the best of our knowledge, the development of a lipid–based (cholesterol) biomaterial to act as a decoy for *H. pylori* is a novelty. Although one study has been found in the literature involving the use of a cell-based decoy, it was dependent on antibiotic *in situ* delivery.

Besides the promising results obtained and the above-presented work, further studies are needed to strengthen this approach.

First, other *H. pylori* strains should be tested for their interaction with the Chol-PEG-SAMs/Chol-Au-NPs, since it is known that infection is commonly multi-strain. Although proof-of-concept results are promising for *H. pylori* J99 strain, different Cholesterol ratios may induce different responses in different strains. The *in vitro* adhesion assays with *H. pylori* can be complemented marking cholesterol fluorescently, for example using Filipin staining, which is specific for cholesterol [164]. This would allow visualizing cholesterol location and correlating it with bacteria adhesion. Adhesion assays performed in cholesterol supplemented medium, instead of PBS, could be performed to understand if when cholesterol is freely available, *H. pylori* behaviour towards the bioengineered surfaces would be impacted. Also, other bacteria widely found on the gut microbiota should be tested to further validate the specificity of the developed strategy and, consequently, safety towards normal gut microbiota.

The proof-of-concept study using SAMs could be extended to further exploring different steroids (cholesterol-like molecules) and their capability to attract *H. pylori*. Additional characterization of SAMs could be performed using AFM techniques for exploring SAMs topography, better understanding alkanethiols arrangement and steroids availability on the surface and how it influences bacteria adhesion.

For cholesterol quantification on the surfaces, the use of cholesterol esterase enzyme for the cleav-

age of the cholesterol moiety could be attempted.
An indirect method of quantification could also be tried. For that, ethanolic solutions of EG4- and Chol-PEG would be collected after 24 hours of incubation with gold surfaces and High Performance Liquid Chromatography (HPLC) would be used to quantify the remaining alkanethiols in solution.

As for studies using NPs, different Chol-PEG/EG4 ratios decorating Gold cores could be tested. These NPs must also be tested against gut microbiota bacteria to ensure its safety in what concerns dysbiosis. The degree of internalization should also be accessed using TEM (on going assays). If required, AMPs can be used in combination with the Chol-Au-NPs, being the latest used to attract the pathogen, while the AMP would lead to *H. pylori* death as previously described in our group [88].
Also, to further understand the mechanisms by which NPs cause *H. pylori* death, evaluation of the presence of intracellular Reactive Oxygen Species (ROS) could be performed, since the presence of ROS leads to bacteria death by inducing intracellular oxidation, variations on membranes potential and release of cellular content such as RNA. Quantification of RNA in solution should be used as a complement [165].

Fourier Transform Infrared Spectroscopy (FTIR) analyses can also be performed in the future to ensure the presence of Cholesterol groups on the surface of the Au-NPs. Potassium Bromide (KBr) pellet should be made with the Chol-Au-NPs and an expected peak at 1744 cm^{-1} (C=O) would confirm the presence of the cholesterol moiety [166].

The sterilization of NPs is another factor that must be studied, as it must not compromise the particles activity. UV irradiation and/or ethylene oxide are options to be considered [167].

Biocompatibility of these Au-NPs may be a concern since cells can recognize cholesterol and thus interact with the developed Chol-Au-NPs. Further studies are needed with different cell lines. In case Chol-Au-NPs are cytotoxic for other cell lines, the cholesterol molecule can be replaced by another steroid previously screened on the proof-of-concept stage, as for instance ergoesterol, a sterol found in fungal cell membranes, very similar to the cholesterol molecule [168].

If and when all the *in vitro* tests are performed and the safety, specificity and excellent biological performance of the designed strategy are ensured, the next step would be to undergo *in vivo* validation using an appropriate model for gastric infection, namely the Black-6 mice model.

Appendix A

Au-NPs characterization after production

A.1 Materials and Methods

1 mg/mL of Au-NPs were diluted in 1:10 ratio in MilliQ water and placed in a clean disposable cuvette. Particle size was also determined using light scattering via Zeta PALS Zeta Potential Analyzer and Zeta Plus Particle Sizing Software, v. 2.27 (Brookhaven Instruments Corporation). Typically, all sizing measurements were performed at 25 °C, and all data were recorded at 90°, with an equilibration time of 5 minutes and individual run times of 60 seconds.

A.2 Results

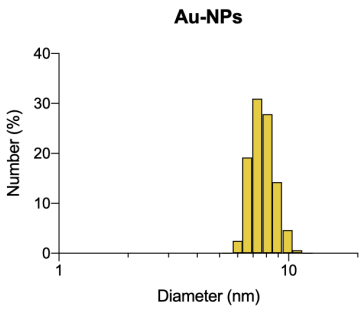


Figure A.1: Histogram of size distribution of the produced Au-NPs after production, revealing a size diameter between 7.1 and and 8.3 nm.

Appendix B

i3S Annual Meeting (2019): "Lipid-based Decoys for Gastric Infection Management: A Proof of Concept Study"

P168

POSTER COMMUNICATION

Lipid-based Decoys for Gastric Infection Management: Proof of Concept Study using Self-Assembled Monolayers

R. M. Pereira[1,2,3], M. Cristina. L. Martins[1,2,4], P. Parreira[1,2]

[1]i3S - Instituto de Investigação e Inovação em Saúde, Universidade do Porto, Portugal; [2]Bioengineered Surfaces Group, INEB - Instituto de Engenharia Biomédica, Portugal [3]FEUP – Faculdade de Engenharia da Universidade do Porto, Portugal; [4]ICBAS, Instituto de Ciências Biomédicas Abel Salazar, Universidade do Porto, Portugal

Helicobacter pylori(*H. pylori*) is linked to increased risk of peptic ulcer disease, gastritis and gastric cancer[1]. Available treatments for *H. pylori* are obsolete, mainly due to antimicrobial resistance to antibiotics[2]. Thus, other therapeutic strategies must be explored. Since *H. pylori* is auxotrophic for cholesterol, extracting this lipid from the host epithelial cells[3], bioengineered cholesterol-based decoys could be of interest for *H. pylori* infection management. Here, the proof of concept studies for development of a lipid (cholesterol)-based decoy are described.

Mixed Self-Assembled Monolayers on gold(SAMs) of Cholesterol-terminated polyethyleneglycol(Chol-PEG) and tetra(ethylene glycol)(EG4) thiols were developed (Chol-SAMs). The PEG chain helps to expose the cholesterol molecule and the EG4 allows having a more compacted and ordered surface[4]. Chol-SAMs were prepared by immersion of gold substrates in solutions containing different ratios of EG4/Chol-PEG (0(100%EG4)/12.5/25/50/75/100%(0 % EG4)) at a final concentration of 0.1mM. Thickness and wettability were determined by ellipsometry and optical contact angle measurements. SAMs thickness and hydrophobicity increased with increasing Chol-PEG concentration as expected, from 37º to 50º (100%Chol-SAMs) and from 2.5nm to 4nm (100% Chol-SAMs), respectively.

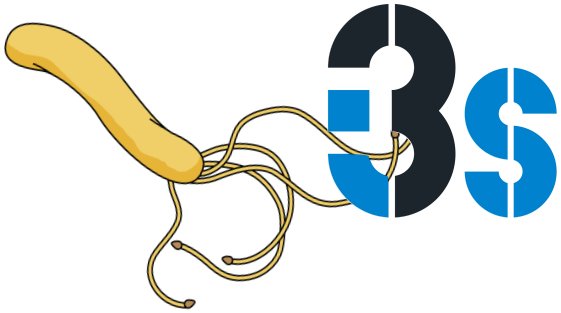
Ability of the bioengineered surfaces to attract *H. pylori* J99 strain was accessed by *in vitro* adhesion assays. Surfaces were incubated with a bacterial suspension(1x10^7 CFU/mL) at 37ºC,microaerophilic conditions,150 r.p.m. After 30min and 2h, surfaces were rinsed and bacteria stained with DAPI as described elsewhere[5]. Surfaces were then visualized under inverted fluorescence microscope, 40x magnification. Bacterial counts were performed based on photographs from 9 random fields.

After 30min, adhesion was higher for Chol-SAMs compared to EG4-SAMs (0% Chol-PEG). Adhesion to SAMs was time dependent, with more bacteria adhered after 2h, in accordance to previous work. After 2h, the number of adhered bacteria increased from 0% to 25%Chol-SAMs, being this surface the one with higher adhesion. A decrease in the number of adherent bacteria from 25 to 100% Chol-SAMs was seen and, more interestingly, the number of adhered bacteria at 100% Chol-SAMs is lower than the one in the control group (EG4; 0% Chol-PEG). These results indicate that an optimum ratio is required to induce bacterial adhesion.

In conclusion, Chol-SAMs were successfully engineered. *H. pylori* adhered to cholesterol presenting surfaces in a time dependent manner. The maximum adhered bacteria were reached after 2h and onto 25% Chol-SAMs. These preliminary assays demonstrate that this strategy may be useful for development of newer therapeutic strategies.

References:
[1] Dang, et. al. Nat Rev Gastro Hepat, 2017
[2] Malfertheiner, *et al*.Maastricht consensus report, 2017
[3] Wanibuchi, et. al, Gastritis-New Approaches and Treatments, 2019
[4] Parreira,*et al*, Acta Biomaterialia, 2013
[5] Parreira,*et al*, J. Biomed. Mater. Res., 2011

Lipid-based Decoys for Gastric Infection Management: A Proof of Concept Study



R. M. Pereira[1,2,3], M. Cristina L. Martins[1,2,4], P. Parreira[1,2]
[1]i3S - Instituto de Investigação e Inovação em Saúde, Universidade do Porto, Portugal; [2]Bioengineered Surfaces Group, INEB - Instituto de Engenharia Biomédica, Portugal; [3]FEUP – Faculdade de Engenharia da Universidade do Porto, Portugal; [4]ICBAS, Instituto de Ciências Biomédicas Abel Salazar, Universidade do Porto, Portugal

Introduction

Helicobacter pylori (*H. pylori*) is linked to an increased risk of peptic ulcer disease, gastritis and gastric cancer, having an estimated prevalence of 50% of the world's population[1]. Available treatments for *H. pylori* are obsolete, mainly due to antimicrobial resistance to antibiotics[2]. Thus, other therapeutic strategies must be explored.

H. pylori is auxotrophic for cholesterol, extracting this lipid from the host epithelial cells[3].Therefore, bioengineered cholesterol-based decoys could present an interesting approach for *H. pylori* infection management.

Here, proof of concept studies for development of a lipid (cholesterol)-based decoy are described. For that, cholesterol presenting Self-Assembled Monolayers on gold (SAMs) were designed. SAMs are well-defined model surfaces that allow to perform proof-of-concept studies at the molecular level[4].

SAMs formation

Mixed SAMs of Cholesterol-terminated polyethyleneglycol (Chol-PEG; Nanocs®), and tetra(ethylene glycol) (EG4; Sigma®) were developed (Chol-SAMs), adapting a previously published protocol[4]. Briefly, SAMs were prepared by immersion of gold substrates in solutions containing different ratios of EG4/Chol-PEG (0.1 mM), from 0% Chol-PEG (100% EG4, control surfaces) to 100%Chol-PEG (0% EG4) (Figure 1).

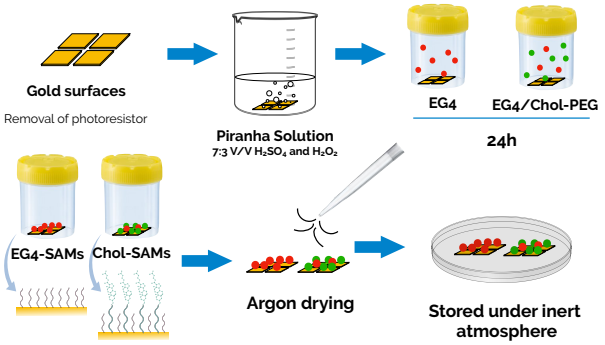


Figure 1. Schematic representation of the Chol-SAMs preparation method. (schematic representation not to scale) ● EG4, ● Chol-PEG.

SAMs characterization

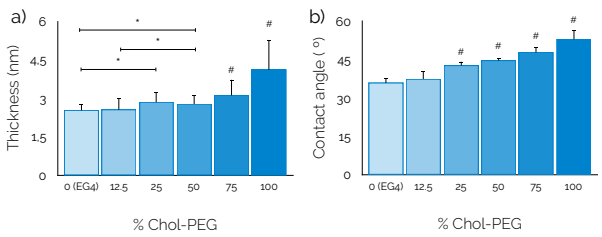


Figure 2. Chol-SAMs characterization: a) Ellipsometry b). Optical contact angle; * - statistically significant different, # - statistically significant from all the other tested surfaces. (Mann-Whitney; $p<0.05$)

Thickness and wettability were determined by ellipsometry and optical contact angle measurements.

- SAMs thickness increased from 2.5 nm to 4 nm with increasing Chol-PEG concentration (Figure 2a);
- Optical contact angle increased from 37° to 50° with increasing Chol-PEG concentration (Figure 2b);

Adhesion assay

H. pylori J99 strain was cultured in blood agar with an antibiotics cocktail as described elsewhere.[4] Surfaces were pre-incubated with Phosphate buffer saline (PBS). Afterwards, surfaces were incubated with a bacterial suspension adjusted to 1x10^7 CFU/mL, 37°C, microaerophilic conditions, 150 r.p.m. After 30min and 2h, surfaces were rinsed twice with PBS, stained with Vectashield® with DAPI and visualized under inverted fluorescence microscope, 40x magnification[5] (Figure 3). Bacterial counts were performed based on photographs from 9 random fields and expressed as bacteria/mm^2.

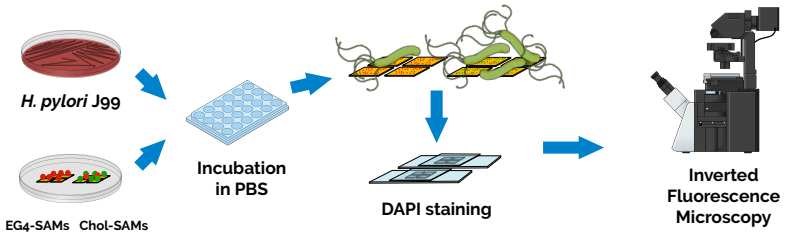


Figure 3. Schematic representation of the adhesion assay to Chol-SAMs. (not to scale)

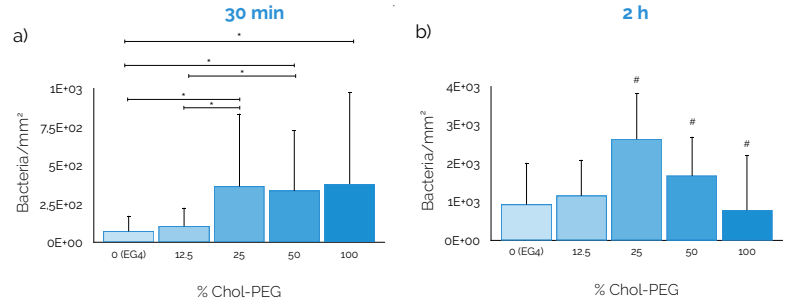


Figure 4. *H. pylori* adhesion to Chol-SAMS after a) 30 minutes and b) 2 hours. * - statistically significant different, # - statistically significant from all the other tested surfaces. (Mann-Whitney; $p<0.05$)

- After 30min, adhesion was higher for all Chol-SAMs compared to EG4-SAMs (0% Chol-PEG).
- After 2h (adhesion plateau[5]), the number of adhered bacteria increased from 0% to 25% Chol-SAMs, being this the one with higher adhesion.
- A decrease in the number of adherent bacteria from 25 to 100% Chol-SAMs was seen which indicate that an optimum ratio is required to induce bacterial adhesion.

Conclusions

- Chol-SAMs were successfully engineered.
- *H. pylori* adhered to Chol.-SAMs in a concentration dependent way.
- The maximum adhered bacteria were reached onto 25% Chol-SAMs.
- These proof of concept assay demonstrate that this strategy may be useful for development of a decoy targeting *H. pylori*.

References

[1]Dang,*et. al.*Nat Rev Gastro Hepat.2017,
[2]Malfertheiner,*et al.*Maastricht consensus report.2017,
[3]Wanibuchi,*et. al.*Gastritis-New Approaches and Treatments.2019,
[4]Parreira,*et al.*Acta Biomaterialia.2013,
[5]Parreira,*et al.*, J. Biomed. Mater. Res.,*2011*

Acknowledgments

This work was supported by FEDER - Fundo Europeu de Desenvolvimento Regional funds through the COMPETE 2020 - Operational Program for Competitiveness and Internationalization (POCI), Portugal 2020 and NORTE-01-0145-FEDER-000012 and by FCT - Fundação para a Ciência e a Tecnologia/Ministério da Ciência, Tecnologia e Inovação through the POCI-01-0145-FEDER-007274.
PyloriBinders - Helicobacter pylori specific biomaterials for antibiotic-free treatment/diagnostic of gastric infection (PTDC/CTM-BIO/4043/2014) UID/QUI/50006/2013 (LAQV-REQUIMTE) projects.
The authors also would like to acknowledge the support of the Biointerfaces and Nanotechnology i3S Scientific Platform (PPBI-POCI-01-0145-FEDER-022122 and UID/BIM/04293/2019, respectively) & Portuguese Platform of Bioimaging i3s Scientific Platform (PPBI-POCI-01-0145-FEDER-022122).

INSTITUTO DE INVESTIGAÇÃO E INOVAÇÃO EM SAÚDE
UNIVERSIDADE DO PORTO

Rua Alfredo Allen, 208
4200-135 Porto
Portugal

+351 220 408 800

www.i3s.up.pt

References

[1] Marina Da Conceição Pinto Azevedo-Vethacke. The effect of proton pump inhibitors (ppis) on the orientation of *Helicobacter pylori* in the gastric mucus of the mongolian gerbil *in vivo*. 2008.

[2] Anthony O'connor, Colm A O'morain, and Alexander C Ford. Population screening and treatment of helicobacter pylori infection. *Nature reviews Gastroenterology & hepatology*, 14(4):230, 2017.

[3] James KY Hooi, Wan Ying Lai, Wee Khoon Ng, Michael MY Suen, Fox E Underwood, Divine Tanyingoh, Peter Malfertheiner, David Y Graham, Vincent WS Wong, Justin CY Wu, et al. Global prevalence of helicobacter pylori infection: systematic review and meta-analysis. *Gastroenterology*, 153(2):420–429, 2017.

[4] Paula Parreira, M Fátima Duarte, Celso A Reis, and M Cristina L Martins. Helicobacter pylori infection: a brief overview on alternative natural treatments to conventional therapy. *Critical reviews in microbiology*, 42(1):94–105, 2016.

[5] Sara Lindén. *Helicobacter pylori binding to gastric mucins and host glycosylation changes after inoculation*. Lund University, 2004.

[6] Holly M Scott Algood and Timothy L Cover. Helicobacter pylori persistence: an overview of interactions between h. pylori and host immune defenses. *Clinical microbiology reviews*, 19(4):597–613, 2006.

[7] Anurag Verma, Juhi Dubey, Rahul Rama Hegde, Vaibhav Rastogi, and JK Pandit. Helicobacter pylori: past, current and future treatment strategies with gastroretentive drug delivery systems. *Journal of drug targeting*, 24(10):897–915, 2016.

[8] Jyh-Ming Liou, Po-Yueh Chen, Yu-Ting Kuo, Ming-Shiang Wu, et al. Toward population specific and personalized treatment of helicobacter pylori infection. *Journal of biomedical science*, 25(1):70, 2018.

[9] Hirofumi Shimomura, Kouichi Hosoda, Shunji Hayashi, Kenji Yokota, and Yoshikazu Hirai. Phosphatidylethanolamine of helicobacter pylori functions as a steroid-binding lipid in the assimilation of free cholesterol and 3β-hydroxl steroids into the bacterial cell membrane. *Journal of bacteriology*, 194(10):2658–2667, 2012.

[10] Kiyofumi Wanibuchi, Hisashi Masui, Takashi Takahashi, and Hirofumi Shimomura. Development of a novel antibacterial medicine that targets a characteristic lipid of the cell membranes of helicobacter pylori. In *Gastritis-New Approaches and Treatments*. IntechOpen, 2019.

[11] Pau Morey and Thomas F Meyer. The sweeping role of cholesterol depletion in the persistence of helicobacter pylori infections. In *Molecular Mechanisms of Inflammation: Induction, Resolution and Escape by Helicobacter pylori*, pages 209–227. Springer, 2019.

[12] JitKang Lim, Swee Pin Yeap, Hui Xin Che, and Siew Chun Low. Characterization of magnetic nanoparticle by dynamic light scattering. *Nanoscale research letters*, 8(1):381, 2013.

[13] Chihiro Kageyama, Mayu Sato, Hiroyuki Sakae, Yuka Obayashi, Yoshiro Kawahara, Takehiko Mima, Osamu Matsushita, Kenji Yokota, Motowo Mizuno, and Hiroyuki Okada. Increase in antibiotic resistant helicobacter pylori in a university hospital in japan. *Infection and Drug Resistance*, 12:597, 2019.

[14] Amro Metwaly Hassan, Muhammad Abd El-Gawad Shawky, Ahmed Qasem Mohammed, Mustafa Ahmed Haridy, and Khaled Abd-El-Azeem Eid. Simvastatin improves the eradication rate of helicobacter pylori: upper egypt experience. *Infection and Drug Resistance*, 12:1529, 2019.

[15] Prashanth Rawla and Adam Barsouk. Epidemiology of gastric cancer: global trends, risk factors and prevention. *Gastroenterology Review/Przegląd Gastroenterologiczny*, 13(1), 2019.

[16] Larissa Spósito, Fernando Bombarda Oda, Júlia Hunger Vieira, Flávio Alexandre Carvalho, Matheus Aparecido dos Santos Ramos, Rogério Cardoso de Castro, Eduardo José Crevelin, Antônio Eduardo Miller Crotti, André Gonzaga Santos, Patrícia Bento da Silva, et al. In vitro and in vivo anti-helicobacter pylori activity of casearia sylvestris leaf derivatives. *Journal of ethnopharmacology*, 233:1–12, 2019.

[17] Nicole Tegtmeyer and Steffen Backert. *Molecular Pathogenesis and Signal Transduction by Helicobacter Pylori*, volume 400. Springer, 2017.

[18] Peter Malfertheiner, Michael Selgrad, Thomas Wex, Benedetta Romi, Erica Borgogni, Fabiana Spensieri, Luisanna Zedda, Paolo Ruggiero, Laura Pancotto, Stefano Censini, et al. Efficacy, immunogenicity, and safety of a parenteral vaccine against helicobacter pylori in healthy volunteers challenged with a cag-positive strain: a randomised, placebo-controlled phase 1/2 study. *The Lancet Gastroenterology & Hepatology*, 3(10):698–707, 2018.

[19] Sho Suzuki, Mitsuru Esaki, Chika Kusano, Hisatomo Ikehara, and Takuji Gotoda. Development of helicobacter pylori treatment: How do we manage antimicrobial resistance? *World Journal of Gastroenterology*, 25(16):1907–1912, 2019.

[20] David J McGee, Alika E George, Elizabeth A Trainor, Katherine E Horton, Ellen Hildebrandt, and Traci L Testerman. Cholesterol enhances helicobacter pylori resistance to antibiotics and ll-37. *Antimicrobial agents and chemotherapy*, 55(6):2897–2904, 2011.

[21] Carlo A Fallone, Steven F Moss, and Peter Malfertheiner. Reconciliation of recent helicobacter pylori treatment guidelines in a time of increasing resistance to antibiotics. *Gastroenterology*, 2019.

[22] Rod R Seeley, TD Stephens, and P Tate. Anatomy & physiology. 6th. *Boston: McGraw Hill*, 21(1116):42, 2017.

[23] Christian Wunder, Yuri Churin, Florian Winau, Dirk Warnecke, Michael Vieth, Buko Lindner, Ulrich Zähringer, Hans-Joachim Mollenkopf, Ernst Heinz, and Thomas F Meyer. Cholesterol glucosylation promotes immune evasion by helicobacter pylori. *Nature medicine*, 12(9):1030, 2006.

[24] C Ciacci and G Mazzacca. The history of helicobacter pylori: A reflection on the relationship between the medical community and industry. *Digestive and liver disease*, 38(10):778–780, 2006.

[25] JW Konturek. Discovery by jaworski of helicobacter pylori. *Journal of physiology and pharmacology*, 54(S3):23–41, 2003.

[26] James Murray Luck and Trilok Nath Seth. Gastric urease. *Biochemical Journal*, 18(6):1227, 1924.

[27] J Robin Warren and Barry Marshall. Unidentified curved bacilli on gastric epithelium in active chronic gastritis. *The lancet*, 321(8336):1273–1275, 1983.

[28] Lydia E Wroblewski, Richard M Peek, and Keith T Wilson. Helicobacter pylori and gastric cancer: factors that modulate disease risk. *Clinical microbiology reviews*, 23(4):713–739, 2010.

[29] Rhonda R Caston, John T Loh, Bradley J Voss, W Hayes McDonald, Matthew B Scholz, Mark S McClain, and Timothy L Cover. Effect of environmental salt concentration on the helicobacter pylori exoproteome. *Journal of proteomics*, 2019.

[30] Paula Cristina Castro Parreira et al. Engineering surfaces to enhance helicobacter pylori specific binding. 2013.

[31] D Forman, DG Newell, F Fullerton, JW Yarnell, AR Stacey, N Wald, and F Sitas. Association between infection with helicobacter pylori and risk of gastric cancer: evidence from a prospective investigation. *Bmj*, 302(6788):1302–1305, 1991.

[32] Genzhu Wang, Jing Pang, Xinxin Hu, Tongying Nie, Xi Lu, Xue Li, Xiukun Wang, Yun Lu, Xinyi Yang, Jiandong Jiang, et al. Daphnetin: A novel anti-helicobacter pylori agent. *International journal of molecular sciences*, 20(4):850, 2019.

[33] Lin Sun, Xiaoyan Zhang, Yuxiao Zhang, Kai Zheng, Qiaoyan Xiang, Ning Chen, Zhiyun Chen, Nan Zhang, Junping Zhu, and Qiushui He. Antibiotic-induced disruption of gut microbiota alters local metabolomes and immune responses. *Frontiers in cellular and infection microbiology*, 9:99, 2019.

[34] Martin J Blaser and John C Atherton. Helicobacter pylori persistence: biology and disease. *The Journal of clinical investigation*, 113(3):321–333, 2004.

[35] NF Azevedo, AP Pacheco, CW Keevil, and MJ Vieira. Adhesion of water stressed helicobacter pylori to abiotic surfaces. *Journal of Applied Microbiology*, 101(3):718–724, 2006.

[36] Howard C Berg and Linda Turner. Movement of microorganisms in viscous environments. *Nature*, 278(5702):349, 1979.

[37] Muhannad Sarem and Rodolfo Corti. Role of helicobacter pylori coccoid forms in infection and recrudescence. *Gastroenterología y Hepatología (English Edition)*, 39(1):28–35, 2016.

[38] J Ferlay, DM Parkin, and E Steliarova-Foucher. Estimates of cancer incidence and mortality in europe in 2008. *European journal of cancer*, 46(4):765–781, 2010.

[39] P Malfertheiner, F Megraud, CA O'morain, JP Gisbert, EJ Kuipers, AT Axon, Franco Bazzoli, A Gasbarrini, John Atherton, David Y Graham, et al. Management of helicobacter pylori infection—the maastricht v/florence consensus report. *Gut*, 66(1):6–30, 2017.

[40] Pelayo Correa and Maria Blanca Piazuelo. Natural history of helicobacter pylori infection. *Digestive and Liver Disease*, 40(7):490–496, 2008.

[41] Pelayo Correa. Human gastric carcinogenesis: a multistep and multifactorial process—first american cancer society award lecture on cancer epidemiology and prevention. *Cancer research*, 52(24):6735–6740, 1992.

[42] Arnoud HM Van Vliet, Florian D Ernst, and Johannes G Kusters. Nikr-mediated regulation of helicobacter pylori acid adaptation. *Trends in microbiology*, 12(11):489–494, 2004.

[43] Bárbara Peleteiro, Ana Bastos, Ana Ferro, and Nuno Lunet. Prevalence of helicobacter pylori infection worldwide: a systematic review of studies with national coverage. *Digestive diseases and sciences*, 59(8):1698–1709, 2014.

[44] FF Vale and JMB Vítor. Transmission pathway of helicobacter pylori: does food play a role in rural and urban areas? *International journal of food microbiology*, 138(1-2):1–12, 2010.

[45] Samantha Morais, Ana Ferro, Ana Bastos, Clara Castro, Nuno Lunet, and Bárbara Peleteiro. Trends in gastric cancer mortality and in the prevalence of helicobacter pylori infection in portugal. *European journal of cancer prevention*, 25(4):275–281, 2016.

[46] Elisabete Coelho, Ana Magalhães, Mário Dinis-Ribeiro, and Celso A Reis. Molecular mechanisms for adhesion and colonization of human gastric mucosa by helicobacter pylori and its clinical implications. *Acta medica portuguesa*, 29(7-8):476–483, 2016.

[47] Leonardo H Eusebi, Rocco M Zagari, and Franco Bazzoli. Epidemiology of helicobacter pylori infection. *Helicobacter*, 19:1–5, 2014.

[48] NF Azevedo. *Survival of Helicobacter pylori in drinking water and associated biofilms*. PhD thesis, 2005.

[49] Ciara Dunne, Brendan Dolan, and Marguerite Clyne. Factors that mediate colonization of the human stomach by helicobacter pylori. *World Journal of Gastroenterology: WJG*, 20(19):5610, 2014.

[50] Cheng-Yen Kao, Bor-Shyang Sheu, and Jiunn-Jong Wu. Helicobacter pylori infection: An overview of bacterial virulence factors and pathogenesis. *Biomedical journal*, 39(1):14–23, 2016.

[51] Jonathan P Celli, Bradley S Turner, Nezam H Afdhal, Randy H Ewoldt, Gareth H McKinley, Rama Bansil, and Shyamsunder Erramilli. Rheology of gastric mucin exhibits a ph-dependent sol- gel transition. *Biomacromolecules*, 8(5):1580–1586, 2007.

[52] Yen-Ting Chu, Ya-Hui Wang, Jiunn-Jong Wu, and Huan-Yao Lei. Invasion and multiplication of helicobacter pylori in gastric epithelial cells and implications for antibiotic resistance. *Infection and immunity*, 78(10):4157–4165, 2010.

[53] Ying Huang, Qi-long Wang, Dan-dan Cheng, Wen-ting Xu, and Nong-hua Lu. Adhesion and invasion of gastric mucosa epithelial cells by helicobacter pylori. *Frontiers in cellular and infection microbiology*, 6:159, 2016.

[54] Terry Kwok, Steffen Backert, Heinz Schwarz, Jürgen Berger, and Thomas F Meyer. Specific entry of helicobacter pylori into cultured gastric epithelial cells via a zipper-like mechanism. *Infection and immunity*, 70(4):2108–2120, 2002.

[55] Ya-Hui Wang, Jiunn-Jong Wu, and Huan-Yao Lei. The autophagic induction in helicobacter pylori-infected macrophage. *Experimental biology and medicine*, 234(2):171–180, 2009.

[56] Ya-Hui Wang, Jean-Pierre Gorvel, Yen-Ting Chu, Jiunn-Jong Wu, and Huan-Yao Lei. Helicobacter pylori impairs murine dendritic cell responses to infection. *PLoS One*, 5(5):e10844, 2010.

[57] Timothy L Cover, CiP Dooley, and MJ Blaser. Characterization of and human serologic response to proteins in helicobacter pylori broth culture supernatants with vacuolizing cytotoxin activity. *Infection and Immunity*, 58(3):603–610, 1990.

[58] JE Crabtree, JD Taylor, RV Heatley, TM Shallcross, BJ Rathbone, JI Wyatt, and DS Tompkins. Mucosal iga recognition of helicobacter pylori 120 kda protein, peptic ulceration, and gastric pathology. *The Lancet*, 338(8763):332–335, 1991.

[59] Martin J Blaser, Guillermo I Perez-Perez, Harry Kleanthous, Timothy L Cover, Richard M Peek, PH Chyou, Grant N Stemmermann, and Abraham Nomura. Infection with helicobacter pylori strains possessing caga is associated with an increased risk of developing adenocarcinoma of the stomach. *Cancer research*, 55(10):2111–2115, 1995.

[60] John C Atherton and Martin J Blaser. Coadaptation of helicobacter pylori and humans: ancient history, modern implications. *The Journal of clinical investigation*, 119(9):2475–2487, 2009.

[61] John C Atherton. The pathogenesis of helicobacter pylori–induced gastro-duodenal diseases. *Annu. Rev. Pathol. Mech. Dis.*, 1:63–96, 2006.

[62] Pau Morey, Lennart Pfannkuch, Ervinna Pang, Francesco Boccellato, Michael Sigal, Aki Imai-Matsushima, Victoria Dyer, Manuel Koch, Hans-Joachim Mollenkopf, Philipp Schlaermann, et al. Helicobacter pylori depletes cholesterol in gastric glands to prevent interferon gamma signaling and escape the inflammatory response. *Gastroenterology*, 154(5):1391–1404, 2018.

[63] Bianca Bauer, Ervinna Pang, Carsten Holland, Mirjana Kessler, Sina Bartfeld, and Thomas F Meyer. The helicobacter pylori virulence effector caga abrogates human β-defensin 3 expression via inactivation of egfr signaling. *Cell host & microbe*, 11(6):576–586, 2012.

[64] Sabine Nuding, Michael Gersemann, Yoshio Hosaka, Sabrina Konietzny, Christian Schaefer, Julia Beisner, Bjoern O Schroeder, Maureen J Ostaff, Katunori Saigenji, German Ott, et al. Gastric antimicrobial peptides fail to eradicate helicobacter pylori infection due to selective induction and resistance. *PLoS One*, 8(9), 2013.

[65] Peter Malfertheiner, F Megraud, C O'morain, APS Hungin, R Jones, A Axon, DY Graham, G Tytgat, and European Helicobacter Pylori Study Group (EHPSG). Current concepts in the management of helicobacter pylori infection—the maastricht 2-2000 consensus report. *Alimentary pharmacology & therapeutics*, 16(2):167–180, 2002.

[66] Chika Kusano, Takuji Gotoda, Sho Suzuki, Hisatomo Ikehara, and Mitsuhiko Moriyama. Safety of first-line triple therapy with a potassium-competitive acid blocker for helicobacter pylori eradication in children. *Journal of gastroenterology*, 53(6):718–724, 2018.

[67] Maria Pina Dore, Hong Lu, and David Y Graham. Role of bismuth in improving helicobacter pylori eradication with triple therapy. *Gut*, 65(5):870–878, 2016.

[68] Pedro Boal Carvalho, Joana Magalhães, Francisca Dias de Castro, Bruno Rosa, and José Almeida Berkeley Cotter. Randomized controlled trial for helicobacter pylori eradication in a naive portuguese population: Is sequential treatment superior to triple therapy in real world clinical setting? 2017.

[69] Rocco Maurizio Zagari, Stefano Rabitti, Leonardo Henry Eusebi, and Franco Bazzoli. Treatment of helicobacter pylori infection: A clinical practice update. *European journal of clinical investigation*, 48(1):e12857, 2018.

[70] Chen-Li Ye, Guo-Ping Liao, Shuai He, Yan-Na Pan, Ying-Bo Kang, and Zhong-Yi Zhang. Levofloxacin and proton pump inhibitor-based triple therapy versus standard triple first-line therapy for helicobacter pylori eradication. *Pharmacoepidemiology and drug safety*, 23(5):443–455, 2014.

[71] Min Jun Song, Dong Il Park, Jung Ho Park, Hong Joo Kim, Yong Kyun Cho, Chong Il Sohn, Woo Kyu Jeon, and Byung Ik Kim. The effect of probiotics and mucoprotective agents on ppi-based triple therapy for eradication of helicobacter pylori. *Helicobacter*, 15(3):206–213, 2010.

[72] Carlo A Fallone, Naoki Chiba, Sander Veldhuyzen van Zanten, Lori Fischbach, Javier P Gisbert, Richard H Hunt, Nicola L Jones, Craig Render, Grigorios I Leontiadis, Paul Moayyedi, et al. The toronto consensus for the treatment of helicobacter pylori infection in adults. *Gastroenterology*, 151(1):51–69, 2016.

[73] William D Chey, Grigorios I Leontiadis, Colin W Howden, and Steven F Moss. Acg clinical guideline: treatment of helicobacter pylori infection. *The American journal of gastroenterology*, 112(2):212, 2017.

[74] Adrian G McNicholl, Dmitry S Bordin, Alfredo Lucendo, Galina Fadeenko, Manuel Castro Fernandez, Irina Voynovan, Natalia Valerievna Zakharova, Aiman Silkanovna Sarsenbaeva, Luis Bujanda, Ángeles Perez-Aisa, et al. Combination of bismuth and standard triple therapy eradicates helicobacter pylori infection in more than 90% of patients. *Clinical Gastroenterology and Hepatology*, 2019.

[75] Florent Ailloud, Xavier Didelot, Sabrina Woltemate, Gudrun Pfaffinger, Jörg Overmann, Ruth Christiane Bader, Christian Schulz, Peter Malfertheiner, and Sebastian Suerbaum. Within-host evolution of helicobacter pylori shaped by niche-specific adaptation, intragastric migrations and selective sweeps. *Nature communications*, 10(1):2273, 2019.

[76] SMA Campo, A Zullo, Cesare Hassan, and S Morini. Antibiotic treatment strategies for helicobacter pylori infection. *Recent patents on anti-infective drug discovery*, 2(1):11–17, 2007.

[77] Ramanan Laxminarayan, Precious Matsoso, Suraj Pant, Charles Brower, John-Arne Røttingen, Keith Klugman, and Sally Davies. Access to effective antimicrobials: a worldwide challenge. *The Lancet*, 387(10014):168–175, 2016.

[78] V Ricci, R Zarrilli, and Marco Romano. Voyage of helicobacter pylori in human stomach: odyssey of a bacterium. *Digestive and Liver Disease*, 34(1):2–8, 2002.

[79] PO Erah, AF Goddard, DA Barrett, PN Shaw, and RC Spiller. The stability of amoxycillin, clarithromycin and metronidazole in gastric juice: relevance to the treatment of helicobacter pylori infection. *The Journal of antimicrobial chemotherapy*, 39(1):5–12, 1997.

[80] Hiroki Tanabe, Katsuyoshi Ando, Kiichi Sato, Takahiro Ito, Mitsuru Goto, Tomonobu Sato, Akihiro Fujinaga, Toru Kawamoto, Tatsuya Utsumi, Nobuyuki Yanagawa, et al. Efficacy of vonoprazan-based triple therapy for helicobacter pylori eradication: a multicenter study and a review of the literature. *Digestive diseases and sciences*, 62(11):3069–3076, 2017.

[81] Richard H Hunt and Carmelo Scarpignato. Potent acid suppression with ppis and p-cabs: what's new? *Current treatment options in gastroenterology*, 16(4):570–590, 2018.

[82] Philip Sutton. Progress in vaccination against helicobacter pylori. *Vaccine*, 19(17-19):2286–2290, 2001.

[83] Filipa F Vale and Mónica Oleastro. Overview of the phytomedicine approaches against helicobacter pylori. *World Journal of Gastroenterology: WJG*, 20(19):5594, 2014.

[84] Yuan-Chuen Wang. Medicinal plant activity on helicobacter pylori related diseases. *World Journal of Gastroenterology: WJG*, 20(30):10368, 2014.

[85] Xiao-Lin Zhang, An-Min Jiang, Zhong-You Ma, Xian-Bao Li, You-Yi Xiong, Jin-Feng Dou, and Jian-Fei Wang. The synthetic antimicrobial peptide pexiganan and its nanoparticles (pnps) exhibit the anti-helicobacter pylori activity in vitro and in vivo. *Molecules*, 20(3):3972–3985, 2015.

[86] Inês C Gonçalves, Ana Magalhães, Ana MS Costa, José R Oliveira, Patrícia C Henriques, Paula Gomes, Celso A Reis, and M Cristina L Martins. Bacteria-targeted biomaterials: Glycan-coated microspheres to bind helicobacter pylori. *Acta biomaterialia*, 33:40–50, 2016.

[87] Catarina Leal Seabra, Cláudia Nunes, Manuela Brás, Maria Gomez-Lazaro, Celso A Reis, Inês C Gonçalves, Salette Reis, and M Cristina L Martins. Lipid nanoparticles to counteract gastric infection without affecting gut microbiota. *European Journal of Pharmaceutics and Biopharmaceutics*, 127:378–386, 2018.

[88] Paula Parreira, Claudia Monteiro, Vanessa Graça, Joana Gomes, Sílvia Maia, Paula Gomes, Inês C Gonçalves, and M Cristina L Martins. Surface grafted msi-78a antimicrobial peptide has high potential for gastric infection management. *Scientific Reports*, 9(1):1–11, 2019.

[89] Chih-Ho Lai, Yuan-Man Hsu, Hung-Jung Wang, and Wen-Ching Wang. Manipulation of host cholesterol by helicobacter pylori for their beneficial ecological niche. *BioMedicine*, 3(1):27–33, 2013.

[90] Anne-Helene Lebrun, Christian Wunder, Janosch Hildebrand, Yuri Churin, Ulrich Zähringer, Buko Lindner, Thomas F Meyer, Ernst Heinz, and Dirk Warnecke. Cloning of a cholesterol-α-glucosyltransferase from helicobacter pylori. *Journal of Biological Chemistry*, 281(38):27765–27772, 2006.

[91] Kai Simons and Julio L Sampaio. Membrane organization and lipid rafts. *Cold Spring Harbor perspectives in biology*, 3(10):a004697, 2011.

[92] Hung-Jung Wang, Wen-Chi Cheng, Hsin-Hung Cheng, Chih-Ho Lai, and Wen-Ching Wang. Helicobacter pylori cholesteryl glucosides interfere with host membrane phase and affect type iv secretion system function during infection in ags cells. *Molecular microbiology*, 83(1):67–84, 2012.

[93] Shin-Yi Du, Hung-Jung Wang, Hsin-Hung Cheng, Sheng-De Chen, Lily Hui-Ching Wang, and Wen-Ching Wang. Cholesterol glucosylation by helicobacter pylori delays internalization and arrests phagosome maturation in macrophages. *Journal of Microbiology, Immunology and Infection*, 49(5):636–645, 2016.

[94] Whitney Fies, Jason W Dugger, Jeffrey E Dick, Logan Wilder, Katie Browning, Mathieu Doucet, James F Browning, and Lauren J Webb. Direct measurement of water permeation in submerged alkyl thiol self-assembled monolayers on gold surfaces revealed by neutron reflectometry. *Langmuir*, 2019.

[95] Laongnuan Srisombat, Andrew C Jamison, and T Randall Lee. Stability: A key issue for self-assembled monolayers on gold as thin-film coatings and nanoparticle protectants. *Colloids and Surfaces A: Physicochemical and Engineering Aspects*, 390(1-3):1–19, 2011.

[96] Colin D Bain, E Barry Troughton, Yu Tai Tao, Joseph Evall, George M Whitesides, and Ralph G Nuzzo. Formation of monolayer films by the spontaneous assembly of organic thiols from solution onto gold. *Journal of the American Chemical Society*, 111(1):321–335, 1989.

[97] Jen-Jr Gau, Esther H Lan, Bruce Dunn, Chih-Ming Ho, and Jason CS Woo. A mems based amperometric detector for e. coli bacteria using self-assembled monolayers. *Biosensors and Bioelectronics*, 16(9-12):745–755, 2001.

[98] Emanuele Ostuni, Robert G Chapman, Michael N Liang, Gloria Meluleni, Gerald Pier, Donald E Ingber, and George M Whitesides. Self-assembled monolayers that resist the adsorption of proteins and the adhesion of bacterial and mammalian cells. *Langmuir*, 17(20):6336–6343, 2001.

[99] Ma Cristina L Martins, Buddy D Ratner, and Mário A Barbosa. Protein adsorption on mixtures of hydroxyl-and methyl-terminated alkanethiols self-assembled monolayers. *Journal of Biomedical Materials Research Part A: An Official Journal of The Society for Biomaterials, The Japanese Society for Biomaterials, and The Australian Society for Biomaterials and the Korean Society for Biomaterials*, 67(1):158–171, 2003.

[100] Xiangping Qian, Steven J Metallo, Insung S Choi, Hongkai Wu, Michael N Liang, and George M Whitesides. Arrays of self-assembled monolayers for studying inhibition of bacterial adhesion. *Analytical chemistry*, 74(8):1805–1810, 2002.

[101] Ramalingam Murugan, Peter Molnar, Koritala P Rao, and James J Hickman. Biomaterial surface patterning of self assembled monolayers for controlling neuronal cell behavior. *International journal of biomedical engineering and technology*, 2(2):104, 2009.

[102] Paula Parreira, Ana Magalhães, Inês C Gonçalves, Joana Gomes, Ricardo Vidal, Celso A Reis, Deborah E Leckband, and M Cristina L Martins. Effect of surface chemistry on bacterial adhesion, viability, and morphology. *Journal of Biomedical Materials Research Part A*, 99(3):344–353, 2011.

[103] P Parreira, A Magalhães, CA Reis, Thomas Borén, D Leckband, and MCL Martins. Bioengineered surfaces promote specific protein–glycan mediated binding of the gastric pathogen helicobacter pylori. *Acta biomaterialia*, 9(11):8885–8893, 2013.

[104] P Parreira, Q Shi, A Magalhaes, CA Reis, Jeanna Bugaytsova, Thomas Borén, D Leckband, and MCL Martins. Atomic force microscopy measurements reveal multiple bonds between helicobacter pylori blood group antigen binding adhesin and lewis b ligand. *Journal of The Royal Society Interface*, 11(101):20141040, 2014.

[105] James N Hilfiker, Greg K Pribil, Ron Synowicki, Andrew C Martin, and Jeffrey S Hale. Spectroscopic ellipsometry characterization of multilayer optical coatings. *Surface and Coatings Technology*, 357:114–121, 2019.

[106] Eva Bittrich, Keith Brian Rodenhausen, Klaus-Jochen Eichhorn, Tino Hofmann, Mathias Schubert, Manfred Stamm, and Petra Uhlmann. Protein adsorption on and swelling of polyelectrolyte brushes: A simultaneous ellipsometry-quartz crystal microbalance study. *Biointerphases*, 5(4):159–167, 2010.

[107] Saul Patai and Zvi Rappoport. *The chemistry of organic derivatives of gold and silver*. John Wiley & Sons Inc, 1999.

[108] Tianyi Zhao and Lei Jiang. Contact angle measurement of natural materials. *Colloids and Surfaces B: Biointerfaces*, 161:324–330, 2018.

[109] Kulveer Singh and Christopher F Blanford. Electrochemical quartz crystal microbalance with dissipation monitoring: A technique to optimize enzyme use in bioelectrocatalysis. *ChemCatChem*, 6(4):921–929, 2014.

[110] Sean X Liu and Jun-Tae Kim. Application of kevin—voigt model in quantifying whey protein adsorption on polyethersulfone using qcm-d. *JALA: Journal of the Association for Laboratory Automation*, 14(4):213–220, 2009.

[111] Chun-Cheng Lin, Yi-Chun Yeh, Chan-Yi Yang, Chan-Long Chen, Gee-Fong Chen, Chia-Chun Chen, and Yi-Chun Wu. Selective binding of mannose-encapsulated gold nanoparticles to type 1 pili in escherichia coli. *Journal of the American Chemical Society*, 124(14):3508–3509, 2002.

[112] Show-Mei Chuang, Yi-Hui Lee, Ruei-Yue Liang, Gwo-Dong Roam, Zih-Ming Zeng, Hsin-Fang Tu, Shi-Kwun Wang, and Pin Ju Chueh. Extensive evaluations of the cytotoxic effects of gold nanoparticles. *Biochimica et Biophysica Acta (BBA)-General Subjects*, 1830(10):4960–4973, 2013.

[113] Narges Elahi, Mehdi Kamali, and Mohammad Hadi Baghersad. Recent biomedical applications of gold nanoparticles: A review. *Talanta*, 184:537–556, 2018.

[114] Ralph A Sperling, Pilar Rivera Gil, Feng Zhang, Marco Zanella, and Wolfgang J Parak. Biological applications of gold nanoparticles. *Chemical Society Reviews*, 37(9):1896–1908, 2008.

[115] Thomas Bürgi. Properties of the gold–sulphur interface: from self-assembled monolayers to clusters. *Nanoscale*, 7(38):15553–15567, 2015.

[116] Lifeng Qi, Zirong Xu, Xia Jiang, Caihong Hu, and Xiangfei Zou. Preparation and antibacterial activity of chitosan nanoparticles. *Carbohydrate research*, 339(16):2693–2700, 2004.

[117] Yan Zhou, Ying Kong, Subrata Kundu, Jeffrey D Cirillo, and Hong Liang. Antibacterial activities of gold and silver nanoparticles against escherichia coli and bacillus calmette-guérin. *Journal of nanobiotechnology*, 10(1):19, 2012.

[118] Ivan Sondi and Branka Salopek-Sondi. Silver nanoparticles as antimicrobial agent: a case study on e. coli as a model for gram-negative bacteria. *Journal of colloid and interface science*, 275(1):177–182, 2004.

[119] Yuyun Zhao, Yue Tian, Yan Cui, Wenwen Liu, Wanshun Ma, and Xingyu Jiang. Small molecule-capped gold nanoparticles as potent antibacterial agents that target gram-negative bacteria. *Journal of the American Chemical Society*, 132(35):12349–12356, 2010.

[120] Yu-Hsin Lin, Chiung-Hung Chang, Yu-Shiun Wu, Yuan-Man Hsu, Shu-Fen Chiou, and Yi-Jen Chen. Development of ph-responsive chitosan/heparin nanoparticles for stomach-specific anti-helicobacter pylori therapy. *Biomaterials*, 30(19):3332–3342, 2009.

[121] Pavimol Angsantikul, Soracha Thamphiwatana, Qiangzhe Zhang, Kevin Spiekermann, Jia Zhuang, Ronnie H Fang, Weiwei Gao, Marygorret Obonyo, and Liangfang Zhang. Coating nanoparticles with gastric epithelial cell membrane for targeted antibiotic delivery against helicobacter pylori infection. *Advanced therapeutics*, 1(2), 2018.

[122] Soumita Das, Pavimol Angsantikul, Christine Le, Denny Bao, Yukiko Miyamoto, Weiwei Gao, Liangfang Zhang, and Lars Eckmann. Neutralization of cholera toxin with nanoparticle decoys for treatment of cholera. *PLoS neglected tropical diseases*, 12(2):e0006266, 2018.

[123] Tamara Escajadillo, Joshua Olson, Brian T Luk, Liangfang Zhang, and Victor Nizet. A red blood cell membrane-camouflaged nanoparticle counteracts streptolysin o-mediated virulence phenotypes of invasive group a streptococcus. *Frontiers in pharmacology*, 8:477, 2017.

[124] Elena Colangelo, Joan Comenge, David Paramelle, Martin Volk, Qiubo Chen, and Raphael Levy. Characterizing self-assembled monolayers on gold nanoparticles. *Bioconjugate chemistry*, 28(1):11–22, 2016.

[125] Jingfang Zhou, John Ralston, Rossen Sedev, and David A Beattie. Functionalized gold nanoparticles: synthesis, structure and colloid stability. *Journal of colloid and interface science*, 331(2):251–262, 2009.

[126] Antonella Badia, Shanti Singh, Linette Demers, Louis Cuccia, G Ronald Brown, and R Bruce Lennox. Self-assembled monolayers on gold nanoparticles. *Chemistry–A European Journal*, 2(3):359–363, 1996.

[127] Mathias Brust, Merryl Walker, Donald Bethell, David J Schiffrin, and Robin Whyman. Synthesis of thiol-derivatised gold nanoparticles in a two-phase liquid–liquid system. *Journal of the Chemical Society, Chemical Communications*, (7):801–802, 1994.

[128] Vasumathi Velachi, Debdip Bhandary, Jayant K Singh, and M Natália DS Cordeiro. Structure of mixed self-assembled monolayers on gold nanoparticles at three different arrangements. *The Journal of Physical Chemistry C*, 119(6):3199–3209, 2015.

[129] Stefaan J Soenen, Bella Manshian, José Maria Montenegro, Faheem Amin, Björn Meermann, Toke Thiron, Maria Cornelissen, Frank Vanhaecke, Shareen Doak, Wolfgang J Parak, et al. Cytotoxic effects of gold nanoparticles: a multiparametric study. *ACS nano*, 6(7):5767–5783, 2012.

[130] Willi Jahnen-Dechent and Ulrich Simon. Function follows form: shape complementarity and nanoparticle toxicity. 2008.

[131] Jelle Penders, Michelle Stolzoff, Daniel J Hickey, Martin Andersson, and Thomas J Webster. Shape-dependent antibacterial effects of non-cytotoxic gold nanoparticles. *International journal of nanomedicine*, 12:2457, 2017.

[132] You Jeong Lee, Eun-Young Ahn, and Youmie Park. Shape-dependent cytotoxicity and cellular uptake of gold nanoparticles synthesized using green tea extract. *Nanoscale research letters*, 14(1):129, 2019.

[133] Mario Jug, Anita Hafner, Jasmina Lovrić, Maja Lusina Kregar, Ivan Pepić, Željka Vanić, Biserka Cetina-Čižmek, and Jelena Filipović-Grčić. An overview of in vitro dissolution/release methods for novel mucosal drug delivery systems. *Journal of pharmaceutical and biomedical analysis*, 147:350–366, 2018.

[134] Samuel K Lai, Ying-Ying Wang, and Justin Hanes. Mucus-penetrating nanoparticles for drug and gene delivery to mucosal tissues. *Advanced drug delivery reviews*, 61(2):158–171, 2009.

[135] Georgia K Hinkley, Paul Carpinone, John W Munson, Kevin W Powers, and Stephen M Roberts. Oral absorption of peg-coated versus uncoated gold nanospheres: does agglomeration matter? *Particle and fibre toxicology*, 12(1):9, 2015.

[136] Wolfgang Mehnert and Karsten Mäder. Solid lipid nanoparticles: production, characterization and applications. *Advanced drug delivery reviews*, 64:83–101, 2012.

[137] Hilde Jans, Xiong Liu, Lauren Austin, Guido Maes, and Qun Huo. Dynamic light scattering as a powerful tool for gold nanoparticle bioconjugation and biomolecular binding studies. *Analytical chemistry*, 81(22):9425–9432, 2009.

[138] Ute Pyell, Alaa H Jalil, Christian Pfeiffer, Beatriz Pelaz, and Wolfgang J Parak. Characterization of gold nanoparticles with different hydrophilic coatings via capillary electrophoresis and taylor dispersion analysis. part i: Determination of the zeta potential employing a modified analytic approximation. *Journal of colloid and interface science*, 450:288–300, 2015.

[139] Clinical and Laboratory Standards Institute. Performance standards for antimicrobial susceptibility testing, 2017.

[140] Frederico Nogueira, Inês C Gonçalves, and M Cristina L Martins. Effect of gastric environment on helicobacter pylori adhesion to a mucoadhesive polymer. *Acta Biomaterialia*, 9(2):5208–5215, 2013.

[141] I Iso. 10993–5: 2009 biological evaluation of medical devices—part 5: tests for in vitro cytotoxicity. *International Organization for Standardization, Geneva*, 2009.

[142] E ISO et al. Biological evaluation of medical devices-part 12: Sample preparation and reference materials, 2012.

[143] JATL MacLachlan, ATL Wotherspoon, RO Ansell, and CJW Brooks. Cholesterol oxidase: sources, physical properties and analytical applications. *The Journal of steroid biochemistry and molecular biology*, 72(5):169–195, 2000.

[144] Christopher ED Chidsey, Carolyn R Bertozzi, TM Putvinski, and AM Mujsce. Coadsorption of ferrocene-terminated and unsubstituted alkanethiols on gold: electroactive self-assembled monolayers. *Journal of the American Chemical Society*, 112(11):4301–4306, 1990.

[145] Yan Guo, Jianwei Zhao, and Junjie Zhu. Study on the intermolecular interactions between the functional moieties in ferrocene-terminated alkanethiol self-assembled monolayer on gold. *Thin Solid Films*, 516(10):3051–3057, 2008.

[146] Seyed R Tabaei, Joshua A Jackman, Seong-Oh Kim, Bo Liedberg, Wolfgang Knoll, Atul N Parikh, and Nam-Joon Cho. Formation of cholesterol-rich supported membranes using solvent-assisted lipid self-assembly. *Langmuir*, 30(44):13345–13352, 2014.

[147] Nuno T Marcos, Ana Magalhães, Bibiana Ferreira, Maria J Oliveira, Ana S Carvalho, Nuno Mendes, Tim Gilmartin, Steven R Head, Céu Figueiredo, Leonor David, et al. Helicobacter pylori induces β3gnt5 in human gastric cell lines, modulating expression of the saba ligand sialyl–lewis x. *The Journal of clinical investigation*, 118(6):2325–2336, 2008.

[148] Gerhard Reuter. The lactobacillus and bifidobacterium microflora of the human intestine: composition and succession. *Current issues in intestinal microbiology*, 2(2):43–53, 2001.

[149] Nathan Crook, Aura Ferreiro, Andrew J Gasparrini, Mitchell W Pesesky, Molly K Gibson, Bin Wang, Xiaoqing Sun, Zevin Condiotte, Stephen Dobrowolski, Daniel Peterson, et al. Adaptive strategies of the candidate probiotic e. coli nissle in the mammalian gut. *Cell host & microbe*, 25(4):499–512, 2019.

[150] Claire Valotteau, Niki Baccile, Vincent Humblot, Sophie Roelants, Wim Soetaert, Christian V Stevens, and Yves F Dufrêne. Nanoscale antiadhesion properties of sophorolipid-coated surfaces against pathogenic bacteria. *Nanoscale Horizons*, 4(4):975–982, 2019.

[151] BVZE Kos, Jagoda Šušković, Snježana Vuković, Miljenko Šimpraga, Jadranka Frece, and Srećko Matošić. Adhesion and aggregation ability of probiotic strain lactobacillus acidophilus m92. *Journal of applied microbiology*, 94(6):981–987, 2003.

[152] S Rajeshkumar. Anticancer activity of eco-friendly gold nanoparticles against lung and liver cancer cells. *Journal of Genetic Engineering and Biotechnology*, 14(1):195–202, 2016.

[153] Akhilesh Rai, Sandra Pinto, Tiago R Velho, André F Ferreira, Catarina Moita, Urvish Trivedi, Marta Evangelista, Michela Comune, Kendra P Rumbaugh, Pedro N Simões, et al.

One-step synthesis of high-density peptide-conjugated gold nanoparticles with antimicrobial efficacy in a systemic infection model. *Biomaterials*, 85:99–110, 2016.

[154] Kenji Aramaki, Yuki Watanabe, Junpei Takahashi, Yusuke Tsuji, Ami Ogata, and Yoshikazu Konno. Charge boosting effect of cholesterol on cationic liposomes. *Colloids and Surfaces A: Physicochemical and Engineering Aspects*, 506:732–738, 2016.

[155] Xiangsheng Liu, Qiao Jin, Ying Ji, and Jian Ji. Minimizing nonspecific phagocytic uptake of biocompatible gold nanoparticles with mixed charged zwitterionic surface modification. *Journal of Materials Chemistry*, 22(5):1916–1927, 2012.

[156] Nouf N Mahmoud, Ala A Alhusban, Jamila Isabilla Ali, Amal G Al-Bakri, Rania Hamed, and Enam A Khalil. Preferential accumulation of phospholipid-peg and cholesterol-peg decorated gold nanorods into human skin layers and their photothermal-based antibacterial activity. *Scientific reports*, 9(1):1–15, 2019.

[157] Nouf N Mahmoud, Dima A Sabbah, Rana Abu-Dahab, Duaa Abuarqoub, Maha Abdallah, Enam A Khalil, et al. Cholesterol-coated gold nanorods as an efficient nano-carrier for chemotherapeutic delivery and potential treatment of breast cancer: in vitro studies using the mcf-7 cell line. *RSC advances*, 9(22):12718–12731, 2019.

[158] M Danaei, M Dehghankhold, S Ataei, F Hasanzadeh Davarani, R Javanmard, A Dokhani, S Khorasani, and MR Mozafari. Impact of particle size and polydispersity index on the clinical applications of lipidic nanocarrier systems. *Pharmaceutics*, 10(2):57, 2018.

[159] A Reznickova, N Slavikova, Z Kolska, K Kolarova, T Belinova, M Hubalek Kalbacova, M Cieslar, and V Svorcik. Pegylated gold nanoparticles: Stability, cytotoxicity and antibacterial activity. *Colloids and Surfaces A: Physicochemical and Engineering Aspects*, 560:26–34, 2019.

[160] Liang Xu, Hai-Wei Liang, Yuan Yang, and Shu-Hong Yu. Stability and reactivity: positive and negative aspects for nanoparticle processing. *Chemical reviews*, 118(7):3209–3250, 2018.

[161] Elina Ikonen. Mechanisms of cellular cholesterol compartmentalization: recent insights. *Current opinion in cell biology*, 53:77–83, 2018.

[162] Shailendra Anoopkumar-Dukie, JB Carey, T Conere, E O'sullivan, FN Van Pelt, and A Allshire. Resazurin assay of radiation response in cultured cells. *The British journal of radiology*, 78(934):945–947, 2005.

[163] Konstantin Präbst, Hannes Engelhardt, Stefan Ringgeler, and Holger Hübner. Basic colorimetric proliferation assays: Mtt, wst, and resazurin. In *Cell viability assays*, pages 1–17. Springer, 2017.

[164] Léa P Wilhelm, Laetitia Voilquin, Toshihide Kobayashi, Catherine Tomasetto, and Fabien Alpy. Intracellular and plasma membrane cholesterol labeling and quantification using filipin and gfp-d4. In *Intracellular Lipid Transport*, pages 137–152. Springer, 2019.

[165] Guomin Wang, Weihong Jin, Abdul Mateen Qasim, Ang Gao, Xiang Peng, Wan Li, Hongqing Feng, and Paul K Chu. Antibacterial effects of titanium embedded with silver nanoparticles based on electron-transfer-induced reactive oxygen species. *Biomaterials*, 124:25–34, 2017.

[166] Leila Büttner Mostaço-Guidolin, Luciana Sayuri Murakami, Marina Ribeiro Batistuti, Auro Nomizo, and Luciano Bachmann. Molecular and chemical characterization by fourier transform infrared spectroscopy of human breast cancer cells with estrogen receptor expressed and not expressed. *Journal of Spectroscopy*, 24(5):501–510, 2010.

[167] Angela França, Beatriz Pelaz, María Moros, Christian Sánchez-Espinel, Andrea Hernández, Cristina Fernández-López, Valeria Grazu, Jesus M de la Fuente, Isabel Pastoriza-Santos, Luis M Liz-Marzán, et al. Sterilization matters: consequences of different sterilization techniques on gold nanoparticles. *small*, 6(1):89–95, 2010.

[168] John D Weete, Maritza Abril, and Meredith Blackwell. Phylogenetic distribution of fungal sterols. *PloS one*, 5(5), 2010.